



NTNU – Trondheim
Norwegian University of
Science and Technology

Earthquake analysis of structures using nonlinear models

Miran Cemalovic

Civil and Environmental Engineering (2 year)

Submission date: June 2015

Supervisor: Amir Kaynia, KT

Co-supervisor: Nina Øystad-Larsen, Rambøll

Norwegian University of Science and Technology
Department of Structural Engineering

Acknowledgements

This masters thesis has been written at Norwegian University of Science and Technology (NTNU), Department of Structural Engineering in collaboration with Rambøll Norway, Oslo. The work has been conducted in the spring semester of 2015.

I would like to thank my supervisors Professor II Amir M. Kaynia (NTNU) and PhD Candidate Nina Øystad-Larsen (Rambøll) for tremendous support and encouragement throughout the entire process. Their insight and genuine interest in this thesis has been invaluable for my accomplishments. I also wish to express my gratitude to PhD, Siv.Eng Emrah Erduran (Rambøll) for sharing his vast knowledge in the fields of earthquake engineering and computational mechanics. A special thanks to Nina I. Eslami for her consistent support and correcting of my English.

Abstract

Throughout the governing design codes, several different methods are presented for the evaluation of seismic problems. This thesis assesses the non-linear static and dynamic procedures presented in EN 1998-1 through the structural response of a RC wall-frame building. The structure is designed in detail according to the guidelines for high ductility (DCH) in EN 1998-1. The applied procedures are meticulously evaluated and the requirements in EN 1998-1 are reviewed. In addition, the finite element softwares SeismoStruct and OpenSees are utilized and evaluated.

The results revealed that even though expecting, and designing for, high ductility, the structural response remained nearly in the elastic range. The elastic behaviour was a result of oversized and heavily reinforced members, with emphasis on the lower storey walls. The reduction of global stiffness caused by the selected time-history ground motions was greater than the recommendation in EN 1998-1. The non-linear static analysis rendered reasonable results in terms of displacements for the first-mode dominated structure. However, it has been demonstrated that the structure's natural sensitivity to multi-degree-of-freedom effects limited the static analysis in terms of revealing possible structural behaviour.

Sammendrag

Flere ulike analytiske metoder er utviklet for evalueringen av seismiske påkjenninger og beskrevet i de forskjellige lands standarder. Denne masteroppgaven vurderer de ikke-lineære statiske og dynamiske prosedyrene presentert i EN 1998-1 gjennom responsen av et vegg-ramme-bygg i armert betong. Bygget er utformet i detalj i henhold til retningslinjene for høy duktilitet (DCH) i EN 1998-1. De anvendte prosedyrene er nøye vurdert og kravene i EN 1998-1 er evaluert. Analysene er utført ved bruk av de elementmetode-baserte programvarene SeismoStruct og OpenSees.

Resultatene viste at selv om konstruksjonen var utformet for høy duktilitet, responderte den nærmest elastisk. Den elastiske oppførselen var et resultat av overdimensjonerte og tungt armerte vegger. Reduksjonen av global stivhet forårsaket av grunnakselerasjonsforløpene var større enn anbefalingen i EN 1998-1. Den ikke-lineære statiske analysen ga rimelige resultater i form av forskyvninger for et bygg dominert av første mode. Det har imidlertid blitt påvist at konstruksjonens naturlige følsomhet for MDOF-effekter begrenset den statiske analysen på grunn av dens manglende evne til å avsløre alternativ oppførsel.

Contents

1	Introduction	1
1.1	Background	1
1.2	Objective of the thesis	2
1.3	Method	2
1.4	Structure of the thesis	3
2	Literature review	4
2.1	Response modification factor	4
2.2	Analytical procedures	5
2.2.1	Linear static analysis	5
2.2.2	Non-linear static analysis	7
2.2.3	Non-linear time history analysis	10
2.3	Distributed inelasticity element-formulation	11
2.3.1	General scheme	11
2.3.2	Finite element formulation	12
2.4	OpenSees	13
3	Design	14
3.1	Basis	14
3.1.1	General	14
3.1.2	Materials	14
3.1.3	Loads	14
3.2	Design for gravity loads	16
3.2.1	Slab	16
3.2.2	Beams	16
3.2.3	Columns	17
3.2.4	Desired formation of mechanism	18
3.2.5	Walls	21
3.3	Analysis based on the linear static method	23
3.3.1	Q-factor	23
3.3.2	Seismic loading	24
3.3.3	Check of the beams	26
3.3.4	Check of the columns	29
3.3.5	Check of the walls	33

3.3.6	Check of the structural system	34
3.4	Final element characteristics	34
4	Establishing the finite element model	36
4.1	Introduction	36
4.2	Model	36
4.2.1	Geometry	36
4.2.2	Material	36
4.2.3	Elements	37
4.2.4	Algorithms and integrators	37
4.3	Eigenvalue analysis	38
4.3.1	Stiffness	39
4.3.2	Effect of RC walls	39
4.3.3	Shear deformations	39
4.4	Concluding remarks	41
5	Non-Linear Static Analysis	42
5.1	Introduction	42
5.2	Basis for procedure	42
5.2.1	SDOF-system	42
5.2.2	Idealized force-displacement relationship	44
5.3	Expected displacement	45
5.4	Safety verifications	45
5.4.1	General	45
5.4.2	Flexural capacity	46
5.4.3	Cyclic shear capacity	47
6	Non-Linear Time-History Analysis	48
6.1	Introduction	48
6.2	Ground motions	48
6.2.1	Selected ground motions	48
6.2.2	Scaling	48
6.3	Response	49
7	Discussion of the results	60
7.1	Introduction	60
7.2	SeismoStruct versus OpenSees	60
7.2.1	Non-linear static response	60
7.2.2	Time-history response	65
7.3	NSA versus NTHA	65
7.3.1	Period elongation	65
7.3.2	Base shear force	72
7.3.3	Interstorey drift ratios	73
7.4	Requirements in EN 1998-1	78

7.4.1	Ductility and over-strength	78
7.4.2	Reduction of stiffness	78
7.4.3	Shear demands in EN 1998-1	80
7.4.4	DCM versus DCH	81
7.5	Effect of integration points	84
8	Conclusion	85
8.1	EN 1998-1	85
8.2	Dynamic versus static procedures	85
8.3	SeismoStruct versus OpenSees	86
	Appendices	90
	Appendix A Calculations	91
A.1	Loads	91
A.2	Effective flange width of the beams	92
A.3	Moment capacities of initial columns	93
A.4	General calculations and equations from Eurocode	94
A.5	Equivalent spacing of shear reinforcement for walls	95
A.6	Ductility demands for beams in the seismic situation	96
A.7	Shear capacities in the seismic design situation	98
A.8	Moment and shear capacity of walls in the seismic design situation	100
	Appendix B Matlab scripts	103
B.1	Response spectrum	103
	Appendix C OpenSees scripts	116
C.1	Main file	116
C.2	Material	116
C.3	Sections	121
C.4	Geometry	134
C.5	Constraints	146
C.6	Gravity loads	146
C.7	Records	148
C.8	Non-linear static analysis	148
C.9	Non-linear time-history analysis	150

List of Figures

2.1	General structural response of a building subjected to monotonically increasing lateral loads. Illustration: Asgarian, B. and Shokrgozar, H.	5
2.2	Distributed inelasticity fibre-element. Illustration: Calabrese, A, Almeida, J.P and Pinho, R.	12
2.3	OpenSees interface and an example of a Tcl-script for the assessment of a dynamic time-history analysis.	13
3.1	Geometry of the structure.	15
3.2	Illustration of the moment capacities at the border joint.	18
3.3	M/N-diagrams for the 440 mm interior and 330 border columns.	19
3.4	Peak ground acceleration and response spectrum.	25
3.5	M/N-diagrams in the seismic design situation.	31
4.1	Illustration of the FEM-model configuration.	37
4.2	Natural periods of the FEM-models.	38
4.3	First 4 natural mode shapes of the structure.	40
5.1	Base shear-displacement relationship.	43
5.2	Interstorey drifts from the non-linear static analysis.	45
5.3	Chord rotation-roof displacement relationship for the 4th storey interior beam in axis B/2-3.	46
5.4	Shear force-roof displacement relationship for the 4th storey interior beam in axis B/2-3.	47
6.1	Selected non-scaled ground motion time histories.	51
6.2	Response spectrum of selected ground motions	52
6.3	Displacement response of the control node.	53
6.4	Displacement response of the control node. Individual time ranges are selected to reveal possible discrepancies between SeismoStruct and OpenSees.	54
6.5	Base shear-time history relationships for the selected ground motions.	55
6.6	Base shear-time history relationships. Individual time ranges are selected to reveal possible discrepancies between SeismoStruct and OpenSees.	56
6.7	Hysteric base shear - roof displacement relationship.	57
6.8	Maximum roof displacements and drift ratios from the non-linear time history analysis.	58

6.9	Maximum base shear forces plotted against maximum displacements for the individual non-linear dynamic analyses.	58
6.10	Interstorey drift ratios from the non-linear time history analyses.	59
7.1	Displacement response of the control node for "Iwate Japan"-ground motion increased by 50 %.	61
7.2	Illustration of the confined concrete model applied in SeismoStruct and OpenSees. Illustration: OpenSeesWiki.	62
7.3	The steel material models applied in SeismoStruct and OpenSees. Note that a) represents the actual steel model in SeismoStruct, while b) is an illustration of the steel model in OpenSees.	62
7.4	Illustration of the 1st storey wall cross section. Observe that the figure only illustrates half of the cross section.	63
7.5	Stress and strain-displacement relationships for the reinforcement illustrated in Figure 7.4. The relationships are assessed from the static analysis. The bars are numbered from left to right. Note that the presented range of displacement differs in the two figures.	63
7.6	Base shear-control displacement relationship. The fracture strain of reinforcement steel in SeismoStruct is set equal to unity.	64
7.7	Displacement response of the control node for "Iwate Japan" ground motion increased by 50 % when the fracture strain of reinforcement steel in SeismoStruct is set equal to unity.	65
7.8	Target displacement from NSA together with maximum displacements/base shear from NTHA.	66
7.9	Scaled response spectrum for $0 \leq T \leq 1.2$ presented in three figures.	68
7.10	Stress and strain-time relationship for the reinforcement illustrated in Figure 7.4.	69
7.11	Extraction of SDOF pushover-curves together with the initial stiffness of the system.	70
7.12	Natural periods of the cracked system. Eigenvalue analysis has been performed after the structure has been exposed to the individual ground motion.	71
7.13	First natural periods from the cracked system plotted against the maximum displacement from the individual ground motions.	71
7.14	First natural periods from the cracked system plotted against the maximum base shear forces from the individual ground motions.	72
7.15	Interstorey drift ratio comparison between NSA and the average values from NTHA.	74
7.16	Interstorey drift ratio comparison between NSA and San Fernando. The drift ratios from NSA are assessed at target displacement equal to maximum roof displacement from San Fernando. The values are obtained from SeismoStruct.	75
7.17	Interstorey drift ratio comparison between NSA and Imperial Valley. The drift ratios from NSA are assessed at target displacement equal to maximum roof displacement from Imperial Vally. The values are obtained from SeismoStruct.	75

7.18	Interstorey drift ratio comparison between NSA and Superstition Hills. The drift ratios from NSA are assessed at target displacement equal to maximum roof displacement from Superstition Hills. The values are obtained from SeismoStruct.	76
7.19	Interstorey drift ratio comparison between NSA and Spitak Armenia. The drift ratios from NSA are assessed at target displacement equal to maximum roof displacement from Spitak Armenia. The values are obtained from SeismoStruct.	76
7.20	Interstorey drift ratio comparison between NSA and Manjil Iran. The drift ratios from NSA are assessed at target displacement equal to maximum roof displacement from Manjil Iran. The values are obtained from SeismoStruct.	77
7.21	Interstorey drift ratio comparison between NSA and Joetsu City. The drift ratios from NSA are assessed at target displacement equal to maximum roof displacement from Joetsu City. The values are obtained from SeismoStruct.	77
7.22	Interstorey drift ratio comparison between NSA and Iwate Japan. The drift ratios from NSA are assessed at target displacement equal to maximum roof displacement from Iwate Japan. The values are obtained from SeismoStruct.	78
7.23	Base shear-displacement relationship, target displacement and first plastic hinge from the non-linear static analysis for $0 \text{ m} \leq d \leq 0.1 \text{ m}$	79
7.24	Base shear-displacement relationship for the structure with 1st storey wall designed in DCM.	83
7.25	Non-linear analysis with varying number of integration points.	84
A.1	M/N-diagrams for the 280 mm interior and border 230 mm border columns.	93
A.2	Moment diagram from the seismic design situation.	99

List of Tables

3.1	Beam characteristics.	17
3.2	Axial loads and moment capacities of the 440 mm and 330 mm columns. . .	20
3.3	Moment capacities of the beams.	20
3.4	Moment capacity ratios.	21
3.5	Column characteristics.	22
3.6	Wall characteristics.	23
3.7	Shear capacities of columns.	24
3.8	Storey forces and displacements.	26
3.9	P - δ effect factor ϑ	26
3.10	Ductility demands for beams without additional reinforcement.	27
3.11	Ductility demands for beams with additional reinforcement.	27
3.12	Moment capacities of the beams with additional reinforcement.	28
3.13	Final moment capacities of beams.	28
3.14	Ductility demands for beams designed for the seismic situation.	29
3.15	Shear capacities of beams in accordance with EN 1998-1	30
3.16	Axial loads and moment capacities of columns in the seismic design situation.	30
3.17	Moment capacity ratios in the seismic design situation.	32
3.18	Final beam characteristics.	35
3.19	Final column characteristics.	35
3.20	Final wall characteristics.	35
5.1	Target displacement calculations according to EN 1998-1, Appendix B.	44
6.1	Selected ground motions from the PEER Ground Motion Database.	49
6.2	Ground motion scaling factors.	49
6.3	Maximum roof displacements and base shear forces from the non-linear time history analysis.	50
7.1	The 1st storey wall designed in DCM.	81
7.2	Target displacement calculations according to EN 1998-1, Appendix B. Structural system with 1st storey wall designed in DCM.	82
A.1	Axial loads and moment capacities of the 280 mm and 230 mm columns. . .	94
A.2	Capacity check of walls after increased forces.	102

Chapter 1

Introduction

1.1 Background

Seismic design is somewhat exceptional in the sense that we accept higher risks of damage than for e.g. wind or gravity design. In general, the forces caused by seismic ground motions are too high to be resisted by realistically designed structures in the elastic range. Therefore, the structure must withstand such forces through energy dissipation, i.e. the structure is expected to deform past the elastic limit when subjected to the design earthquake. The current design codes give a number of prescribed requirements that must be met. Seismic design based on such predefined demands is commonly referred to as "Conventional seismic design". Several simplified methods have been developed for both the linear and non-linear response of structures and are incorporated in the current design codes with the purpose of providing the industry with easy and time-efficient guidelines. It is the author's opinion that such methods often become rigorous step-by-step procedures that limit the engineers ability to exercise creativity and perform rational design. In contrast, "Performance-based seismic design" (PBSD) implies the evaluation of the buildings *performance* with regards to the expectations of owners, users and society in general. The design, i.e. structural configuration, selection of materials, member dimensions and reinforcement etc., is assessed depending on how the structure responds to the design seismic actions instead of the aforementioned prescribed set of requirements. The state-of-the-art understanding of PBSD indicates the assessment of displacements and strains rather than forces and stresses. The key to understanding the basic principles and concepts of seismic design is to recognize the fact that for the inelastic range of response, deformations are better indicators of damage than forces.

Due to the dynamic nature of seismic loading and the corresponding inelastic structural response, sufficiently accurate analytical solutions are non-existing. As for any non-linear problem, the evaluation must be performed numerically. Theoretically, the finite element method formulated in the various commercialized programs allows for element-formulations and algorithms that produce nearly accurate results. However, these formulations are still too complicated and time-consuming to be implemented when assessing the global response of real-life structures subjected to seismic ground motions. There has therefore been developed,

and is still developing, alternative element-formulations that allow for reasonable computational efforts and time consumptions. As will be demonstrated throughout this thesis, the application, and especially the output interpretation of such elements is not straight-forward and must be exercised with caution. It is the author's understanding that the finite element method, generally formulated and no matter how simple the program appears to be, is not nor will it ever be a plug-and-play sort of application. Design of structures in accordance with the basic principles of PBSB is dependent on the establishment of a rational and sufficiently accurate FEM-model. In addition, the evaluation and validity of the results are contingent of understanding the general formulations implemented in the given finite element tool. This thesis will therefore emphasize the computational part of seismic engineering in addition to the general principles of code-and performance based seismic design together with the various types of linear and non-linear analysis.

1.2 Objective of the thesis

The main objectives of this thesis are listed below.

- Evaluate the strength capacity demand in EN 1998-1 [1].
- Evaluate and compare the non-linear analytical procedures provided in EN 1998-1 [1], i.e. the Non-linear Static Analysis (NSA) and the Non-Linear Time-History Analysis (NTHA).
- Evaluate and compare the finite element based softwares SeismoStruct [2] and OpenSees [3].

1.3 Method

First, a structure is designed in detail according to EN 1998-1 [1]. Though simple in geometry, the building represents a realistic design without non-realistic simplifications. The validity of evaluating the demands in EN 1998-1 depend on meticulous evaluation in accordance with the given guidelines. Therefore, conscientious design of members and structural configuration has been emphasized. Next, the finite element model is established by evaluating the eigenvalue-problem and comparing the results from several finite elements softwares. The aim is to establish a sufficiently accurate mathematical model prior to embarking on the different analyses. Finally, the structural response is evaluated through the application of non-linear static and dynamic procedures. The results are thoroughly investigated to reveal strengths and weaknesses of dynamic and static methods, potential discrepancies in the respective softwares and also to evaluate the capacity demands in EN 1998-1 in comparison with the obtained results.

1.4 Structure of the thesis

Chapter 2 - Literature review

This chapter contains a concise review over the topics that are dealt with in the thesis. Section 2.1 explains the modification factor q incorporated in EN 1998-1 [1], Section 2.2 describes the different analytical procedures, Section 2.3 elucidates the element-formulation applied in the finite elements models and Section 2.4 briefly introduces OpenSees [3].

Chapter 3 - Design

The example structure is designed in accordance with the governing design codes.

Chapter 4 - Establishing the finite element model

The procedure for establishing the finite element model is presented.

Chapter 5 - Non-Linear Static Analysis

This chapter contains the assessment of the Non-Linear Static Analysis. The results are presented and safety verifications are performed on a selected member.

Chapter 6 - Non-Linear Time-History Analysis

This chapter contains the assessment of the Non-Linear Time-History Analysis. The results are presented.

Chapter 7 - Discussion of the results

This chapter discusses the results from the static and dynamic non-linear analyses assessed in Chapters 5 and 6. Section 7.2 compares the results from OpenSees with those obtained in SeismoStruct, Section 7.3 evaluates and compares the static and dynamic procedures and Section 7.4 reviews the requirements in EN 1998-1 in relation to the acquired results.

Chapter 8 - Conclusion

Concluding remarks are presented.

Appendices

Appendix A shows the calculations from Chapter 3, Appendix B contains the Matlab-script written for the assessment of the response spectra from the selected ground motion records and Appendix C presents the OpenSees-script developed for the various analyses of the example structure. Additional Matlab-scripts and results from computer programs are added digitally.

Chapter 2

Literature review

2.1 Response modification factor

Simplified methods for estimating seismic actions given in current design codes take into account ductility and over-strength by reducing forces determined by linear models. The presence of over-strength in buildings is associated with the fact that code-designed structures possess strength beyond the design values due to the conservative determination of material properties, member dimensions, reinforcement and acting loads. In EN 1998-1 [1], the force reduction is incorporated through a modification factor q that depends on the structural type (e.g. concrete frames, wall-systems) and regularity. This factor represents the ratio of maximum acting force if the structure was to remain elastic to the design force [4]. The estimation of q has been criticized throughout the literature [5] suggesting that ductility in concrete and masonry structures depend on a wide range of factors such as axial loads, reinforcement and geometry. The theoretical approach, e.g. suggested by Asgarian and Shokrgozar [4], defines the modification factor by utilizing the force-displacement relationship of a structure where the non-linear behaviour is idealized by a elastic-perfectly plastic relationship. With reference to Figure 2.1, the part of the modification factor that accounts for ductility can be expressed as

$$\mu = \frac{V_{\max}}{V_y} \quad (2.1)$$

where V_{\max} is the maximum force considering elastic behaviour and V_y is the yield force corresponding to the idealized system. Throughout the literature, μ is also referred to as the force reduction factor. The over-strength factor is defined as

$$\Omega = \frac{V_y}{V_s} \quad (2.2)$$

where V_{ym} is the actual maximum occurring force and V_s is acting force at the formation of the first plastic hinge. The modification factor is expressed as the product of the factors accounting for ductility and over-strength, i.e.,

$$q = \mu \times \Omega \quad (2.3)$$

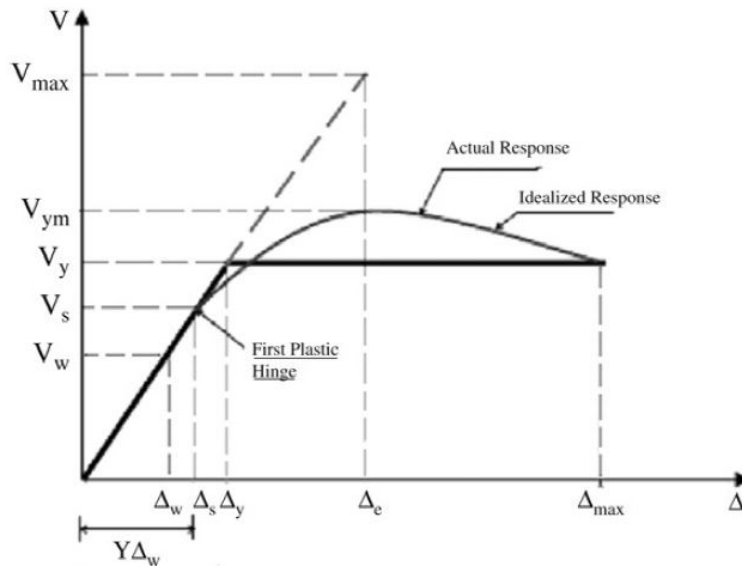


Figure 2.1: General structural response of a building subjected to monotonically increasing lateral loads. Illustration: Asgarian, B. and Shokrgozar, H.

2.2 Analytical procedures

This section briefly explains the type of analyses performed and evaluated in the thesis. In general, four types of analyses are considered in seismic design.

- Linear Static Analysis
- Linear Dynamic Analysis
- Non-linear static analysis
- Non-linear time-history analysis

The Linear Dynamic Analysis is not applied in this thesis and will therefore not be explained in this section. The reader is referred to the to section 3-10 in FEMA 356 [6].

2.2.1 Linear static analysis

Background

The linear static analysis is the most elementary and straight-forward procedure for the determination of internal loads and displacements due to seismic excitation of buildings presented in EN 1998-1 [1]. The simple guidelines allow for easy and less time-consuming evaluation of seismic problems. However, since earthquakes by nature are dynamic and not static problems, the method has several limitations and should be chosen with caution.

Basis of the procedure

The application is restricted to structures that are dominated by one mode in each of the main directions. NS-EN 1998-1 allows for the method if

$$T_1 \leq \min\{4 \times T_c, 2.0s\} \quad (2.4)$$

and if the criteria for regularity according to EN 1998-1, section 4.2.3.3 is fulfilled.

Loads

The linear static method is based on a elastic building model. The lateral loads are determined such that when applied to the model, it will result in design displacements approximating maximum displacements expected during the design earthquake [6]. The magnitude of loads are determined by estimating the base shear force,

$$F_b = S_d(T_1) \times m \times \lambda. \quad (2.5)$$

where $S_d(T_1)$ is the design spectral acceleration, m is the total mass of the structure and λ is a correction factor depending on the natural period and the number of stories in the structure. The force distribution over the height can be approximated as

$$F_i = F_b \times \frac{z_i \times m_i}{\sum(z_j \times m_j)} \quad (2.6)$$

where m_i and m_j are the floor masses and z_i and z_j are the floor heights.

Period determination

The period can either be evaluated analytically, empirically or it can be estimated. EN 1998-1 gives guidelines for all three alternatives. For further explanation, the reader is referred to the literature [1, 7].

Torsional effects

EN 1998-1, section 4.3.3.2.4 gives guidelines for the effects from torsion. For structures with symmetrically distributed mass and stiffness that are modelled in two dimensions, the effects from accidental torsion are safeguarded by multiplying the acting design forces with a factor

$$\delta = 1 + 1.2 \times \frac{X}{L_e} \quad (2.7)$$

where X is the distance from the mass center to the element in question, measured horizontally, and L_e is the distance between the two elements that resist horizontal forces and are the farthest from each other.

Disadvantages

The validity of the method is restricted by significant contributions from higher modes. The procedure should therefore only be considered for structures that are heavily dominated by one mode. Linear methods are applicable if the structure is expected to deform primarily within the elastic range. If not, which is often the case for seismic problems, non-linear methods will produce more reliable results since deformations are better indicators of damage level than forces. Also, when the structure responds past the elastic range, the modal properties will change, hence making the method less valid.

2.2.2 Non-linear static analysis

Background

Despite the fact that most practising engineers, if not all, have access to powerful computers and advanced finite element software, there is still a need for simple, sufficiently accurate analytical procedures for non-linear behaviour. Methods such as the non-linear time-history analysis can be perceived as being too complicated and/or time consuming for practical tasks. Such analyses require above-average knowledge and experience in the fields of computational mechanics and earthquake engineering. Moreover, time-history analysis demands selection and application of multiple, suitable ground motions. The selection itself is not straightforward, and multiple ground motions increase the computational efforts significantly. The non-linear static analysis provides a simple option for estimating deformations and strength capacities in the inelastic range. This technique also provides solid information of how the structure will perform, i.e. the sequence of yielding in each and every element, hence making it applicable in performance-based seismic design.

Basis of the procedure

Conveniently referred to as the "pushover analysis", the primary step in the assessment of the non-linear static analysis is to determine a force-displacement relationship by applying monotonically increasing lateral loads until a horizontal target displacement is reached. The lateral loads represent the inertia forces and the target displacement represents the maximum displacement expected to occur during the design earthquake. The mathematical model must directly incorporate the non-linear stress-strain relationships of all elements expected to deform past the elastic limit.

It can be shown that $P-\delta$ effects are of great importance for the static post-yield behaviour of structures [8]. It is therefore important that all gravity loads are included during the analysis. For the utmost seismic effects, the lateral loads must be applied in all necessary directions and both primary and secondary lateral-force-resisting elements must be included the model. The control displacement node, i.e. the node where the displacement is assessed, should be located at the center of mass at the top of the structure [6].

Lateral load distribution

EN 1998-3 [9] demand that at least two different lateral force distributions are applied. The first distribution is based on a modal pattern, while the second is based on a vertical mass distribution regardless of elevation. However, the application of the latter has been shown unnecessary since it underestimates drifts in upper stories and overestimates them in lower stories [10].

Target displacement

EN 1998-1 [1] defines the target displacement as the seismic design displacement taken from the elastic response spectrum when considering an equivalent SDOF-system, i.e. an equivalent force-displacement relationship with a corresponding mass m^* . The method, as presented in the design codes [1, 6] and applied in this thesis, is also known as the *N2-method* developed at the University of Ljubljana [11, 12]. The force F^* and displacement d^* of the equivalent system are determined by a transformation factor Γ .

$$m^* = \sum m_i \times \Phi_i \quad (2.8)$$

$$\Gamma = \frac{m^*}{\sum(m_i \times \Phi_i^2)} \quad (2.9)$$

$$F^* = \frac{F_b}{\Gamma} \quad (2.10)$$

$$d^* = \frac{d_n}{\Gamma} \quad (2.11)$$

Here, m_i is the lumped storey mass, Φ_i is the normalized value of the mode shape at storey i , F_b is the base shear force and d_n is the real displacement. Simplified procedures such as those given in EN 1998-1 require constant stiffness properties. The equivalent force-displacement relationship between the base shear force and control node displacement must be replaced with an idealized bi-linear relationship by stating that the strain energy up till the target displacement is equal for both relationships.¹ Simple geometrical considerations give then the yield deformation and natural period of the equivalent system. The yield force F_y^* , which is to be considered as the yield force for both the modelled and idealized system, represents the base shear force at the formation of the first mechanism.

$$d_y^* = 2 \times \left(d_m^* - \frac{E_m^*}{F_y^*} \right) \quad (2.12)$$

$$T^* = 2 \times \pi \times \sqrt{\frac{m^* \times d_y^*}{F_y^*}} \quad (2.13)$$

¹EN 1998-1, Appendix B gives guidelines for the determination of the target displacement. Note that the *assumed* target displacement is set equal to the displacement at the formation of the first mechanism.

According to EN 1998-1, Appendix B.5, the target displacement depends on whether the response is elastic or inelastic. For short periods, i.e.

$$T^* \leq T_c \quad (2.14)$$

the response is elastic if

$$\frac{F_y^*}{m^*} \geq S_e(T^*) \quad (2.15)$$

and the target displacement can be calculated as

$$d_t^* = d_{et}^* \quad (2.16)$$

where

$$d_{et}^* = S_e(T^*) \times \left(\frac{T^*}{2 \times \pi} \right)^2 \quad (2.17)$$

The response is inelastic if

$$\frac{F_y^*}{m^*} \leq S_e(T^*) \quad (2.18)$$

and the target displacement can be calculated as

$$d_t^* = \frac{d_{et}^*}{q_u} \times \left(1 + (q_u - 1) \times \frac{T_c}{T^*} \right) \quad (2.19)$$

where

$$q_u = \frac{S_e(T^*) \times m^*}{F_y^*} \quad (2.20)$$

For long periods, i.e.

$$T^* \geq T_c \quad (2.21)$$

the target displacement can be calculated according to Equation 2.16. As an initiation, the target displacement must first be assumed. If the calculated target displacement d_t^* differs significantly from the assumed, an iteration process should be performed. The target displacement d_t of the MDOF-system, i.e. the real system, is given as

$$d_t = \Gamma \times d_t^* \quad (2.22)$$

Disadvantages

Due to the static nature of the method, the most obvious disadvantage is that viscous damping and duration effects are completely overlooked [13]. When a structure is exposed to hysteric motions such as those during an earthquake, material properties are likely to change if the elements deform past the elastic range. For well-detailed RC structures, stiffness degradation is to be expected. For poorly detailed RC structures both stiffness and strength degradation can occur [14]. These effects cannot be captured due to the static nature of the method [13]. Perhaps the most valid concern with regards to utilizing this method in

performance-based seismic design, is the lack of predictions of the behaviour after the first mechanism is formed. As the structure begins to yield and form plastic hinges, the modal properties will change. Hence, the method will not expose weaknesses that will occur when the structure responds into the inelastic range. The static non-linear analysis is based on the assumption that the response of a structure can be based on an equivalent SDOF-system. This implies that the response is governed by a single mode shape. Hence, the method is sufficiently accurate for structures that are dominated by one mode. There have been developed methods for combining several mode shapes, e.g. modal pushover analysis [8]. However, this method lacks a rigorous theoretical background and is reasonable only when modes are weakly coupled [8]. Moreover, the argument of simplicity somewhat diminishes when several mode shapes are utilized.

For inelastic response, EN 1998-1, Appendix B gives the target displacement as

$$d_t^* = A \times S_e(T^*) \times \left(\frac{T^*}{2 \times \pi} \right)^2 \quad (2.23)$$

Here, A is an empirical factor that accounts for non-linear behaviour due to the fact that the response spectrum is based on a linear system. Ergo, the calculated target displacement is inaccurate.

2.2.3 Non-linear time history analysis

Background

The non-linear time-history analysis (NTHA) is the most accurate analytical method. However, it is also time consuming and complicated. The method should be applied when the structure is expected to deform into the inelastic range of response and the contribution from more than one mode is of significance. NTHA is also the only valid option when the structural behaviour after the first mechanism is of interest. For the retrofit of buildings, especially for old, poorly detailed ones where strength and stiffness degradation is of importance, the application of the NTHA becomes well-argued.

Basis of the procedure

As for the non-linear static analysis, the basis for the procedure is a mathematical model that directly incorporates the non-linearity of materials. In addition, the representation of materials must include the material response to hysteric loading. The numerical model is subjected directly to an earthquake loading represented by a ground motion history [6]. Since the mathematical model directly accounts for the non-linear behaviour of materials, the calculated internal forces and displacements will be reasonable estimates of those expected during the considered earthquake.

Ground motions

Calculated response is highly sensitive to the characteristics of the ground motion history [8]. Therefore, several ground motions must be applied. EN 1998-1 [1], section 4.3.3.4.3 states that if at least seven time histories are applied, the average response parameter can be utilised in design. If only three are applied, the most unfavourable response values must be used. The selection of individual time-histories must be aimed representable for the site in question. Parameters such as peak ground acceleration and velocity, fault distance, shear wave velocity and ground type should be reasonably consistent throughout the different time-history records. Once the ground motions are chosen, they are manipulated either by *scaling*, *spectrum matching* or both. *Scaling* is a process where the individual recordings are scaled to match a single period or create a "best fit" to a range of periods. *Spectrum matching* implies that the the frequency content of records is manipulated to fit the elastic design spectrum in the governing design code [15]. To this day, there is no agreement amongst experts on which approach is preferable for the non-linear time history analysis as there is pros and cons for both methods. Also, alternative approaches have been suggested. The reader is referred to the literature for further insight on the topic [15].

Disadvantages

Opposed to e.g. wind-engineering where the analyst usually has access to vast and solid statistical data, records of large ground motions are a rarity. Therefore, the design must be based on actual recordings rather than statistically founded predicaments. The number of individual time-history recordings that match the criteria is often inadequate to represent the true variety in earthquake ground motions. As previously mentioned, the main arguments against this method is the complexity and time consumption. Firstly, the evaluation prior to the actual analysis is not straightforward. Secondly, the analysis itself can be quite time consuming due to limited computational capacity. Also, NTHA does not give a clear image of the stiffness, strength and ductility of the structure. Therefore, NTHA is often supplemented with NSA in research.

2.3 Distributed inelasticity element-formulation

2.3.1 General scheme

In the early days of finite element applications in seismic design, non-linearity was accounted for using *lumped* inelasticity elements, commonly known as plastic-hinge elements. It is evident throughout the literature that these elements have limitations that are not effortless to overcome. The main issue is the determination of the plastic hinge length that depends on level of axial loading, moment gradient, the value of shear stress in the plastic hinge region, the amount of reinforcement, concrete strength, level of confinement and ground motion characteristics [16]. Due to the substantial improvement and easy access to computational tools over the last decades, the adaptation of *distributed* inelasticity elements is becoming the standard. The advantage is implied in the description, i.e. inelasticity can be spread

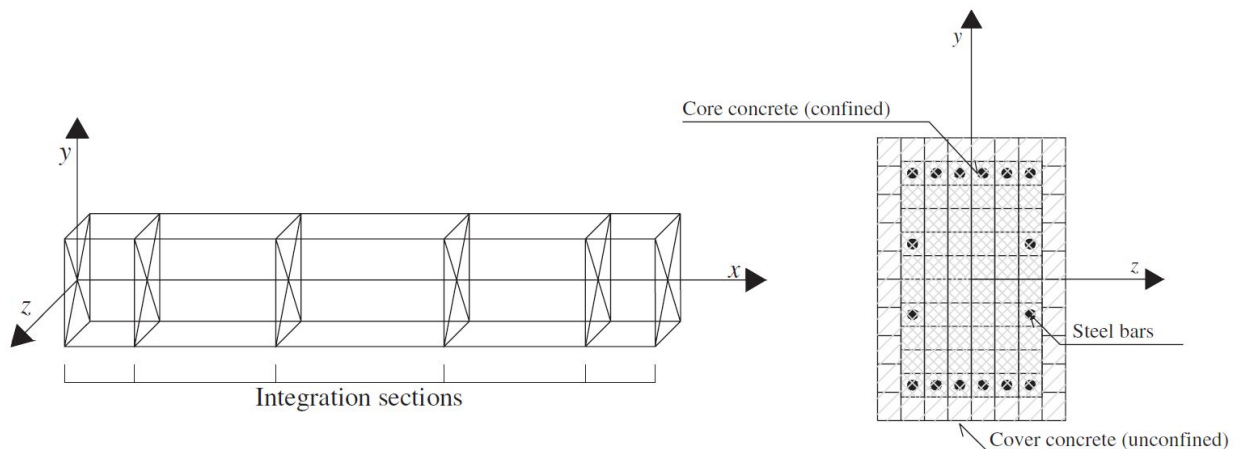


Figure 2.2: Distributed inelasticity fibre-element. Illustration: Calabrese, A, Almeida, J.P and Pinho, R.

throughout the length of an element and is not restricted to a prescribed length at the ends. The inelasticity is assessed by integrating the element at pre-defined control sections, or points. This is illustrated on the left hand side of Figure 2.2. The number of integration points (IPs) may depend on the problem at hand [16, 2], but the SeismoStruct [2] manual recommends between 4 and 7 IPs. The location and weight of each IP is most commonly defined through the Gauss-Lobatto quadrature rule². Locally, non-linearity is accounted for by including fibre models. The cross section is defined by a user-specified number of fibres, where each fibre is assigned a material model. This allows for cross sections with multiple material properties, e.g. confined reinforced concrete. See right hand side of Figure 2.2. The number of fibres depend on the shape and material of the cross section. A reasonable approach is to apply approximately 100 fibres for single-material sections and 200 fibres for more complicated sections where high levels of inelasticity are expected [2].

2.3.2 Finite element formulation

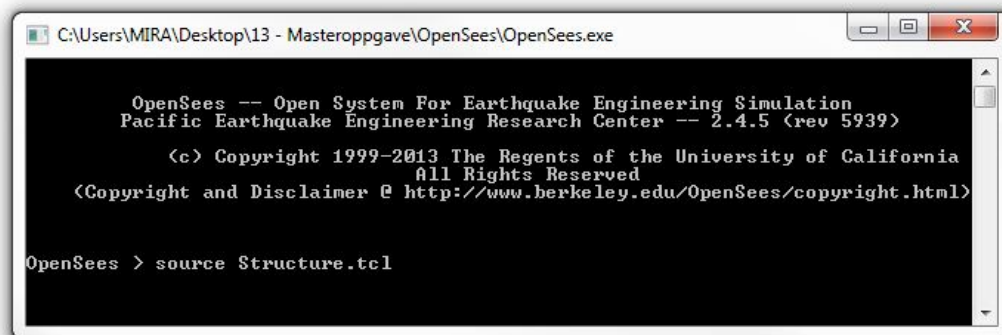
The distributed inelasticity elements are formulated based on two different approaches. The first is the displacement-based formulation (DB), which is the textbook finite element formulation. The element is imposed with a displacement field and the governing equations are solved based on the stiffness. In the assessment of seismic problems, or any non-linear problem for that matter, such formulations are not ideal. Imposing displacement fields when the response is non-linear may produce spurious results for coarsely meshed models [16]. The other is the force-based formulation (FB), where instead of displacement fields, force and moment field variations are imposed. The governing equations are solved based on flexibility. The FB-formulation is "exact" in the sense that it does not restrict the displacement field and thus allows for non-linear behaviour. The only approximation is the discrete number of

²The Gauss-Lobatto rule places one IP point at each element end. The minimum number of IPs is therefore 3 [17].

IPs. The main advantage with the FB-formulation is that, theoretically, only one element is necessary for each structural member due to fact that the force field is always exact [16].

2.4 OpenSees

Open System for Earthquake Engineering Simulation (OpenSees) is a open source software framework created for the assessment of structural response caused by seismic loading. It is developed at the Pacific Earthquake Engineering Research Center (PEER) by Frank McKenna and Gregory L. Fenves. The framework itself is an *interpreter* of the programming language Tcl in combination with unique commands incorporating the finite element method and earthquake engineering. Since it is a non-commercialized application created for academic purposes, it lacks a graphical interface. The users creates scripts which are sourced by the framework. See Figure 2.3. The application differs from commercialized softwares in the sense that the user manually creates every step throughout the assessment of analytical procedures. First-time usage is therefore a laborious process, but once that threshold is crossed, the framework allows for vast opportunities in terms of finite element applications.



```
C:\Users\MIRA\Desktop\13 - Masteroppgave\OpenSees\OpenSees.exe

OpenSees -- Open System For Earthquake Engineering Simulation
Pacific Earthquake Engineering Research Center -- 2.4.5 (rev 5939)

(c) Copyright 1999-2013 The Regents of the University of California
All Rights Reserved
(Copyright and Disclaimer @ http://www.berkeley.edu/OpenSees/copyright.html)

OpenSees > source Structure.tcl
```

```
1 # Define time series
2 set Scalefactor 1;timeSeries Path 992 -dt 0.005 -filePath JC_scaled.txt -factor $Scalefactor;
3 # Apply time series
4 pattern UniformExcitation 2 1 -accel 992;
5 # Define damping
6 set alphaM 0.83775733;set betaK 0.00169765;set betaKinit 0.00;set betaKcomm 0.00;
7 rayleigh $alphaM $betaK $betaKinit $betaKcomm;wipeAnalysis;
8 # Analysis
9 constraints Plain;numberer RCM;system UmfPack;test NormDispIncr 1.0e-3 200;algorithm Linear;
10 # Hilber-Hughes-Taylor Method
11 set HHTalpha 0.9;
12 integrator HHT $HHTalpha;
13 analysis Transient;
14 set NTHA [analyze 10015 0.01];
15 if {$NTHA == 0} {puts "All steps have converged. Non-linear time history analysis OK."}
16 if {$NTHA != 0} {puts "Convergence issues. Non-linear time history analysis not OK."}
```

Figure 2.3: OpenSees interface and an example of a Tcl-script for the assessment of a dynamic time-history analysis.

Chapter 3

Design

3.1 Basis

3.1.1 General

The example structure is a RC residential building situated in southern Europe. It withstands lateral forces through frames and shear walls. The structure is designed for high ductility (DCH), and the design is performed in collaboration with Nina Øystad-Larsen. The geometry is shown in Figure 3.1. The design is performed according to EN 1990 [18], EN 1992-1-1 [19], EN 1998-1 [1] and EN 1998-3 [9]. However, the design for gravity loads is performed according to NS-EN 1992-1-1:NA 2008 due to the fact that the programs at hand performed verifications according to the Norwegian Annex. For simplicity, the materials were also determined according to NS-EN 1992-1-1:NA 2008. Throughout this chapter, only general equations and the results are presented. Simple calculations are shown in Appendix A and extensive procedures are performed in Matlab [20].

3.1.2 Materials

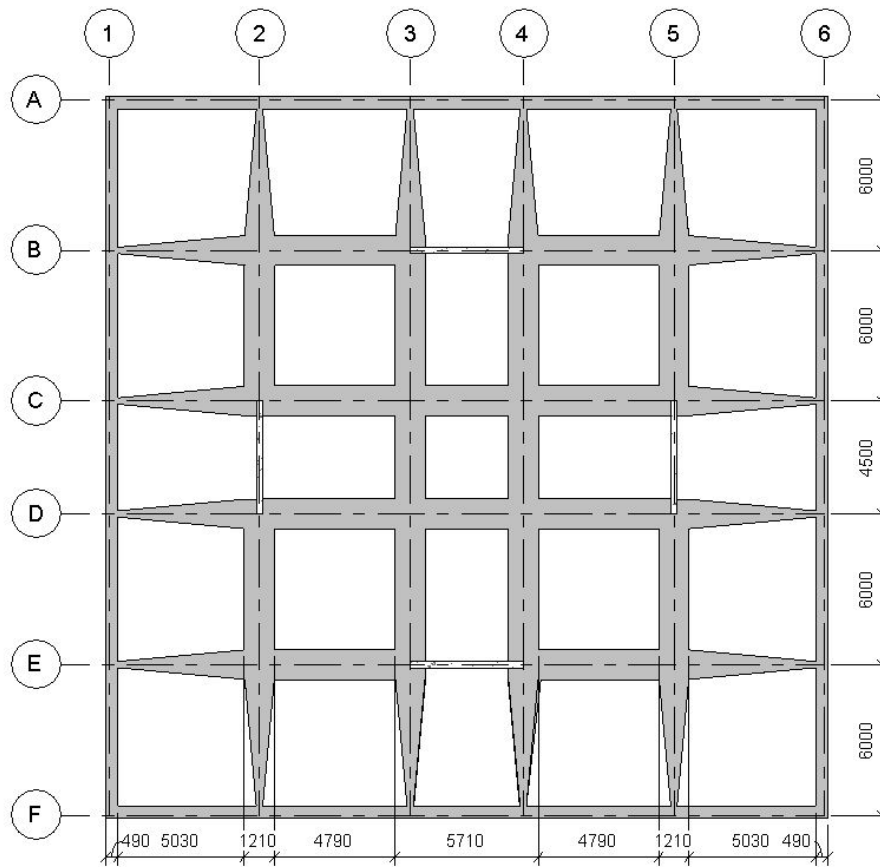
The concrete elements belong to XC3/M60. The elements are built in concrete class B25 with 25+/-10 mm cover. The reinforcement is B500NC.

3.1.3 Loads

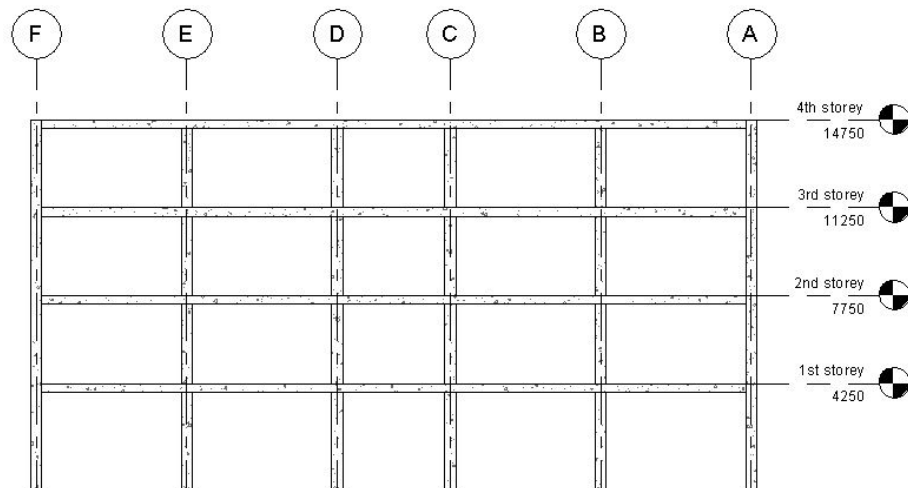
The slab thickness is assumed to be 120 mm. The density of the reinforced concrete is 25 kN/m³. Additional dead load is assumed to be 0.5 kN/m². This gives dead load $Q_D = 3.5$ kN/m². According to EN 1998-3 [9], live load $Q_L = 2.0$ kN/m² and snow load $Q_S = 0.0$ kN/m². Load combinations are set according to EN 1998-1 [1], section 3.2.4, i.e.,

$$Q_G = \sum G_{k,j} + \sum (\Phi \times \Psi_{2,i} \times Q_{k,i}) \quad (3.1)$$

Here, Q_G is the gravity load, $G_{k,j}$ are the dead loads, Φ is a reduction factor that takes into account simultaneous use of separate stories, $\Psi_{2,i}$ considers the permanent part of the



(a) Plan view including the effective beam flanges.



(b) Vertical projection of the structure.

Figure 3.1: Geometry of the structure.

variable load and $Q_{k,i}$ is the live load. The distributed gravity loads in accordance with Equation 3.1 are $Q_{G, \text{Roof}} = 3.5 \text{ kN/m}^2$ and $Q_{G, \text{Story}} = 4.0 \text{ kN/m}^2$.

3.2 Design for gravity loads

3.2.1 Slab

The maximum span is $6.0 \times 6.0 \text{ m}$. For simplicity, and due to the symmetry of the structure, the two-way slab is calculated as an one-way slab carrying 70 % of the total load, i.e. $Q_D = 2.5 \text{ kN/m}^2$ and $Q_L = 1.4 \text{ kN/m}^2$. The design is performed in G-Prog [21]. The result is a 120 mm slab with $\varphi c150$ as both top and bottom reinforcement.

3.2.2 Beams

Design load

For simplicity, only two types of beams are considered; beams at the border of the slab and interior beams. According to EN 1990 [18], table A1.2, the load combinations are given as

$$Q_{Ed} = [1.35 \times Q_D + 1.05 \times Q_L, 1.15 \times Q_L + 1.05 \times Q_L] \quad (3.2)$$

Combining Equation 3.2 with the results from Section 3.1.3, the distributed line loads become $q_{Ed, \text{bdr}} = 18.4 \text{ kN/m}$ and $q_{Ed, \text{bdr}} = 45.3 \text{ kN/m}$.

Effective flange

The effective beam flange, b_{eff} , is determined according to EN 1998-1 [1], section 5.5.3.1.1 and depends on the column width and slab thickness. The column width is assumed to be 250 mm. EN 1998-1 does not clearly define border and interior columns. It is therefore assumed that all the columns along the structure boundary are defined as border columns, and all other columns are defined as interior columns. It is also assumed that the height of the interior beam is larger than the height of the border beam. For the border beam connected to the border column, $b_{\text{eff}} = 490 \text{ mm}$. For the interior beam connected to the border column, $b_{\text{eff}} = 250 \text{ mm}$, since the transverse beams are border beams. For the interior beam connected to the interior column, $b_{\text{eff}} = 1210 \text{ mm}$. The effective flange is interpolated linearly between the joints, and the flange widths of the beams are illustrated in Figure 3.1a.

Dimensions

First, the beams are designed for gravitational loads. For simplicity, the addition of the effective flanges is neglected. By doing so, one has to be aware of that the moment diagram slightly changes as we now assume constant stiffness throughout the beams, and that the moment capacity where the beams connect to the interior columns is larger than assumed. The latter is of great importance when designing in accordance the the strong column-weak

beam principle. The beam design is performed in G-Prog [21] according to NS-EN 1992-1-1:NA2008 [19]. The load factor is set to 0.9-1.15 for dead loads and 0.0-1.5 for live loads. Full anchoring of both top and bottom reinforcement is assumed. At the border, the result is a 200×350 mm beam with $2\phi 20$ at both bottom and top, with stirrups $\phi 6c140$. For the interior beam, the result is a 250×400 mm beam with $2\phi 25$ at both bottom and top, with stirrups $\phi 10c100$.

Local detailing

According to the strong column-weak beam principle, plastic hinges should form at the end of the beams. To safeguard the ductility needed, EN 1998-1 demands special detailing within the critical area l_{cr} . According to EN 1998-1, section 5.5.3.1.3,

$$l_{cr} = 1.5 \times h_w \quad (3.3)$$

$$d_{bw} \geq 6\text{mm} \quad (3.4)$$

$$s = \min\{h_w/4; 24 \times d_{bw}; 6 \times d_{bL}\} \quad (3.5)$$

where h_w is the beam section height, d_{bw} is the stirrup diameter, d_{bL} is the minimum longitudinal bar diameter and s is the stirrup spacing. For the border beams, the stirrups must be increased to $\phi 6c85$ within the critical area. The characteristics of the two beams are presented in Table 3.1.

Table 3.1: Beam characteristics.

Beam	h_w (mm)	b (mm)	Top reinf.	Bottom reinf.	l_{cr} (mm)	Stirrups	Stirrups l_{cr}
Border	350	200	$2\phi 20$	$2\phi 20$	525	$\phi 6c85$	$\phi 6c140$
Interior	400	250	$2\phi 25$	$2\phi 25$	600	$\phi 10c100$	$\phi 10c100$

3.2.3 Columns

Design loads

The design will only differ between border and interior column. The diminution of axial forces throughout the stories will not be considered. This might seem highly conservative, but it will become evident in the following sections that the axial forces acting on the columns are not necessarily deterministic of the design. According to the results from the beam calculations, the largest axial force in the interior columns occur where axis 2 and 5 cross B and E, and the largest axial force in the border columns occur where axis 2 and 5 cross A and F. In accordance with the demands in EN 1990 [18], table A1.2, the column forces are $Q_{G,int} = 1032$ kN and $Q_{G,bdr} = 449$ kN. The buckling length is set to the entire column length.

Dimensions

The columns are design in BtSnitt [22] according to NS-EN 1992-1-1:NA2008 [19]. For the border column, the result is a 230×230 mm column with $8\phi 12$. For the interior column, the result is a 280×280 mm column with $8\phi 16$.

3.2.4 Desired formation of mechanism

Strong column-weak beam

An important principle of earthquake engineering is to ensure that plastic hinges form in the beams rather than in the columns. This is known as the strong column-weak beam principle. EN 1998-1 [1], section 4.4.2.3 demands that the sum of moment capacities of columns exceeds the sum of moment capacities of beams in a joint by a factor of 1.3, i.e.,

$$\sum M_{RC} \geq 1.3 \times \sum M_{RB} \quad (3.6)$$

Critical joints

The ratio demand does not apply for the beam-column joints at the roof level because there is only one column present at the these joints. For the interior columns, the most critical joints are the ones where two interior beams connect, i.e. the joints where axes 3 and 4 cross C and D, respectively. For the border columns, the critical joints are located where axes 1 and 6, cross B and E, respectively. At this joint, bending about axes B and E is most critical since the total moment capacity of two border beams exceeds the moment capacity of one interior beam. An illustration of the border joint is given Figure 3.2.

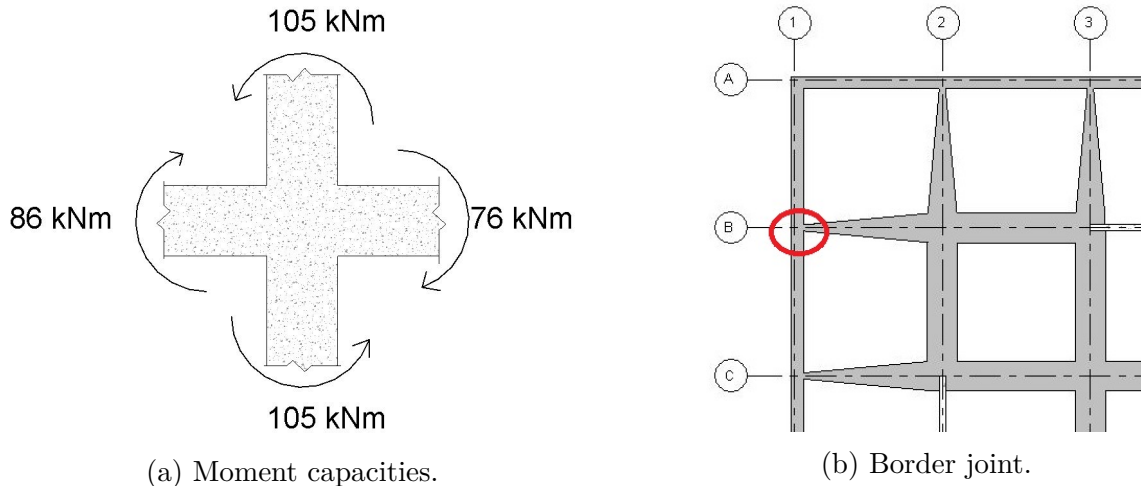
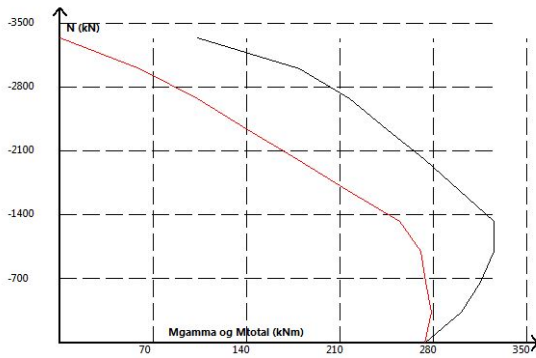


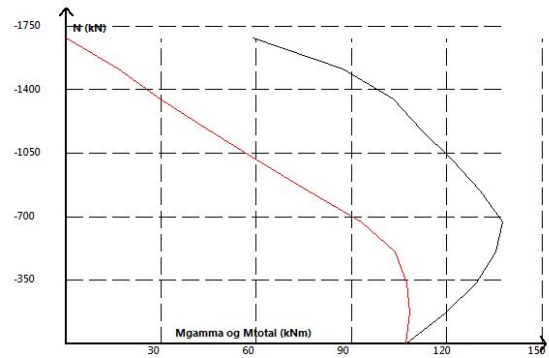
Figure 3.2: Illustration of the moment capacities at the border joint.

Moment capacity ratios

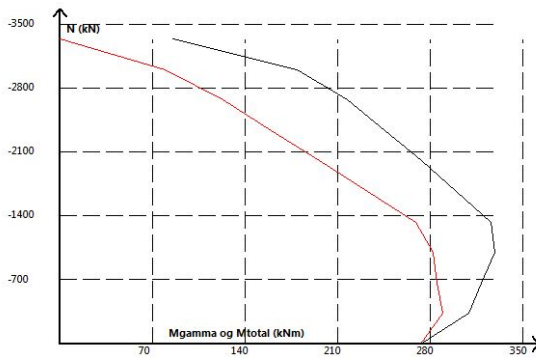
The moment capacities of columns are evaluated by using M/N-diagrams generated in BtSnitt [22]. The axial loads are calculated in the seismic design situation. The M/N-diagrams, together with the acting axial loads and corresponding moment capacities, are shown in Appendix A.3. Observe that 1st storey columns have separate M/N-diagrams due to different buckling lengths. As previously mentioned, it is important to include the effective beam flanges when considering the moment capacity of the beams. However, the results from G-Prog [21] show that the moment capacities of the border and interior beams, without the contribution from the effective flanges, are $M_{RB,bdr} = 72 \text{ kNm}$ and $M_{RB,int} = 168 \text{ kNm}$. Compared to the results in Appendix A.3, it becomes evident that the demand in EN 1998-1, section 4.4.2.3 is clearly not satisfied. Therefore, the interior columns are increased to $440 \times 440 \text{ mm}$ with $8\phi 25$ and the border columns are increased to $330 \times 330 \text{ mm}$ with $8\phi 20$ in all stories. The new M/N-diagrams of the columns are shown in Figure 3.3. The black curve illustrates the capacity when dead load and live load acting on the column are considered. The red curve illustrates the capacity when an additional moment due to minimum eccentricity is included. The acting axial loads with the corresponding moment capacities of the new columns are presented in Table 3.2.



(a) 1st storey 440 mm interior column.



(b) 1st storey 330 mm border column.



(c) 2nd, 3rd, 4th storey 440 mm interior column. (d) 2nd, 3rd, 4th 330 mm storey border column.

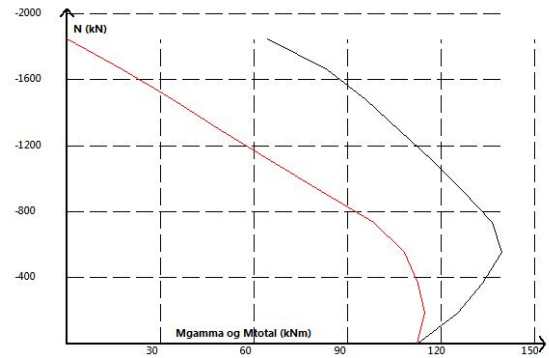


Figure 3.3: M/N-diagrams for the 440 mm interior and 330 border columns.

Table 3.2: Axial loads and moment capacities of the 440 mm and 330 mm columns.

Column	Storey	Axial force (kN)	M_{RC} (kNm)
Interior 440 × 440 mm	4th	153	280
	3rd	237	290
	2nd	500	285
	1st	675	270
Interior 330 × 330 mm	4th	69	110
	3rd	149	115
	2nd	228	110
	1st	307	105

Increase of effective flanges

The increase of column dimensions and reinforcement results in new effective flanges of the beams, which increases their the moment capacity. For the border beam connected to the border column, $b_{\text{eff}} = 570$ mm. For the interior connected to the border column, $b_{\text{eff}} = 330$ mm, since the transverse beams are border beams. For the interior beam connected to the interior column, $b_{\text{eff}} = 1400$ mm. The new moment capacities of the beams are checked in BtSnitt [22] and the results are shown in Table 3.3. The reinforcement of the slab is included. The new moment capacity ratios are presented in Table 3.4 which shows that the demand in EN 1998-1, section 4.4.2.3 is satisfied. The ratios might seem unnecessarily high, but it is expected that the seismic analysis, together with the various demands in EN 1998-1, will lead to increased moment capacities of the beams.

Table 3.3: Moment capacities of the beams.

Beam	$M_{RB,T}$ (kNm)	$M_{RB,B}$ (kNm)
Border beam	86	76
Interior beam, border column	125	128
Interior beam,interior column	182	141

Table 3.4: Moment capacity ratios.

Column	Story	$\sum M_{RC}$ (kNm)	$\sum M_{RB}$ (kNm)	$\sum M_{RC}/\sum M_{RB}$
Interior 440 × 440 mm	4th	-	-	-
	3rd	580	323	1.8
	2nd	570	323	1.8
	1st	540	323	1.7
Interior 330 × 330 mm	4th	-	-	-
	3rd	230	162	1.8
	2nd	220	162	1.8
	1st	210	162	1.7

Local detailing

As for the beams, EN 1998-1 demands special detailing within the critical area l_{cr} of the columns. According to EN 1998-1, section 5.5.3.2.2,

$$l_{cr} = \max\{1.5 \times h_c; l_{cl}/6; 0.6\} \quad (3.7)$$

$$d_{bw} \geq 0.4 \times d_{bL,max} \times \sqrt{\frac{f_{ydL}}{f_{ydw}}} \quad (3.8)$$

$$s = \min\{b_0/3; 125\text{mm}; 6 \times d_{bL}\} \quad (3.9)$$

where h_c is the largest cross-sectional dimension of the column, l_{cl} is the clear length of the column, d_{bw} is the diameter of the horizontal reinforcement, $d_{bL,max}$ is the diameter of the thickest longitudinal reinforcement, f_{ydL} is the design yield stress of thickest longitudinal reinforcement, f_{ydw} is the design yield stress of horizontal reinforcement, s is the stirrup spacing and b_0 is the minimum dimension of the concrete core. Between the critical areas, the maximum spacing of the stirrups is determined according to EN 1992-1-1 [19], section 9.5.3, i.e.

$$s_{cl,max} = \min\{b; 400\text{mm}; 20 \times d_{bL,max}\} \quad (3.10)$$

The column characteristics are shown in Table 3.5.

3.2.5 Walls

The wall is designed according to EN 1998-1 [1], section 5.5.1.2.3. The thickness,

$$b_{wo} \geq \max\{150; h_s/20\} \quad (3.11)$$

Table 3.5: Column characteristics.

Column	b (mm)	h (mm)	Vert. reinf.	l_{cr} (mm)	Stirrups	Stirrups l_{cr}
Interior	440	440	8 ϕ 25	660	ϕ 10c400	ϕ 10c125
Border	330	330	8 ϕ 20	645	ϕ 8c330	ϕ 8c120

where h_s is the maximum free storey height. For the 1st storey, $b_{wo,1st} = 220$ mm. For the other stories, $b_{wo, 2nd, 3rd, 4th} = 175$ mm. According to EN 1992-1-1 [19], section 9.6.2, $A_{s,min} = 440$ mm². By choosing ϕ 12c250 both horizontally and vertically, the demands in EN 1992-1-1 [19], section 9.6.2 and EN 1998-1, section 5.5.3.4.2 are satisfied. EN 1998-1, section 5.4.3.4.1, demands that the normalized axial force must be less than 0.35, i.e.,

$$v_d = \frac{N_{Ed}}{h_c \times b_c \times f_{cd}} \leq 0.35 \quad (3.12)$$

EN 1998-1 also demands special detailing within the critical length and height above the base. According to EN 1998-1, section 5.4.3.4.2, the critical height from the bottom wall,

$$h_{cr} = \max\{l_w; h_w/6\} \leq h_s \quad (3.13)$$

where l_w is the length, h_w is the total height and h_s is the clear height of the wall. For the 1st storey, $h_{cr,wall,1st} = 4$ 130 mm. The critical horizontal length,

$$l_c = x_u \times \left(1 - \frac{\varepsilon_{cu2}}{\varepsilon_{cu2,c}}\right) \geq \min\{0.15 \times I_w; 1.5 \times b_w\} \quad (3.14)$$

Here, x_u is the depth of the confined compression zone at ultimate curvature estimated from equilibrium for a constant width b_0 of the confined compression zone, i.e.,

$$x_u = \frac{(v_d + \omega_v) \times I_w \times b_c}{b_0} \quad (3.15)$$

and ω_v is the mechanical ratio of vertical web reinforcement in the boundary elements, i.e.

$$\omega_v = \frac{A_{sv} \times f_{yd,v}}{h_c \times b_0 \times f_{cd}} \quad (3.16)$$

where v_d is the normalized axial force, A_{sv} is the vertical web reinforcement, h_c is the largest dimension of the web, b_0 is the width of the core, ε_{cu2} is the compressive strain at which spalling is expected and $\varepsilon_{cu2,c}$ is ultimate strain of the confined concrete. According to EN 1998-1, section 5.4.3.4.2,

$$\varepsilon_{cu2,c} = 0.0035 + 0.1 \times \alpha \times \omega_{wd} \quad (3.17)$$

Here, α is the confinement effectiveness factor equal to $\alpha_n \times \alpha_s$, where α_n and α_s account for the loss of confined area in the horizontal and vertical plane, respectively. For a rectangular cross section,

$$\alpha_n = 1 - \sum_{i=1}^n \left(\frac{b_i}{6 \times b_0 \times h_0} \right) \quad (3.18)$$

$$\alpha_s = \left(1 - \frac{s}{2 \times b_0} \right) \times \left(1 - \frac{s}{2 \times h_0} \right) \quad (3.19)$$

where h_0 is height of the core and h_i is the distance between the longitudinal reinforcement. The mechanical volumetric ratio of stirrups in the critical area must be at least 0.12, i.e,

$$\omega_{wd} = \frac{V_s \times f_{yd}}{V_c \times f_{cd}} \geq 0.12 \quad (3.20)$$

Here, V_s is the volume of the stirrups and V_c is the volume of the concrete core in the boundary area. EN 1998-1, section 5.5.3.4.5, demands that

$$\alpha \times \omega_{wd} \geq 30 \times \mu_\varphi \times \nu_d \times \omega_v \times \varepsilon_{sy,d} \times \frac{b_c}{b_o} - 0.035 \quad (3.21)$$

EN 1998-1, section 5.5.3.4.5 also demands boundary areas for at least one storey above the first, with shear reinforcement equal to half of what is required in the 1st storey critical boundary. The aforementioned requirements are evaluated in Matlab [20], and the wall characteristics are presented in Table 3.6.

Table 3.6: Wall characteristics.

Story	b_c (mm)	b_{wo} (mm)	l_c (mm)	Vert. reinf.	Vert. reinf. l_c	Hor. reinf.	Stirrups l_c
3rd and 4th	-	175	-	$\varphi 12c250$	-	$\varphi 12c250$	-
2nd	300	175	675	$\varphi 12c250$	$\varphi 16c200$	$\varphi 12c250$	$\varphi 8c175$
1st	300	220	675	$\varphi 12c250$	$\varphi 16c100$	$\varphi 12c250$	$\varphi 8c90$

3.3 Analysis based on the linear static method

3.3.1 Q-factor

The lateral force method is explained in Section 2.2.1. According to EN 1998-1 [1], section 5.2.2.2,

$$q = q_0 \times k_w \quad (3.22)$$

Here, q_0 depends on the type of structural system and its regularity in elevation and k_w reflects the dominating mechanism in structural systems containing shear walls.

Structural system

The type of structural system is determined by evaluating the shear capacity of walls and columns in the 1st storey in accordance with EN 1998-1 [1], section 5.5.3.4.2 and EN 1992-1-1 [19], section 6.2.3, i.e

$$V_{Rd,c} = (A_{sw} \times z \times f_{ywd} \times \cot \vartheta) / s \quad (3.23)$$

$$V_{Rd,max} = (\alpha_{cw} \times b_w \times z \times v_1 \times f_{cd}) / (\cot \vartheta + \tan \vartheta) \quad (3.24)$$

$$v_1 = 0.6 \times \left(1 - \frac{f_k}{250} \right) \quad (3.25)$$

The shear capacities of columns are calculated in Matlab [20] and the results are shown Table 3.7. The total shear capacity, $V_{Rd,c,total} = \sum V_{Rd,c} = 2492$ kN. Equation 3.23 and Equation 3.24 also apply for walls. However, according to EN 1998-1, section 5.5.3.4.2, $\cot \vartheta = 1$ and $z = 0.8 \times l_w$ for walls. Since the shear reinforcement is different inside and outside the confined area, an equivalent spacing must be determined. The calculation is shown in Appendix A.5 and the result is $s_{eqv,\varphi12} = 182$ mm. The shear capacities of the 1st storey walls are calculated in the same manner as for the columns. The result is $V_{Rd,w} = 1\,426$ kN and $V_{Rd,w,total} = 2852$ kN. Since $V_{Rd,w,total} \geq V_{Rd,c,total}$, the system is wall-equivalent. This gives $q_0 = 5.4$. For the wall equivalent system,

$$k_w = \frac{1 + \alpha_0}{3} \geq 0.5 \quad (3.26)$$

Here, α_0 is the predominant height to length ratio, i.e.,

$$\alpha_0 = \frac{\sum h_{wi}}{\sum I_{wi}} \quad (3.27)$$

For the 1st storey walls, $\alpha_0 = 0.94$, $k_w = 0.65$ and $q = 3.51$.

Table 3.7: Shear capacities of columns.

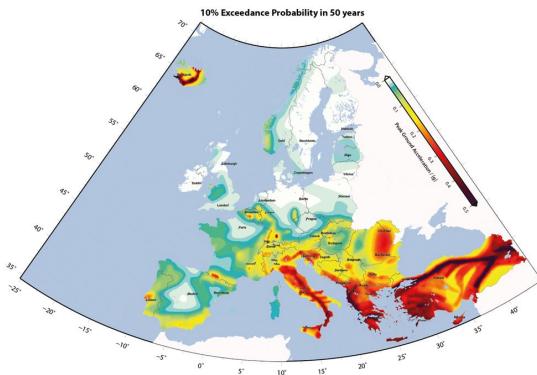
Column	V_{Rd} (kN)	$V_{Rd,max}$ (kN)	Number of columns	Total shear capacity (kN)
Interior	134	430	8	1072
Border	71	219	20	1420

3.3.2 Seismic loading

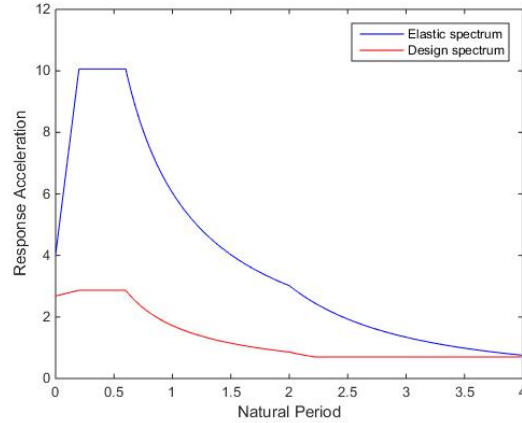
Response spectrum

PGA is set to 3.5 m/s^2 , which is representative for southern Europe according to SHARE [23]. See Figure 3.4a. Assuming ground type C and response spectrum Type 1, EN 1998-1

[1] gives the soil factor $S = 1.15$ and control periods $T_B = 0.2$, $T_C = 0.6$ and $T_D = 2.0$. The elastic and design response spectrum is determined according to EN 1998-1 [1], section 3.2.2.5 and it is shown in Figure 3.4b.



(a) European Seismic Hazard Map 2013 [23]



(b) Response spectrum.

Figure 3.4: Peak ground acceleration and response spectrum.

Seismic forces and displacements

The natural periods and storey displacements of the structure are calculated in Robot [24]. Dead and live loads acting in the seismic design situation are converted into equivalent masses. The stiffness is reduced by 50 % in all columns and beams on the account of cracking in the seismic situation. The first natural period is equal to 0.51 s, which gives

$$S_d(T_1) = \frac{3.5 \text{ m/s}^2 \times 1.15 \times 2.5}{3.51} = 2.87 \text{ m/s}^2 \quad (3.28)$$

The structure mass is lumped in the stories. The mass calculations are performed in Matlab [20] and the result is $m_{\text{roof}} = 370\,550 \text{ kg}$, $m_{3\text{rd}} = 383\,580 \text{ kg}$, $m_{2\text{nd}} = 383\,580 \text{ kg}$ and $m_{1\text{st}} = 386\,370 \text{ kg}$. The total mass of the structure $m_{\text{total}} = 1\,524\,100 \text{ kg}$. The base shear force F_b is determined according Equation 2.5 and is equal to 3 718 kN. The vertical force distribution is determined according to Equation 2.6 and presented in Table 3.8. Since the displacements are calculated by an elastic model, the actual displacements are obtained by multiplying the values with $q = 3.51$. The results are shown in Table 3.8.

P- δ -effects

According to EN 1998-1 [1], section 4.4.2.2, P- δ -effects need to be considered by evaluating the sensitivity factor which must be less than 0.10, i.e.,

$$\vartheta = \frac{P_{\text{total}} \times d_r}{V_{\text{total}} \times h} \leq 0.10 \quad (3.29)$$

Table 3.8: Storey forces and displacements.

Storey	Vertical force (kN)	Displacements form Robot (mm)	Actual displacements (mm)
4th	1 412	24	84
3rd	1 115	16	56
2nd	768	9	32
4th	424	3	11

Here, P_{total} is the total gravitational load over and above the storey in question, d_r is the relative displacement between the stories, V_{total} is the total seismic shear in the respective storey and h is the storey height. Table 3.9 presents the sensitivity factors. Since ϑ is less than 0.10 for all stories, the P - δ effects can be neglected.

Table 3.9: P - δ effect factor ϑ .

Storey	P_{total} (kN)	d_r (mm)	V_{total} (kN)	h (mm)	ϑ
4	2 843	28	1 412	3 500	0.02
3	6 092	24	2 527	3 500	0.02
2	9 341	21	3 295	3 500	0.02
1	12 590	11	3 718	4 250	0.01

Accidental torsion

Accidental torsion effects are determined according to Equation 2.7. The distance between the two horizontal force-resisting elements that are the farthest from each other, L_e , is equal to 28.5 m. For axes 1, 6, A and F, $\delta = 1.600$. For axes 2, 5, B and E, $\delta = 1.347$. For axes 3, 4, C and D, $\delta = 1.094$.

3.3.3 Check of the beams

Ductility demands

EN 1998-1 [1] demands sufficient local ductility in potential plastic regions. According to EN 1998-1, section 5.2.3.4, the demand is met if at least half of the reinforcement in the tension zone is placed in the compression zone (in addition to the reinforcement needed in

the seismic design situation) and if the reinforcement ratio ρ in the tension zone does not exceed the maximum value

$$\rho_{\max} = \rho' + \frac{0.0018 \times f_{cd}}{\mu_{\varphi} \times f_{yd}} \quad (3.30)$$

Here, ρ is the maximum normalized reinforcement ratio of the tension zone when the reinforcement from the slab is included, ρ' is the reinforcement ratio in the compression zone and μ_{φ} is the curvature ductility.

$$\mu_{\varphi} = 1 + 2 \times (q_0 - 1) \times \frac{T_c}{T_1} \quad (3.31)$$

For the structure in question, $\mu_{\varphi} = 11.35$. The calculation of ρ and ρ_{\max} is given in Appendix A.6 and the results are presented in Table 3.10. The ductility demand is not met for the interior beam connecting to the interior column. Therefore, the bottom reinforcement of the interior beams is increased to $3\phi 25$. The new calculation of ρ and ρ_{\max} is given in Appendix A.6 and the results are presented in Table 3.11. The demands are met for all beam sections.

Table 3.10: Ductility demands for beams without additional reinforcement.

Beam	ρ	ρ_{\max}	ρ/ρ_{\max}	A_s (mm ²)	A_s' (mm ²)	A_s'/A_s
Border	0.0134	0.0134	1.00	785	628	0.8
Interior beam, border column	0.0116	0.0147	0.82	982	982	1
Interior beam, interior column	0.0172	0.0147	1.22	1 453	982	0.68

Table 3.11: Ductility demands for beams with additional reinforcement.

Beam	ρ	ρ_{\max}	ρ/ρ_{\max}	A_s (mm ²)	A_s' (mm ²)	A_s'/A_s
Border	0.0134	0.0134	1.00	785	628	0.8
Interior beam, border column	0.0116	0.020	0.58	982	1 472	1.5
Interior beam, interior column	0.0172	0.020	0.86	1 453	1 472	1.01

Moment capacities

Since the interior beams now have additional reinforcement, their moment capacities are increased. The calculations are performed in BtSnitt [22] and the results are presented in Table 3.12. The acting moments in the seismic design situation are calculated in Robot [24] and the moment diagram is presented Figure A.2. These values have to be multiplied with the respective δ -values due to accidental torsion. For the border beams, the maximum acting moments are $M_{Ed,Top} = 118$ kNm and $M_{Ed,Bottom} = 50$ kNm. The capacity is not sufficient, so reinforcement in the border beam is increased to $2\phi 25$ at both top and bottom. For the interior beams connected to the border columns, the maximum acting moments are $M_{Ed,Top} = 164$ kNm and $M_{Ed,Bottom} = 101$ kNm. The capacity is not sufficient, so the reinforcement in the interior beams is increased to $2\phi 32$ at the top and $3\phi 32$ at the bottom. For the interior beams connected to the interior columns, the maximum acting moments are $M_{Ed,Top} = 269$ kNm and $M_{Ed,Bottom} = 144$ kNm. Even if the interior beams now have $2\phi 32$ at the top and $3\phi 32$ at the bottom, there is still not sufficient capacity. The reinforcement is therefore increased to $3\phi 32$ at both top and bottom. The moment capacities of all three cross sections are checked in BtSnitt [22]. The results, together with the acting design moments, are presented in Table 3.13, which shows that the beams have sufficient moment capacities.

Table 3.12: Moment capacities of the beams with additional reinforcement.

Beam	$M_{RB,T}$ (kNm)	$M_{RB,B}$ (kNm)
Border beam	86	76
Interior beam, border column	125	182
Interior beam, interior column	182	206

Table 3.13: Final moment capacities of beams.

Beam	$M_{RB,Top}$ (kNm)	$M_{RB,Bot}$ (kNm)	$M_{Ed,Top}$ (kNm)	$M_{Ed,Bot}$ (kNm)
Border beam	120	114	118	50
Interior beam, border column	290	304	164	101
Interior beam, interior column	336	336	269	144

Ductility demands for beams designed for seismic loads

Since the reinforcement is increased for both beams, the ductility demand in EN 1998-1, section 5.2.3.4 must be checked once more. The calculations are shown in Appendix A.6. The results are given in Table 3.14 and show that the demands are satisfied. The final beam characteristics are shown in Table 3.18. Note that the interior beams have additional 2 ϕ 12 at the bottom.

Table 3.14: Ductility demands for beams designed for the seismic situation.

Beam	ρ	ρ_{\max}	ρ/ρ_{\max}	A_s (mm ²)	A_s' (mm ²)	A_s'/A_s
Border	0.0194	0.0198	0.98	1 184	982	0.83
Interior beam, border column	0.0286	0.0343	0.83	2 413	2 639	1.09
Interior beam, interior column	0.0341	0.0343	0.99	2 844	2 639	0.93

Shear capacities of beams designed for seismic loads

The shear capacities of the beams are checked according to EN 1998-1, section 5.4.2.2, which states that in addition to any gravitational loading, end moments $M_{i,d}$ must be added when evaluating the shear force.

$$M_{i,d} = \gamma_{Rd} \times M_{RB,i} \times \min\{1, \sum M_{RC} / \sum M_{RB}\} \quad (3.32)$$

Here, γ_{Rd} is a factor that safeguards the over-strength due to steel hardening (for DCH, $\gamma_{Rd} = 1.2$), $M_{RB,i}$ is the design moment at the end i of the beam and $\sum M_{RC} / \sum M_{RB}$ is the moment capacity ratio. According to EN 1998-1, section 5.5.3.1.2, the shear capacity must be calculated according to EN 1992-1-1 [19] when the ratio

$$\zeta = V_{Ed,\min} / V_{Ed,\max} \geq -0.5 \quad (3.33)$$

The calculation of the shear capacities is given in Appendix A.7. The results are presented in Table 3.15, which shows sufficient shear capacities for both beams.

3.3.4 Check of the columns

Increase of moment capacity

The increase in the moment capacity of beams also affects the column design due to the strong column-weak beam principle. The results in Table 3.2 and Table 3.13 clearly show that the demand regarding the strong column-weak beam principle in EN 1998-1 [1], section

Table 3.15: Shear capacities of beams in accordance with EN 1998-1

	Beam	$V_{Rd,b}$ (kN)	$V_{Rd,max}$ (kN)
Inside critical length l_{cr}	Border	86	267
	Interior	232	307
Outside critical length l_{cr}	Border	130	185
	Interior	302	296

Table 3.16: Axial loads and moment capacities of columns in the seismic design situation.

Column	Storey	Axial force (kN)	M_{RC} (kNm)
Interior 440×440 mm columns with $12\phi 32$	4th	153	595
	3rd	237	580
	2nd	500	570
	1st	675	560
Border 330×330 mm columns with $8\phi 25$	4th	69	165
	3rd	149	165
	2nd	228	160
	1st	307	150

4.4.2.3, is not satisfied. Therefore, the reinforcement in the interior column is increased to $12\phi 32$. EN 1992-1-1 [19], section 8.2, states that the free distance between parallel bars,

$$S_{\min} \geq \max\{k_1 \times \phi_{\max}; d_g + k_2; 20\text{mm}\} \quad (3.34)$$

Here, $k_1 = 1$, d_g is the largest aggregate size (assumed 16 mm) and $k_2 = 5$ mm. This gives $S_{\min} = 32$ mm. For the interior column, $S = 62$ mm. Thus, the demand is satisfied. The reinforcement in the border column is increased to $8\phi 25$, which also satisfies the Equation 3.34. Figure 3.5 shows the MN-diagrams of the new columns, Table 3.16 shows the moment capacities and Table 3.17 shows that the ratio demand is satisfied for both columns.

Normalized axial force

EN 1998-1, section 5.4.3.2.1 requires that the normalized axial force v_d is equal or less than 0.55. For the border column, $v_d = 0.17$. For the interior column, $v_d = 0.21$. Thus, the demand is satisfied for both columns.

Ductility demands

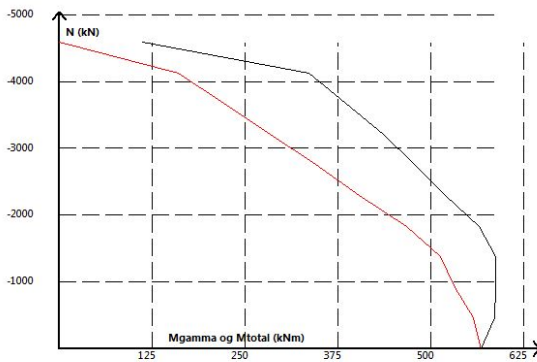
According to EN 1998-1, section 5.4.3.2.2, ductility is ensured if

$$\alpha \times \omega_{wd} \geq 30 \times \mu_\varphi \times v_d \times \varepsilon_{sy,d} \times \frac{b_c}{b_0} - 0.035 \quad (3.35)$$

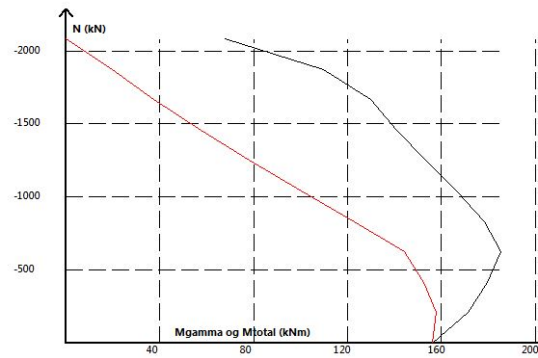
Here, ω_{wd} is the mechanical volumetric ratio between the stirrups in the critical areal, i.e.

$$\omega_{wd} = \frac{V_{stirrup} \times f_{yd}}{V_{core} \times f_{cd}} \quad (3.36)$$

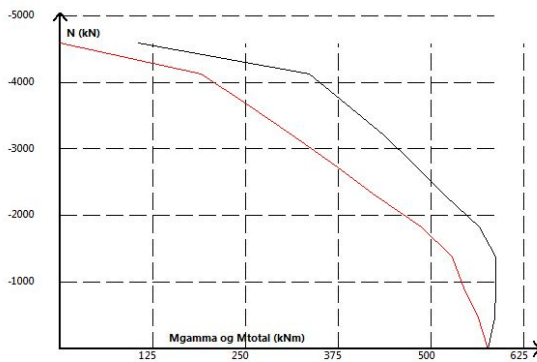
The calculations are performed in Matlab [20]. For the border column, $\alpha \times \omega_{wd} = 0.38$ and the right hand side of Equation 3.35 is equal to 0.19. For the interior column, $\alpha \times \omega_{wd} =$



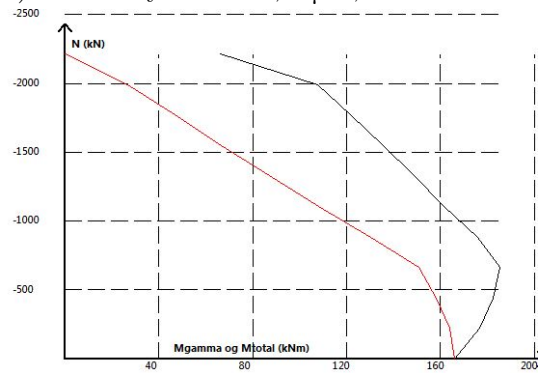
(a) 1st storey 440 mm, 12φ32, interior columns.



(b) 1st storey 330 mm, 8φ25, border columns.



(c) 2nd, 3rd and 4th storey 440 mm, 12φ32, interior columns.



(d) 2nd, 3rd and 4th storey 330 mm, 8φ25, border columns.

Figure 3.5: M/N-diagrams in the seismic design situation.

Table 3.17: Moment capacity ratios in the seismic design situation.

Column	Story	$\sum M_{RC}$ (kNm)	$\sum M_{RB}$ (kNm)	$\sum M_{RC}/\sum M_{RB}$
Interior 440 × 440 mm columns with 12 ϕ 32	4th	-	-	-
	3rd	1 160	672	1.7
	2nd	1 140	672	1.7
	1st	1 120	672	1.7
Border 330 × 330 mm columns with 8 ϕ 25	4th	-	-	-
	3rd	330	234	1.4
	2nd	320	234	1.4
	1st	300	234	1.3

0.22 and the right hand side of Equation 3.35 is equal to 0.16. The demand is satisfied for both columns.

Moment capacities of columns designed for seismic loads

The moment diagram from the the seismic design situation (Figure A.2) shows that the moments acting on columns are substantially lower than the respective capacities, thus no further evaluation is necessary.

Shear capacities of columns designed for seismic loads

The design shear force is determined according to EN 1998-1, section 5.5.2.2, which states that the acting shear force should be determined from end moments,

$$M_{i,d} = \gamma_{Rd} \times M_{RB,i} \times \min\{1, \sum M_{RB}/\sum M_{RC}\} \quad (3.37)$$

For the interior columns, $M_{bottom,d} = 437$ kNm, $M_{top,d} = 774$ kNm and $V_{Ed} = 346$ kN along the entire column. The shear capacities are calculated in Matlab [20]. The result is $V_{Rd} = 131$ kN, which clearly is not sufficient. Therefore, the shear reinforcement outside the critical boundary must be increased. Since the longitudinal reinforcement is now increased, d_{bw} must be larger or equal to 0.4×32 mm = 12.8 mm inside the critical boundary. Thus, the shear reinforcement is increased to $\phi 16c125$ within the critical boundary and $\phi 16c250$ outside the critical boundary. This gives $V_{Rd} = 370$ kN for interior columns. The border columns are evaluated in the same manner. $M_{bottom,d} = 152$ kNm, $M_{top,d} = 215$ kNm and $V_{Ed} = 105$ kN. The shear capacity V_{Rd} is equal to 69 kN. The longitudinal reinforcement

was also increased in the border columns. Hence, d_{bw} must be larger or equal to 0.4×25 mm = 10 mm inside the critical boundary. The shear reinforcement in the border column is therefore increased to $\phi 10c120$ inside the critical boundary and $\phi 10c330$ outside the critical boundary. This gives $V_{Rd} = 106$ kN for border columns. The shear capacity is sufficient for both columns and the final column characteristics are given in Table 3.19.

3.3.5 Check of the walls

The base shear force in the seismic design situation is calculated in Robot [1]. The shear force in the first storey wall, V_{Ed}' , is equal to 1 770 kN. Increase due to accidental torsion must be considered. Since there are no distributed forces along the wall height, the design moment M_{Ed} is calculated considering storey forces, i.e.,

$$M_{Ed} = 415 \text{ kN} \times 14.75 \text{ m} + 602 \text{ kN} \times 11.25 \text{ m} + 441 \text{ kN} \times 7 \text{ m} + 312 \text{ kN} \times 3.5 \text{ m} = 23\,758 \text{ kNm} \quad (3.38)$$

The wall is checked is BtSnitt [22] and does not have sufficient capacity. Therefore, the vertical reinforcement within the critical boundary is increased to $\phi 32c90$ and the vertical reinforcement outside the critical boundary is increased to $\phi 16c250$. This gives $M_{Rd} = 26\,600$ kNm, thus satisfying the demand. According to EN 1998-1 [1], section 5.5.2.4.1, the design shear force in the walls,

$$V_{Ed} = V_{Ed}' \times \varepsilon \quad (3.39)$$

where V_{Ed}' is shear force obtained from the analysis and ε is an amplification factor that accounts for redistribution of forces and dynamic effects, i.e.,

$$\varepsilon = q \times \sqrt{\left(\frac{\gamma_{Rd} \times M_{Rd}}{q \times M_{Ed}}\right)^2 \times \left(\frac{S_e(T_c)}{S_e(T_1)}\right)^2} \leq q \quad (3.40)$$

Here, $\gamma_{Rd} = 1.2$. The reinforcement factor is calculated in Matlab and equal to 1.74. The design base shear force,

$$V_{Ed} = 1.347 \times 1.74 \times 1\,770 \text{ kN} = 4\,148 \text{ kN} \quad (3.41)$$

EN 1998-1, section 5.5.3.4.3 defines

$$\alpha = M_{Ed} / (V_{Ed} \times l_w) \quad (3.42)$$

EN 1998-1 [1], section 5.5.3.4.3 also states that if $\alpha \leq 2$, the shear capacity with regards to tensile failure should be calculated as

$$V_{Rd,c} + 0.75 \times \rho_h \times f_{yd,h} \times b_{wo} \times \alpha_s \times I_w \quad (3.43)$$

For the 1st storey wall, $\alpha_s = 1.27$. The capacity was calculated to be 1 426 kN in Section 3.3.1. Since V_{Ed} is equal to 4 148 kN, the shear demand is clearly not satisfied. Therefore, the wall width in the 1st storey is increased to 400 mm along the entire length, the horizontal

reinforcement is increased to $\phi 16c225$, the stirrups in the confined boundary are increased to $\phi 16c125$ and the quality of the concrete is increased to B45. Due to premature cracking, the vertical reinforcement between the boundary areas must also be increased to $\phi 16c225$. The result is $V_{Rd} = 4\,251$ kN, which satisfies the shear demand. The other demands in EN 1998-1, section 5.5.3.4.5 are also satisfied. The walls in the other stories are calculated in the same manner and the calculations are shown in Appendix A.8. The walls are also evaluated for the demands described in Section 3.2.5. The calculations are performed in Matlab [20] and the final wall characteristics are presented in Table 3.20.

3.3.6 Check of the structural system

Q-factor

Due to changes of both walls and columns, a check of the structural system must be performed. The type of structural system is determined first. The shear capacity of the walls at the base was calculated in Section 3.3.5, i.e. $V_{Rd,w,total} = 2 \times 4\,251$ kN = 8 502 kN. The shear capacity of columns was calculated in Section 3.3.4, i.e. $V_{Rd,col,total} = 106$ kN \times 20 + 370 kN \times 8 = 5080 kN. The system is still wall-equivalent and the q-factor remains the same, i.e. $q = 3.51$.

Dynamic properties

The finite element model in Robot is updated and a new modal analysis is performed. The first natural period $T_1 = 0.45$ s. The response spectrum given in Figure 3.4b shows that the acting seismic forces remain the same. The slight increase of mass is negligible for all practical purposes.

Check of the walls due to increased forces

Since the walls have larger stiffness properties than in the previous analysis, they will carry a slightly larger portion of the total seismic loads than initially calculated. The acting forces are calculated in Robot [24]. Note that these forces are increased in the same manner as in Section 3.3.5. The final shear and moment capacities, together with the acting forces, are presented in Table A.2.

P- δ -effects

The results from Robot [24] show that relative displacement decrease for the updated structural system. Further evaluation of the P- δ -effects is therefore not necessary.

3.4 Final element characteristics

Table 3.18: Final beam characteristics.

Beam	h_w (mm)	b (mm)	Top reinf.	Bot. reinf.	l_{cr} (mm)	Stirrups	Stirrups l_{cr}
Border	350	200	2 ϕ 25	2 ϕ 25	525	ϕ 6c85	ϕ 6c140
Bdr. beam, bdr. col.	400	250	3 ϕ 32	3 ϕ 32 + 2 ϕ 12	600	ϕ 10c100	ϕ 10c100
Int. beam, int. col.	400	250	3 ϕ 32	3 ϕ 32 + 2 ϕ 12	600	ϕ 10c100	ϕ 10c100

Table 3.19: Final column characteristics.

Column	b (mm)	h (mm)	Vert. reinf.	l_{cr} (mm)	Stirrups	Stirrups l_{cr}
Interior	440	440	12 ϕ 32	660	ϕ 16c250	ϕ 16c125
Border	330	330	8 ϕ 25	645	ϕ 10c330	ϕ 10c120

Table 3.20: Final wall characteristics.

Storey	b_c (mm)	b_{wo}	l_c (mm)	Vert. reinf.	Vert. reinf. l_c	Hor. reinf.	Stirrups l_c
4th	-	175	-	ϕ 12c250	-	ϕ 16c200	-
3rd	-	175	-	ϕ 12c250	6 ϕ 25	ϕ 16c150	-
2nd	300	220	675	ϕ 12c250	ϕ 32c125	ϕ 16c150	ϕ 16c250
1st	400	400	675	ϕ 16c225	ϕ 32c90	ϕ 16c225	ϕ 16c125

Chapter 4

Establishing the finite element model

4.1 Introduction

Prior to embarking on the different analysis in this thesis, a sufficiently accurate finite element model must first be in place. In order to obtain such a model, the structure is modelled both in SeismoStruct [2] and in OpenSees [3]. The models are then compared to each other by evaluating the eigenvalue-properties. The first step is to create an elastic model which is directly comparable to the already established Robot-model. Next, inelastic materials and elements are introduced. The reason for using two different software is twofold. Firstly, establishing two matching models strengthens the credibility of the results. Secondly, this thesis aims to compare the somewhat easy-to-use SeismoStruct with the complex, but perhaps more acknowledged OpenSees.

4.2 Model

4.2.1 Geometry

According to EN 1998-1 [1], Table 4.1, the seismic analysis can be performed using a 2D-model if the structure is regular in the plan view. The model consists therefore of the three frames in axes A, B and C (see Figure 3.1) connected with rigid links. All the nodes are constrained against displacements and rotations out of the plane. The illustration is given in Figure 4.1.

4.2.2 Material

In both SeismoStruct and OpenSees, different concrete material models are used for the inside and outside of the confined area. In SeismoStruct [2], the confined concrete parameters are automatically computed when the material model is assigned to the cross section. In

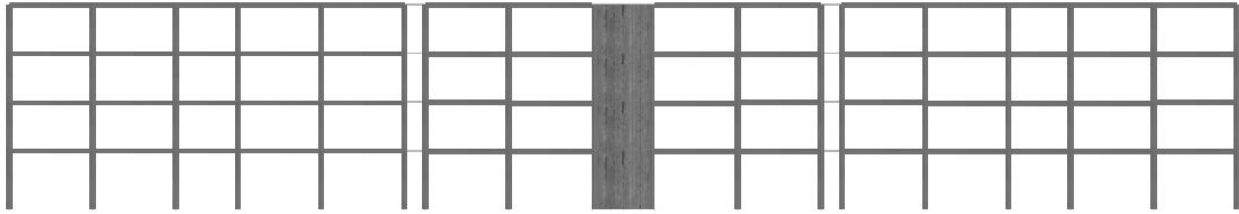


Figure 4.1: Illustration of the FEM-model configuration.

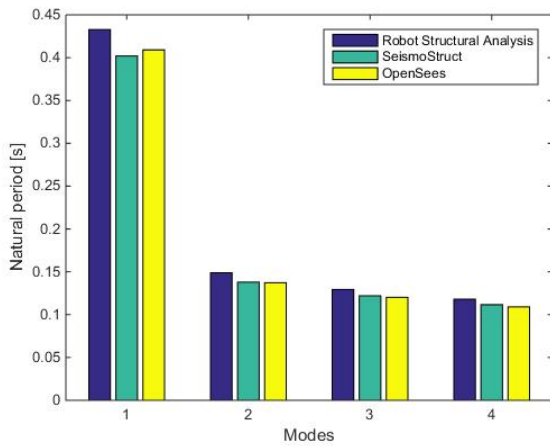
OpenSees [3], assigning such materials is slightly more cumbersome since a pre-defined material model must be assigned to each confined cross section. Nevertheless, the concrete model *ConfinedConcrete01* in OpenSees computes the material properties by allowing the user to assign simple cross sectional parameters. The material concrete model in OpenSees includes tension softening outside the confined area, while the tensile strength in SeismoStruct [2] is abruptly lost when the maximum tensile strain is reached. The reinforcement in both programs is modelled using a bilinear steel model that accounts for kinematic hardening.

4.2.3 Elements

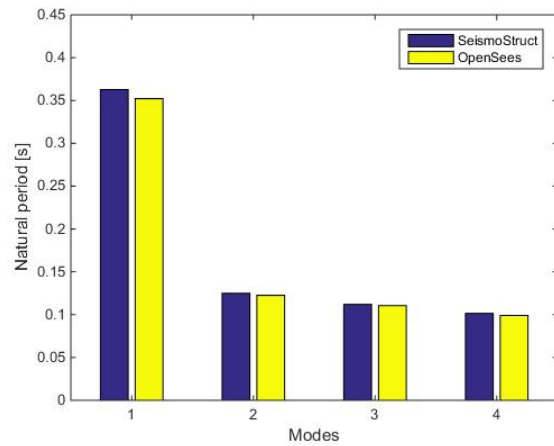
The elastic model consists of beam-column elements with six degrees of freedom which account for bending and axial deformations. For the two-dimensional problem, the cross sectional properties are represented by E , I_z and A . In OpenSees [3], the user must define the above-mentioned parameters manually. This allows the user to include reinforcement when defining the cross sectional area (A) and the second 2nd moment of area (I_z). In SeismoStruct [2], the user must first define a cross section which is then *assigned* to the element type. If the cross section consists of multiple materials, e.g. reinforced concrete members, the reinforcement will not be accounted for when considering stiffness. Another noteworthy difference is that OpenSees allows geometrical non-linearity on local level for elastic elements while SeismoStruct does not. However, P - δ -effects on a global level are considered for both elastic and inelastic elements in both programs. The non-linear model consists of inelastic force-based beam-column elements that are similar to the elastic elements in the sense that they are able to represent bending and axial deformations. In addition, they account for inelasticity along the member length and across the sectional area. The element formulation is explained in Section 2.3.

4.2.4 Algorithms and integrators

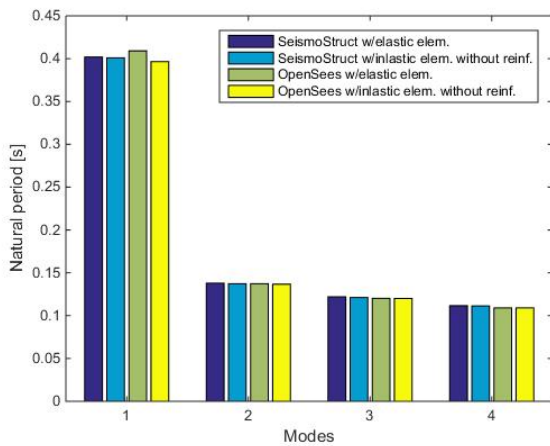
In both OpenSees [3] and SeismoStruct [2], the iterative solution procedures are based on the *Newton-Raphson-method* [25]. Due to the nature of structural response caused by seismic loading, prescribed displacement increments are chosen rather than load increments. In OpenSees, other iterative strategies are applied as *correction steps*. This is shown in Appendix C. The non-linear time-history response is assessed by the *HHT-method*. The integration procedure is a modification of the Newmark's method and has the advantage of suppressing high-frequency noise more effectively [25]. It can be shown that for the model in question,



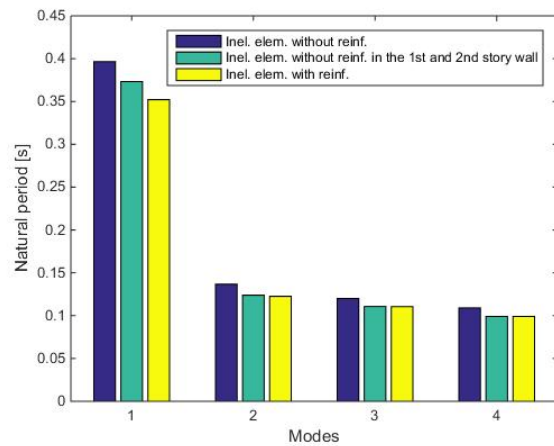
(a) Elastic models.



(b) Inelastic models.



(c) Elastic models versus inelastic models without reinf.



(d) Effects of the 1st and 2nd storey walls (OpenSees).

Figure 4.2: Natural periods of the FEM-models.

there is no considerable difference in the dynamic response between the two methods. For details regarding the non-linear solution procedures and finite element method in general, the reader is referred to the literature [25].

4.3 Eigenvalue analysis

Several eigenvalue analysis are performed in both programs with varying configuration and the results are shown in Figure 4.2. The acting loads in the seismic design situation are included and converted into equivalent masses. The elastic models are compared in Figure 4.2a which shows agreement between OpenSees [3] and SeismoStruct [2]. The walls in Robot [24] are modelled using shell elements that account for shear deformations, which is partly the reason for the slightly softer system.

4.3.1 Stiffness

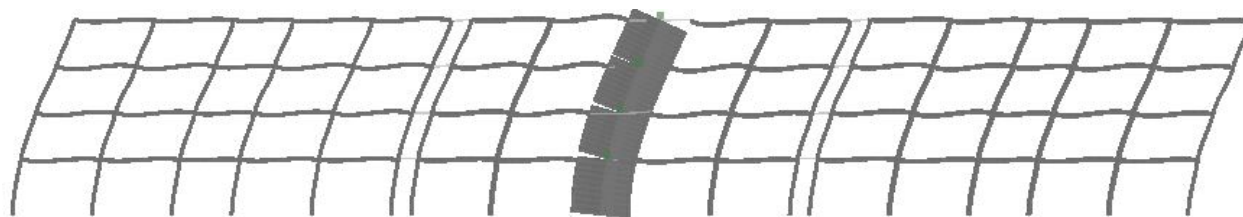
Figure 4.2b shows compliance between the two softwares using inelastic elements. Comparison with Figure 4.2a reveals that the inelastic model is significantly stiffer than the elastic. As was explained in Section 4.2.3, the elastic elements do not account for reinforcement. As opposed to the elastic elements, the inelastic elements are assigned uniaxial non-linear material that accounts for confinement. In practice, confinement increases the compressive strength of the material. The confined concrete material models applied are formulated such that the initial stiffness is equal to the non-confined material models. Thus, the difference between the results in Figure 4.2a and 4.2b are due to reinforcement. Making sure that reinforcement has been modelled properly in OpenSees, the elastic model has been compared to an inelastic model without reinforcement. The result is shown in Figure 4.2c. There is overall agreement between the results, which suggest correct modelling of reinforcement in OpenSees. A slight difference in the first mode is observed between the elastic and inelastic model in OpenSees [3]. It is however negligible for all practical purposes.

4.3.2 Effect of RC walls

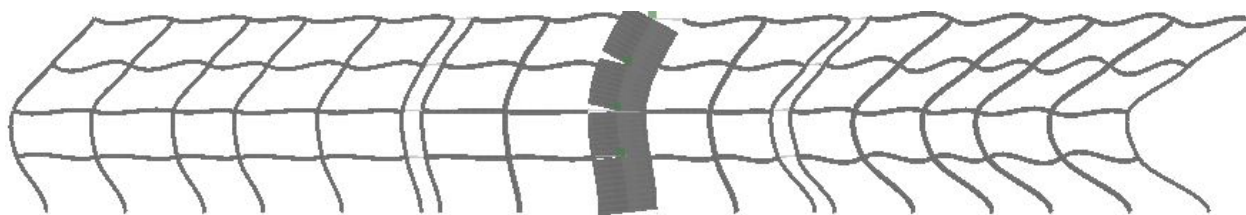
The effects of the reinforcement in the 1st and 2nd storey wall have been evaluated in OpenSees [3] by establishing a model where the reinforcement from the aforementioned walls is removed. The results are presented in Figure 4.2d and reveal that first natural period which increases as the reinforcement is removed. Table 3.20 shows that the 1st and 2nd storey walls are heavily reinforced for bending at the critical areas, i.e. the section ends. Given the fact that the cross sectional height is 4.5 m, it is reasonable that the reinforcement in these areas contributes substantially to the bending stiffness. Note that the reinforcement does not impact the other modes. This can be explained by the fact that the 1st and 2nd storey walls are primarily excited in the first mode. See Figure 4.3.

4.3.3 Shear deformations

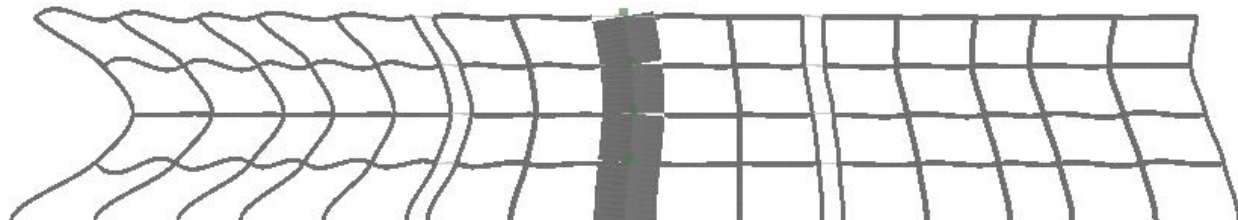
It is observed from Figure 4.2a that Robot [24] gives somewhat softer elastic system. As previously mentioned, this is probably due to the fact that the walls in Robot are modelled with shell elements that account for shear deformations. Since the total wall height is substantially larger than the cross sectional height, the shear deformations become less significant in comparison with bending deformations. For lower buildings however, the shear deformations will have a larger impact on modal properties. In that case, SeismoStruct is limited in the sense that there is no beam-column elements, neither elastic nor inelastic, that account for shear deformations. In OpenSees however, the user can apply the elastic *Timoshenko Beam-Column element* which directly incorporates shear strains. It also possible to include shear deformations for inelastic elements through *Section Aggregators* [26]. The latter is tested for the reinforced inelastic system and the results is an increase in the first natural period from 0.35 s to 0.37 s. It however emphasized that elements accounting for shear deformations will not be applied when assessing the various types of analyses in this thesis.



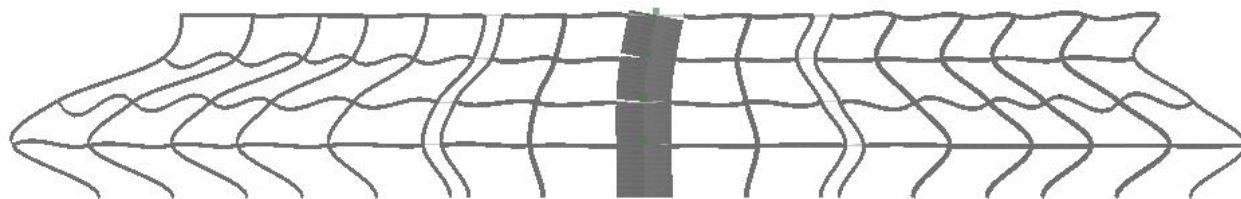
(a) 1st mode shape.



(b) 2nd mode shape.



(c) 3rd mode shape.



(d) 4th mode shape.

Figure 4.3: First 4 natural mode shapes of the structure.

4.4 Concluding remarks

Altogether, the results suggests that a reasonable finite model has been established both in SeismoStruct [2] and in OpenSees [3]. During the comparison, differences between the elastic and inelastic element types have been revealed. Even though the eigenvalue analysis is a purely elastic type of structural analysis, the results suggest that it is not always beneficial to use elastic elements. This applies particularly for SeismoStruct, since there is no possibility of including the stiffness contribution from reinforcement. Also, geometrical non-linearities on the local level are not considered for elastic elements in SeismoStruct. Key remarks are listed below.

- In the case of RC structural members, the effects of the longitudinal reinforcement and confined concrete are fully accounted for when applying inelastic elements, without the user having to calculate the sectional properties manually.
- The effects of the reinforcement vary with the quantity. Structures that partly consists of members with large cross sectional heights and heavy longitudinal reinforcement, such as the 1st and 2nd storey wall, are more sensitive to the presence of reinforcement and should be considered modelled with inelastic elements even if the user only wishes to carry out the eigenvalue analysis.
- There is no possibility, neither in SeismoStruct [2] nor in OpenSees [3], to manually modify the second moment of area for inelastic elements, which might be desirable if the user wishes to evaluate the eigen-problem when accounting for cracking. The only option is to modify the elasticity modulus E .
- OpenSees has a clear advantage over SeismoStruct in the element assortment when assessing modal properties for structures where shear deformations are expected to be of significance.

Chapter 5

Non-Linear Static Analysis

5.1 Introduction

This chapter contains the assessment of the Non-Linear Static Analysis. The results are presented and safety verifications are performed on a selected member. The results are discussed in Chapter 7.1.

5.2 Basis for procedure

The general procedure of the non-linear static analysis is explained in Section 2.2.2. According to EN 1998-3, section 2.1, fundamental requirements refer to the stage of damage in the structure defined through three Limit States, (1) Near Collapse (NC), (2) Significant Damage (SD) and (3) Damage Limitation (DL). Due to time limitations, this thesis will only assess the Significant Damage Limit State. The return period in Significant Damage Limit State is 475 years. The response spectrum in Figure 3.4b is based on EN 1998-1, section 2.1, which gives a return period $T_{NCR} = 475$ years. Therefore, the same response spectrum will also be used in the non-linear static analysis in this section. The basis for the procedure is the pushover curves presented in Figure 5.1a and Figure 5.1b. The displacement is assessed at the top middle node of the 4th storey wall. The analysis in this chapter is based on the curve from OpenSees [3].

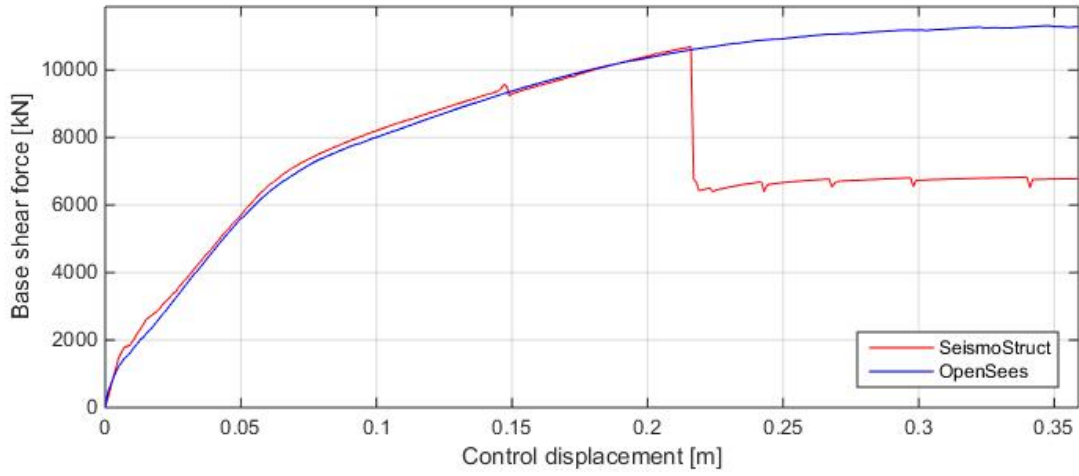
5.2.1 SDOF-system

First, the mass of the equivalent SDOF-system is determined. The first mode shape is assessed by performing a modal analysis in Robot. The result is a first mode shape vector

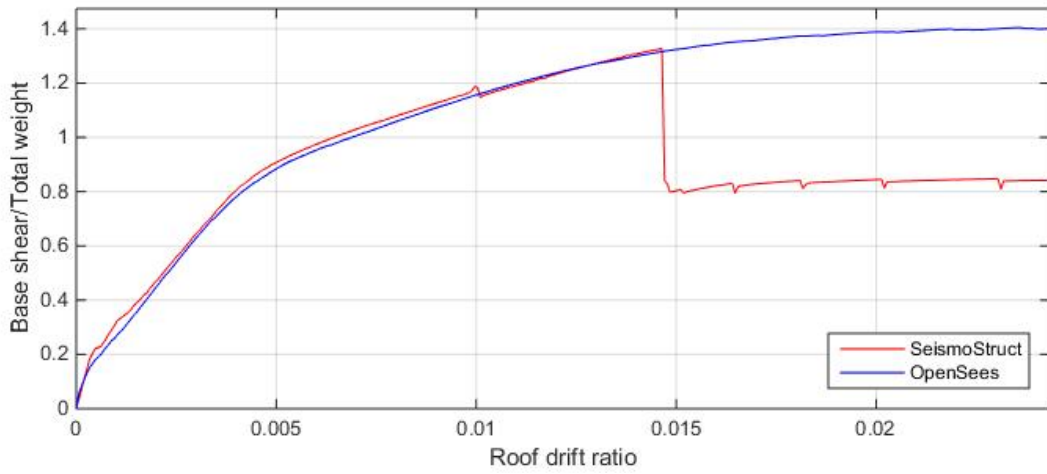
$$\Phi_1 = [1 \quad 0.673 \quad 0.363 \quad 0.137] \quad (5.1)$$

Applying the floor masses calculated in Section 3.3.2,

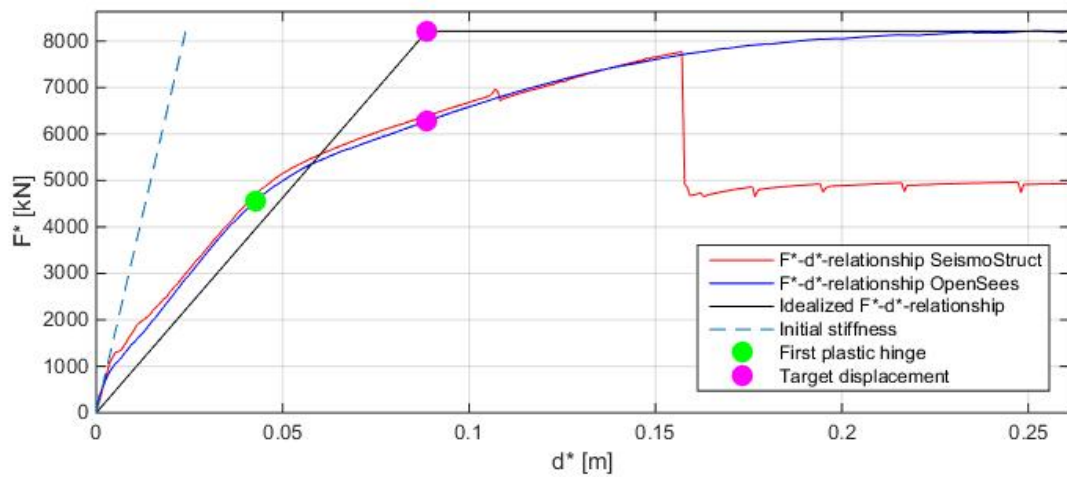
$$m^* = 370\,550 \text{ kg} \times 1 + 383\,580 \text{ kg} \times 0.673 + 383\,580 \text{ kg} \times 0.363 + 386\,370 \text{ kg} \times 0.137 = 820\,872 \text{ kg} \quad (5.2)$$



(a) Base shear-control displacement relationship.



(b) Normalized base shear-roof drift ratio relationship.



(c) F^* - d^* -relationship.

Figure 5.1: Base shear-displacement relationship.

The transformation factor

$$\Gamma = \frac{820\,872 \text{ kg}}{(370\,550 \text{ kg} \times 1^2 + 383\,580 \text{ kg} \times 0.673^2 + 383\,580 \text{ kg} \times 0.363^2 + 386\,370 \text{ kg} \times 0.137^2)} = 1.363 \quad (5.3)$$

The force F^* and displacement d^* of the equivalent SDOF-system are determined in accordance with Equations 2.10 and 2.11. The F^* - d^* relationship is presented in Figure 5.1c.

5.2.2 Idealized force-displacement relationship

Next, the idealized elasto-perfectly plastic force-displacement relationship is determined. According to Figure 5.1c, $d_m^* = 0.250 \text{ m}$ and $F_y^* = 8\,217 \text{ kN}$. As an initiation, the assumed target displacement is equal to d_m^* . The deformation energy is calculated in Matlab and the result is $E_m^* = 1\,602 \text{ (kN} \times \text{m)}$. This gives yield displacement and period,

$$d_y^* = 2 \times \left(0.250 \text{ m} - \frac{1\,602 \text{ (kN} \times \text{m)}}{8\,217 \text{ kN}} \right) = 0.110 \text{ m} \quad (5.4)$$

$$T^* = 2 \times \pi \times \sqrt{\frac{820\,872 \text{ kg} \times 0.110 \text{ m}}{8\,217\,000 \text{ N}}} = 0.66 \text{ s} \quad (5.5)$$

Since $T^* \geq T_c$, the response is calculated in accordance with Equation 2.16. The result is $d_t^* = 0.111 \text{ mm}$. The assumed target displacement d_m^* differs significantly from the calculated target displacement d_t^* . Therefore, an iteration process is initiated. The calculations are performed in Matlab [20] and the results are presented in Table 5.1. Figure 5.1c shows the idealized F^* - d^* -relationship.

Table 5.1: Target displacement calculations according to EN 1998-1, Appendix B.

Iteration	d_m^* (m)	F_y^* (kN)	E_m (kN \times m)	d_y^* (m)	T (s)	d_t^* (m)	d_t^*/d_m^*
0	0.250	8 217	1 602	0.110	0.66	0.111	0.444
1	0.111	8 217	507	0.099	0.62	0.099	0.891
2	0.099	8 217	434	0.092	0.60	0.093	0.929
3	0.093	8 217	391	0.089	0.59	0.090	0.968
4	0.090	8 217	377	0.088	0.59	0.089	0.989
5	0.089	8 217	369	0.088	0.59	0.089	0.100

5.3 Expected displacement

The real target displacement is obtained by multiplying d_t^* with Γ , i.e.,

$$d_t = 0.089 \text{ m} \times 1.363 = 0.121 \text{ m} \quad (5.6)$$

As previously mentioned, d_t is the maximum expected displacement during the design earthquake. The corresponding base shear is equal to 8 767 kN. The inter-storey drifts at target displacement are shown in Figure 5.2.

5.4 Safety verifications

5.4.1 General

According to the definition of Significant Damage Limit State in EN 1998-3 [9], section 2.1, the structure must be able to resist vertical loads after the target displacement is reached. This section contains the assessment of flexure and shear capacities according to EN 1998-3, Annex A, when the building has reached the target displacement calculated in the previous section. The verification of all elements is performed in SeismoStruct [2]. As a validation, a single member is chosen and checked manually. The selected element is the 4th storey interior beam in axis B/2-3 (denoted Bibl41 in the output-file). According to the results in SeismoStruct [2], this element obtains the largest chord rotations when the target displacement is reached. It should be noted that this member is not necessarily the most critical due to variations in cross sections and axial forces.

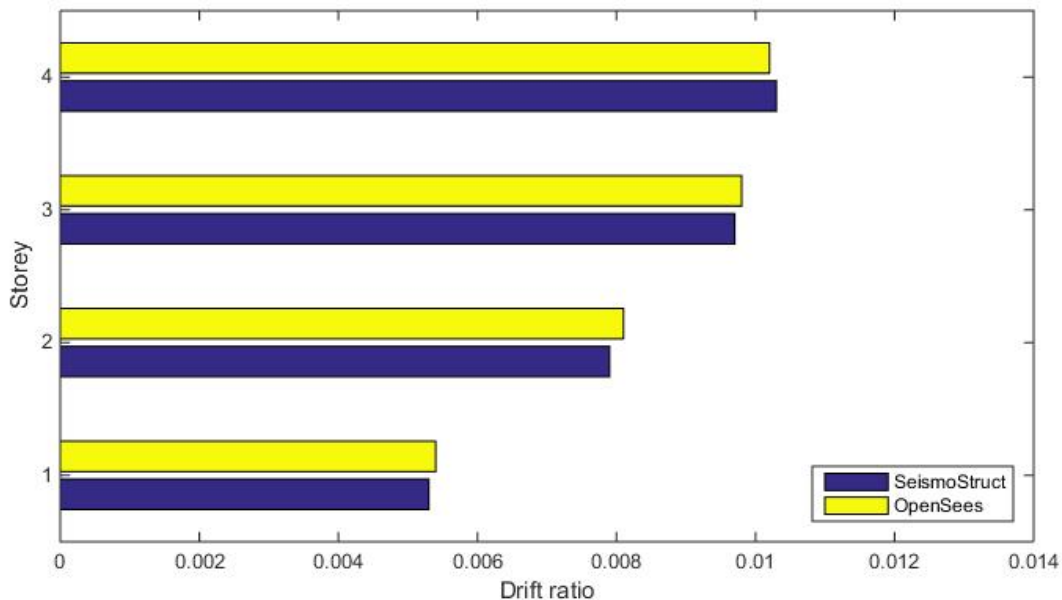


Figure 5.2: Interstorey drifts from the non-linear static analysis.

5.4.2 Flexural capacity

According to EN 1998-3, section A.3.2.1, the flexural performance of elements is assessed by evaluating the total chord rotation. Equation 5.7 gives the chord capacity.

$$\Theta_{um}^{pl} = (3/4) \times (1/y_1) \times 0.016 \times 0.3^v \times ((\max\{0.01; \omega'\}/\max\{0.01; \omega\}) \times f_c)^{0.225} \times (L_v/h)^{0.35} \times 25^\alpha \times \rho_{sx} \times (f_{ywc}/f_c) \times 1.25^{100} \times \rho_d \quad (5.7)$$

Here, y_1 is equal to 1.5 for primary seismic elements and 1.0 for secondary seismic elements, h is the height of the cross section, L_v is the moment/shear ratio at the end section, v is the normalized force in the compression zone, ω is the mechanical reinforcement ratio of the longitudinal reinforcement in tension, ω' is the mechanical reinforcement ratio of the longitudinal reinforcement in compression, ρ_{sx} is the ratio of transverse steel parallel to direction x of loading, ρ_d is the steel ratio of diagonal reinforcement ratio in each direction and α is explained in section 3.2.5. According to the results from the analysis, the acting shear force and moment at target displacement are equal to 147 kN and 262 kNm, respectively. For the 4th storey interior beam, the chord rotation capacity $\Theta_{um, elem} = 0.038$ rad. The capacity according to SeismoStruct is calculated to be 0.043 rad. The reason for the slight disagreement is probably due to inaccurate calculations of α . The total, i.e. elastic plus inelastic, base shear - chord rotation relationship for the above-mentioned element is calculated in SeismoStruct and given in Figure 5.3. The figure shows that the total chord rotation at target displacement $\Theta_{total, elem} = 0.012$ rad. $\Theta_{total, elem}/\Theta_{um, elem} = 0.012 \text{ rad}/0.043 \text{ rad} = 0.279$. The element has sufficient capacity. The results from SeismoStruct [2] show that all the elements have sufficient chord rotation capacities.

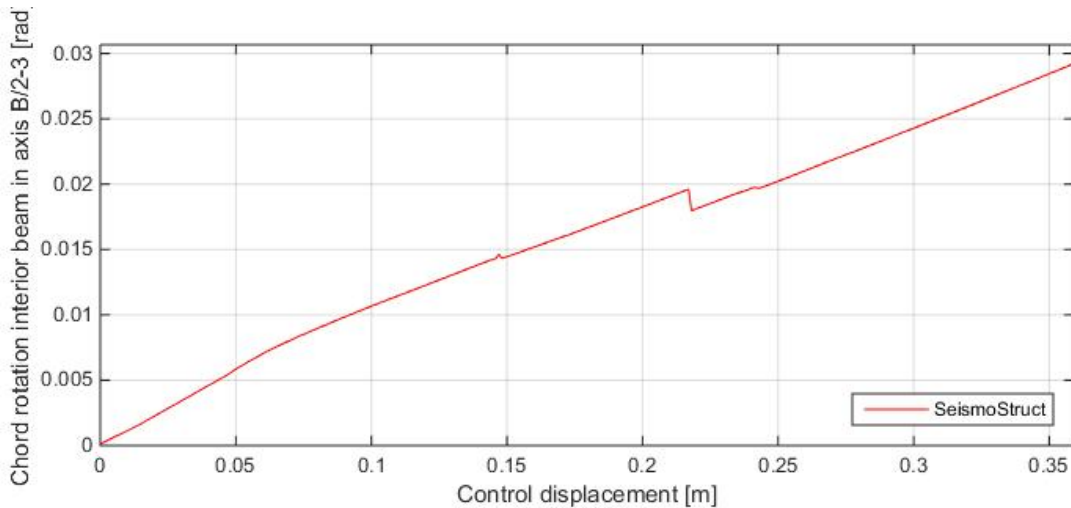


Figure 5.3: Chord rotation-roof displacement relationship for the 4th storey interior beam in axis B/2-3.

5.4.3 Cyclic shear capacity

As for the flexural capacity verification, the 4th storey interior beam connected to the wall will be checked for shear. EN 1998-3 [9], section A.3.3.2 gives the cyclic shear resistance as

$$V_R = (1/y_{el}) \times [((h-x)/(2 \times L_v)) \times \min\{N; 0.55 \times A_c \times f_c\} + (1 - 0.05 \times \min\{5; \mu_{\Delta}^{pl}\}) \times [0.16 \times \max\{0.5; 100 \times \rho_{tot}\} \times (1 - 0.16 \times \min\{5; L_v/h\}) \times f_c^{0.5} \times A_c + V_w]] \quad (5.8)$$

where x is the compression zone depth (assumed $0.5 \times d$), y_1 is equal to 1.15, N is the compressive axial force (zero for tension), A_c is the cross sectional area ($b_w \times d$ for rectangular cross sections), ρ_{tot} is the longitudinal reinforcement ratio and

$$V_w = \rho_w \times b_w \times z \times f_{ywd} \quad (5.9)$$

Here, ρ_w is the transverse reinforcement ratio. The calculation of the factor μ_{Δ}^{pl} is a cumbersome process and it is therefore conservatively assumed equal to 5. The calculation of V_R is performed in Matlab [20]. For the 4th storey interior beam, $V_R = 200$ kN. The capacity according to SeismoStruct is calculated to be 227 kN. As for the chord rotation capacity, the discrepancy might partly be due to inaccurate calculations. Also, the factor μ_{Δ}^{pl} is most likely less than 5, which implies that the calculated shear capacity is higher. According to EN 1998-3, section A.3.3.1, the minimum of the shear resistance determined in accordance with EN 1992-1-1, i.e. $V_{Rd,b}$, and V_R should be used as the design shear resistance. $V_{Rd,b}$ was determined equal to 232 kN in Section 3.3.3. Hence, $V_R = 278$ kN is the design shear force resistance. Since the acting shear force at target displacement is equal to 147 kN, the element has sufficient shear capacity. The shear force-roof displacement relationship for the interior beam is presented in Figure 5.4. According to the results from SeismoStruct [2], all elements except for one have sufficient cyclic shear capacity. The element in question is the 3rd storey interior beam in Frame B, where the capacity is breached by less than 0.5 %.

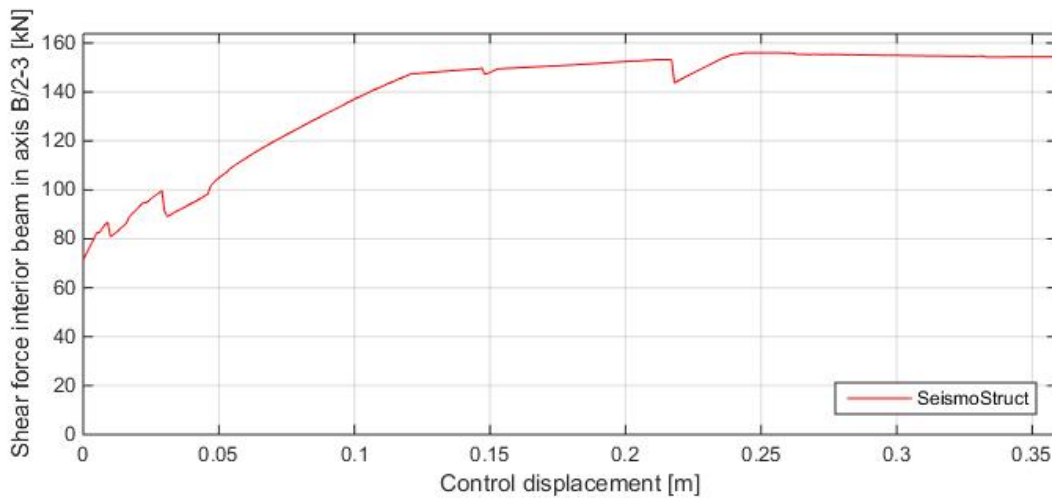


Figure 5.4: Shear force-roof displacement relationship for the 4th storey interior beam in axis B/2-3.

Chapter 6

Non-Linear Time-History Analysis

6.1 Introduction

This chapter contains the assessment of the Non-Linear Time-History Analysis. The results are discussed in Chapter 7.1.

6.2 Ground motions

6.2.1 Selected ground motions

The analysis is based on the seven ground motions shown in Table 6.1 and in Figure 6.1. As previously mentioned, the selection itself is not straight-forward and will not be discussed in detail. The ground motion are selected from the PEER Ground Motion Database [27] in collaboration with Nina Øystad-Larsen. The selection is based on the criteria listed below.

- Solely horizontal far-fault recordings are considered, i.e. $R_{rup} \leq 20$ km
- PGA is at least 2.00 m/s^2 .
- $240 \text{ m/s} \leq V_{s30} \leq 360 \text{ m/s}$
- Moment magnitude larger than 6.5.

6.2.2 Scaling

The ground motions are scaled such that they fit the elastic response spectrum given Figure 3.4b for the first natural period of the structure. Such record manipulation seems reasonable due to the fact that the structure in question is heavily dominated by the first mode. Both the fitted and non-fitted response spectrum for the selected ground motions are developed in

Table 6.1: Selected ground motions from the PEER Ground Motion Database.

RSN	Earthquake	M	Rjb (kM)	Rrup (kM)	V _{s30} (m/s)	PGA (m/s ²)
68	"San Fernando"	6.6	23	23	316	3.04
169	"Imperial Valley"	6.5	22	22	242	4.21
724	"Superstition Hills-02"	6.5	27	27	317	2.16
730	"Spitak Armenia"	6.8	24	24	355	2.65
1634	"Manjil Iran"	7.4	76	76	303	2.45
4853	"Joetsu City"	6.8	26	28	295	3.43
5786	"Iwate Japan"	6.9	35	35	300	2.45

Matlab [20] using Newmarks's method. The script is shown in Appendix B and the results are presented in Figure 6.2. For example, the spectral acceleration for the San Fernando-ground motion is 2.87 m/s^2 at the first natural period. The spectral acceleration given in EN 1998-1 [1] and in Figure 3.4b is equal to 10.06 m/s^2 at the first natural period. Thus, the scaling factor is equal to $10.06 \text{ m/s}^2 / 2.87 \text{ m/s}^2 = 3.502$. The load curve, i.e. the ground motion input-file, is then equal to the original ground motion multiplied with the scaling factor. The same procedure is applied for all ground motions and the scaling factors are presented in Table 6.2.

Table 6.2: Ground motion scaling factors.

San Fern.	Imperial V.	Supers. Hills	Spitak A.	Manjil I.	Joetsu C.	Iwate J.
3.502	1.636	1.837	2.939	1.273	1.638	3.149

6.3 Response

The time-history roof displacements for the selected and scaled ground motions are presented in Figures 6.3 and 6.4. The roof displacement is assessed at the same node as the target displacement in the non-linear static analysis. The maximum roof displacements are presented in Table 6.3 and in Figure 6.8. The hysteric base shear-roof displacement relationship is given in Figure 6.7 and the maximum base shear forces are presented in Table 6.3. Also, a graphical presentation of the maximum displacements and base shear forces is given in Figure 6.9. The interstorey drift ratios are presented in Figure 6.10. According to EN 1998-1

[1], section 4.3.3.4.3, the average response parameter of the seven analysis must be used as the design value. Hence, the expected maximum roof displacements are equal to

$$d_{\max} = 0.118 \text{ m (SeismoStruct)}$$

$$d_{\max} = 0.120 \text{ m (OpenSees)}$$

and the maximum base shear forces are equal to

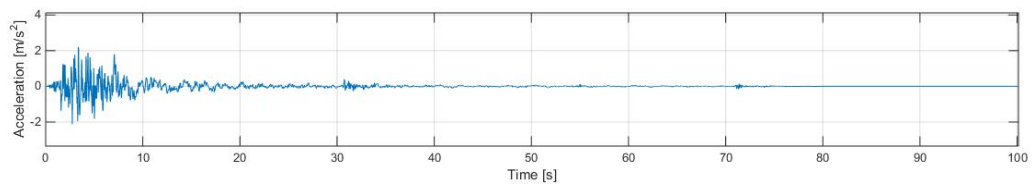
$$F_{b,\max} = 11\,042 \text{ kN (SeismoStruct)}$$

$$F_{b,\max} = 13\,010 \text{ kN (OpenSees)}$$

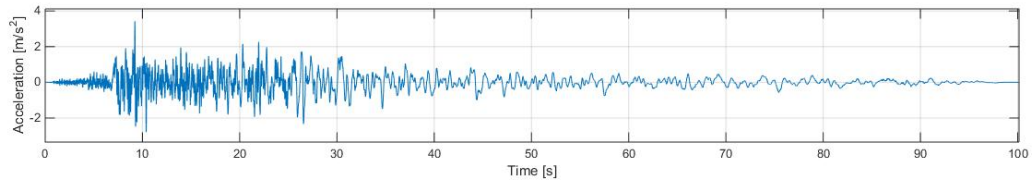
Figure 6.10h shows the average interstorey drift ratios from the seven ground motions.

Table 6.3: Maximum roof displacements and base shear forces from the non-linear time history analysis.

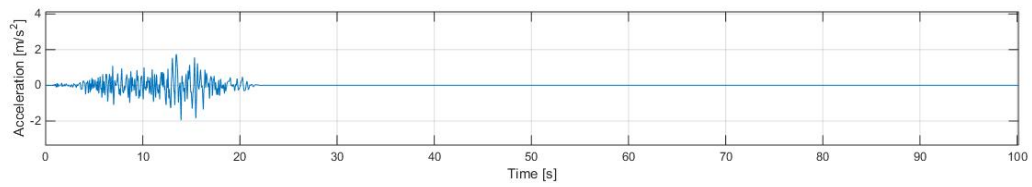
Software	Response	S. F.	I. V.	S. H.	S. A.	M. I.	J. C.	I. J.
SeismoStruct	d_{\max} (m)	0.101	0.109	0.079	0.141	0.059	0.164	0.170
	$F_{b,\max}$ (kN)	13 327	10 866	8 302	12 396	7 887	12 387	12 130
OpenSees	$d_{m,\max}$ (m)	0.096	0.110	0.086	0.147	0.063	0.169	0.172
	$F_{b,\max}$ (kN)	15 250	13 059	9 981	14 816	9 128	14 213	14 622



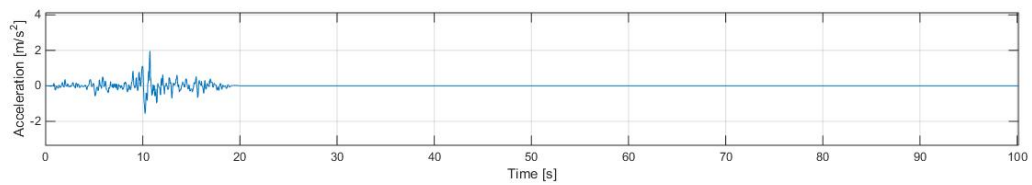
(a) San Fernando



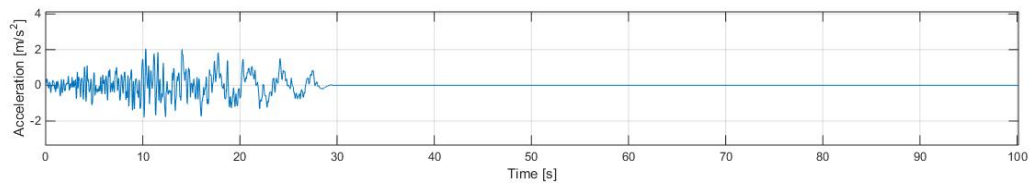
(b) Imperial Valley



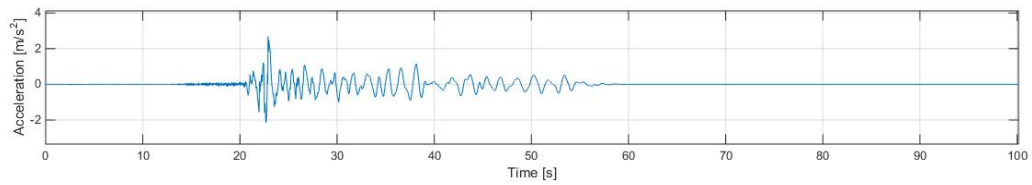
(c) Superstition Hills-02



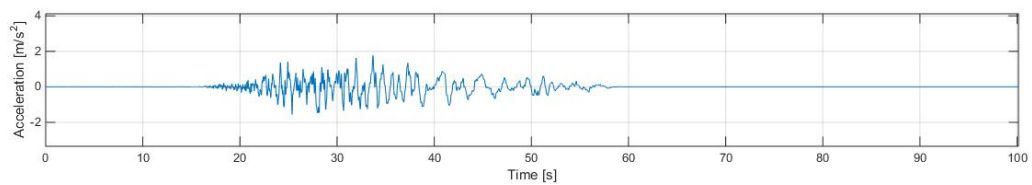
(d) Spitak Armenia



(e) Manjil Iran

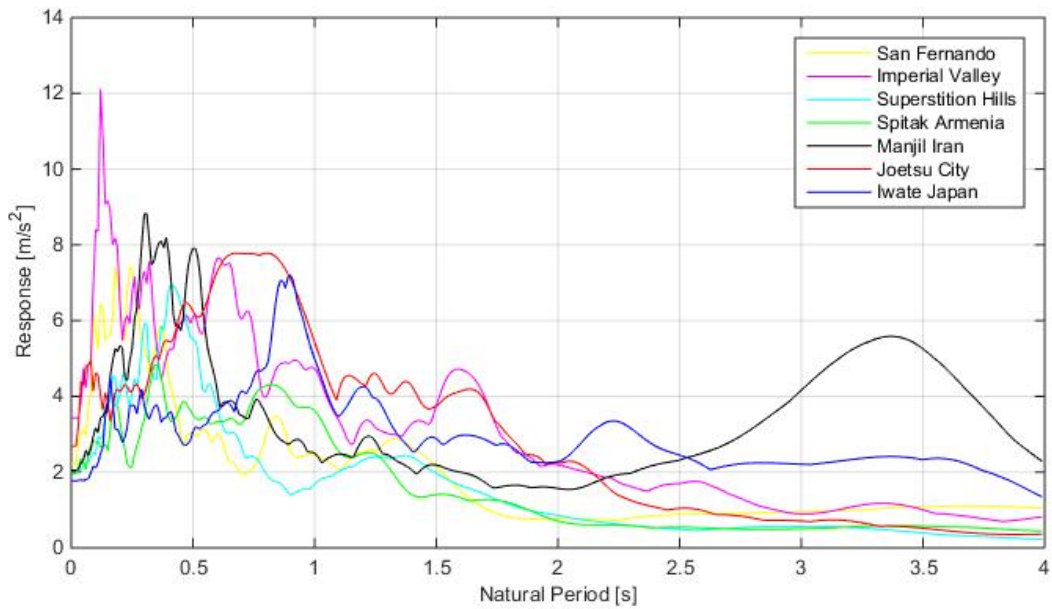


(f) Joetsu City

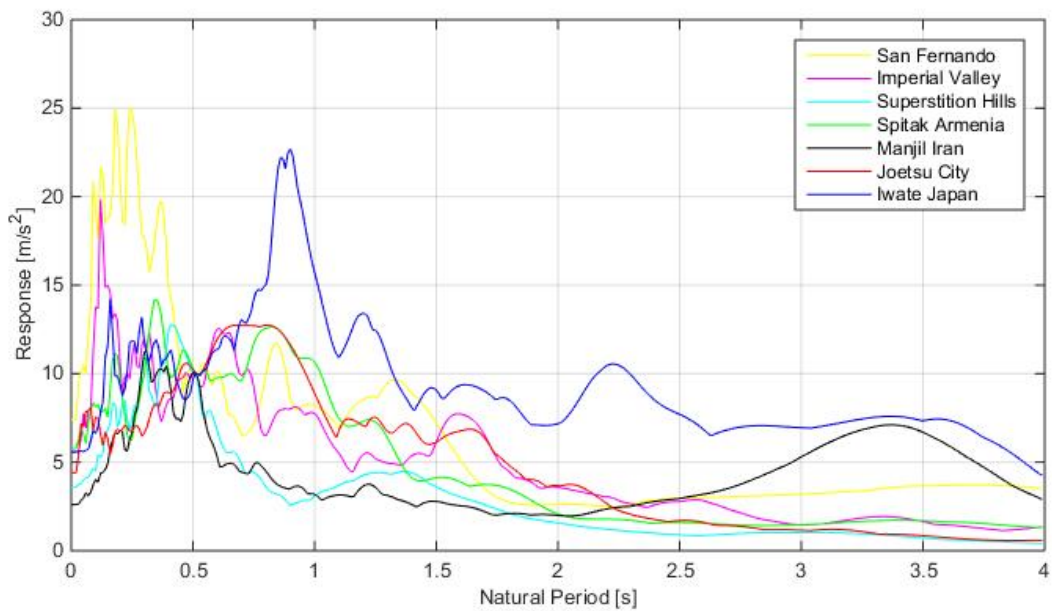


(g) Iwate Japan

Figure 6.1: Selected non-scaled ground motion time histories.

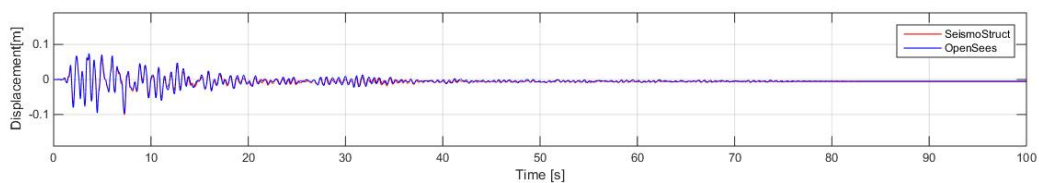


(a) Unscaled response spectrum.

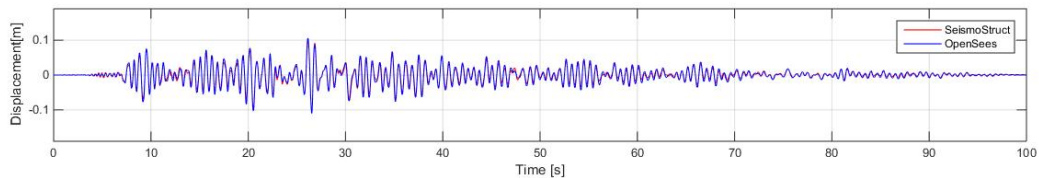


(b) Scaled response spectrum.

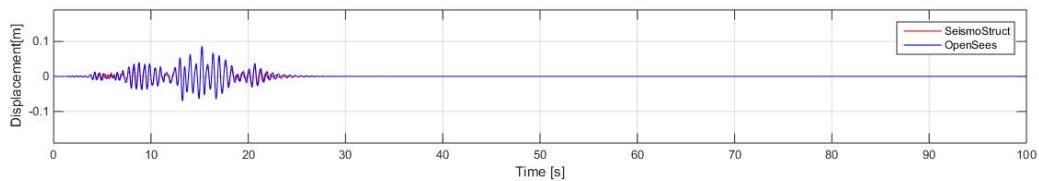
Figure 6.2: Response spectrum of selected ground motions



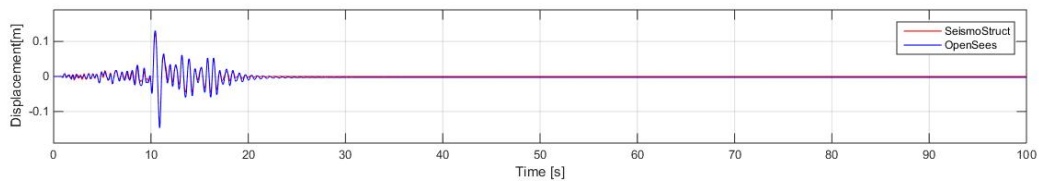
(a) San Fernando



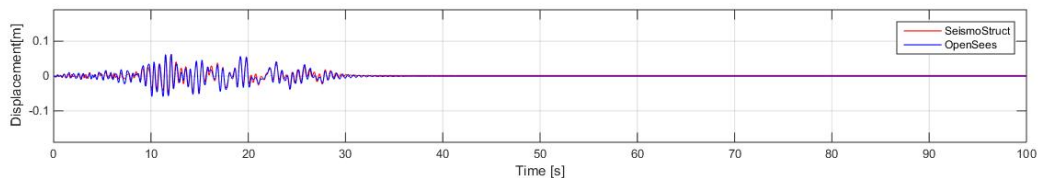
(b) Imperial Valley



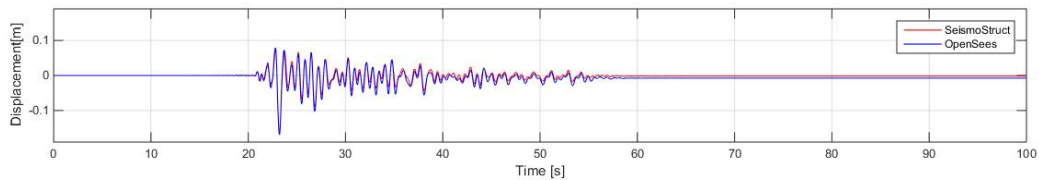
(c) Superstition Hills-02



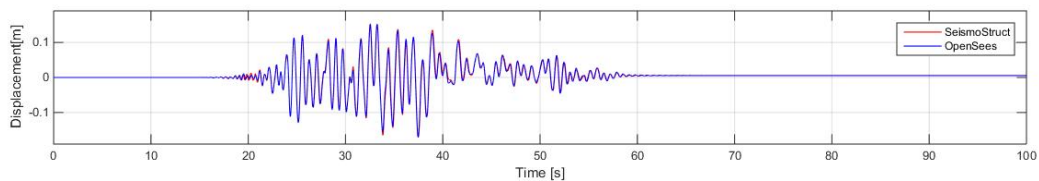
(d) Spitak Armenia



(e) Manjil Iran



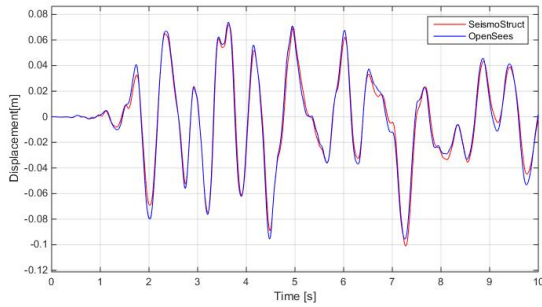
(f) Joetsu City



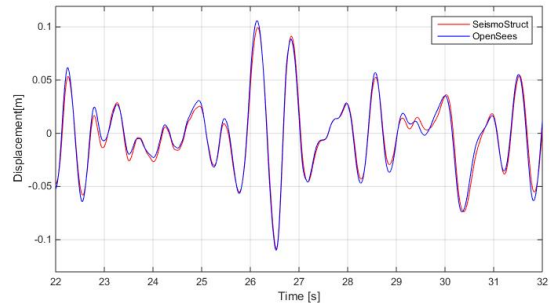
(g) Iwate Japan

Figure 6.3: Displacement response of the control node.

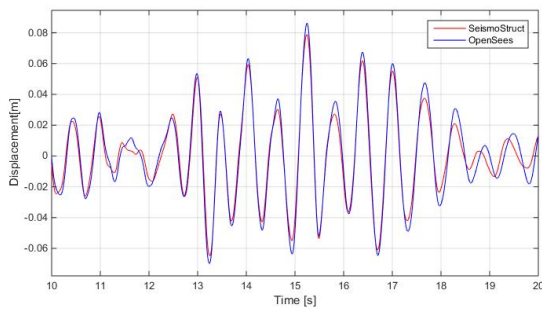
Response



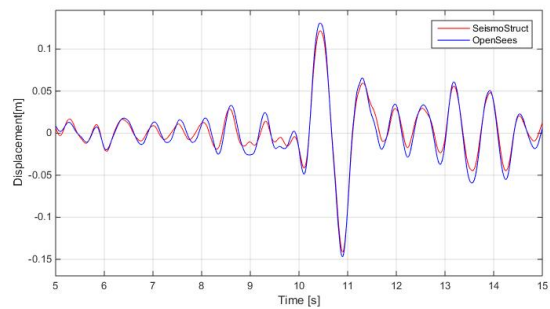
(a) San Fernando



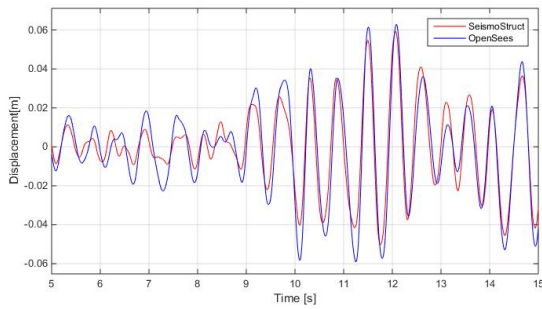
(b) Imperial Valley



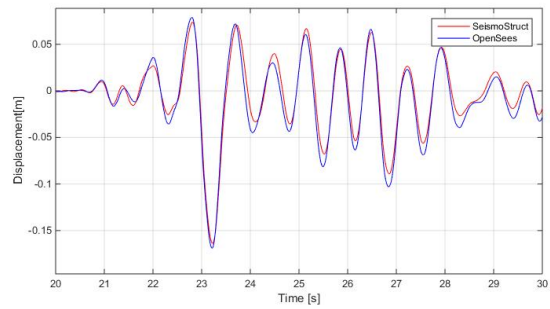
(c) Superstition Hills-02



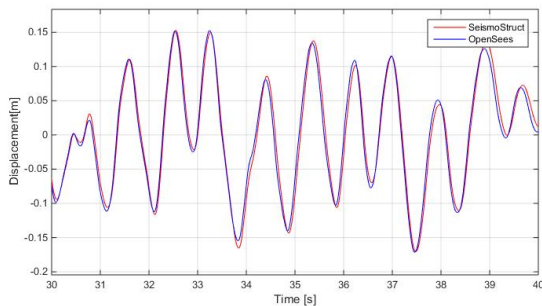
(d) Spitak Armenia



(e) Manjil Iran

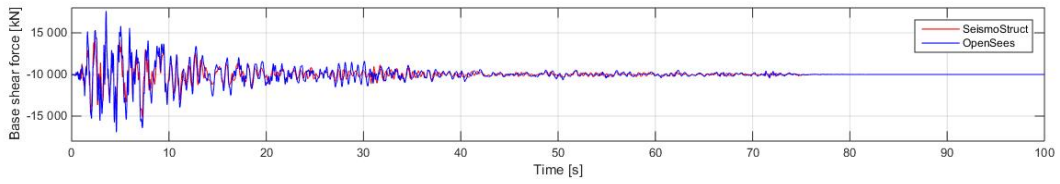


(f) Joetsu City

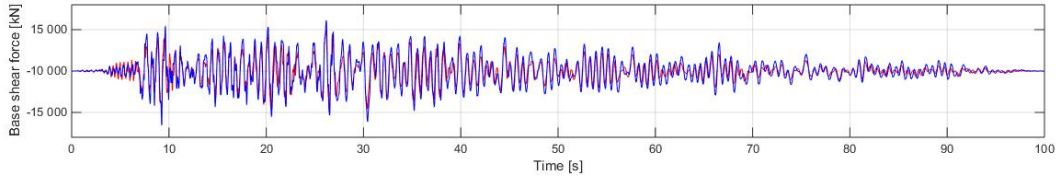


(g) Iwate Japan

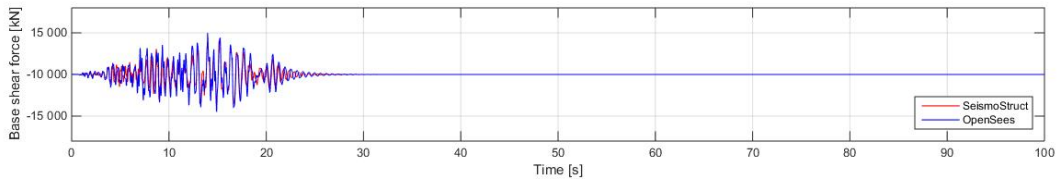
Figure 6.4: Displacement response of the control node. Individual time ranges are selected to reveal possible discrepancies between SeismoStruct and OpenSees.



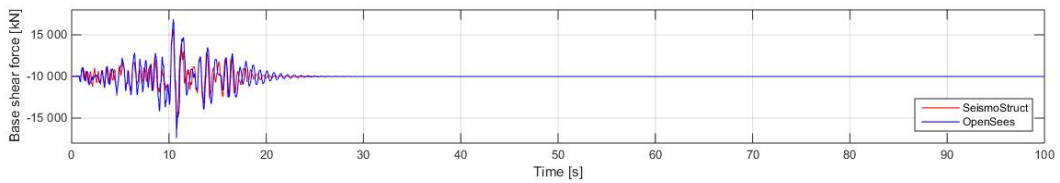
(a) San Fernando



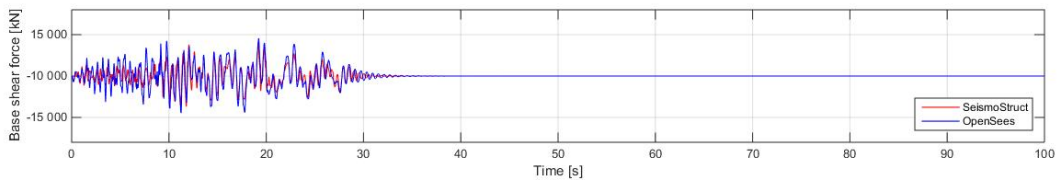
(b) Imperial Valley



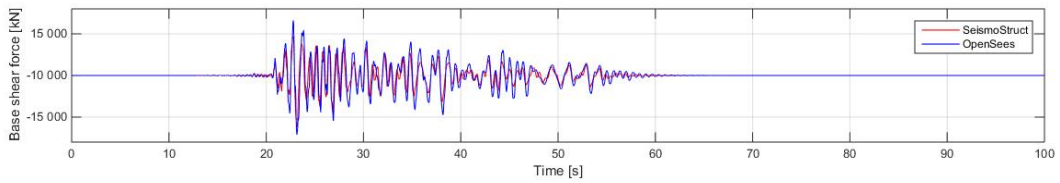
(c) Superstition Hills-02



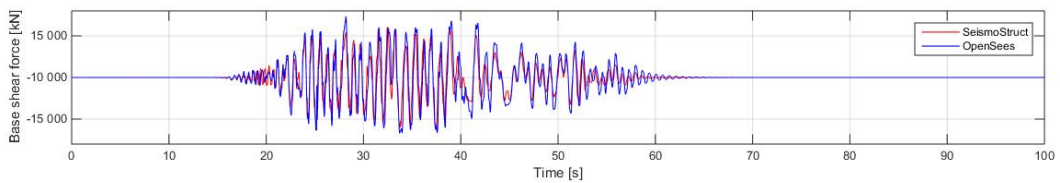
(d) Spitak Armenia



(e) Manjil Iran

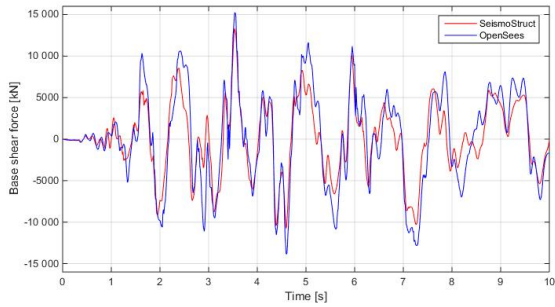


(f) Joetsu City

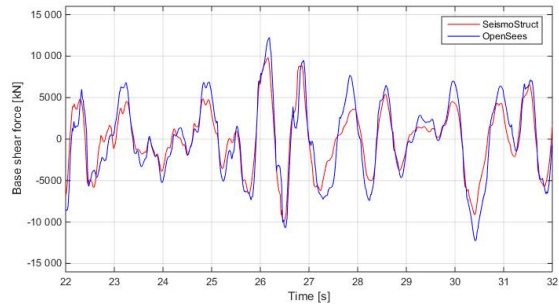


(g) Iwate Japan

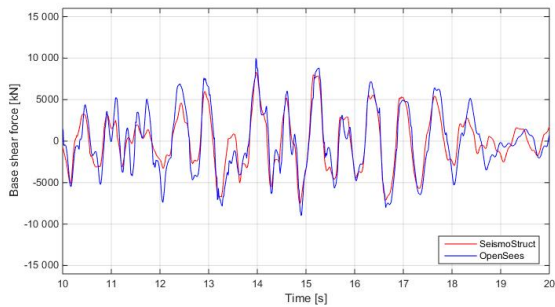
Figure 6.5: Base shear-time history relationships for the selected ground motions.



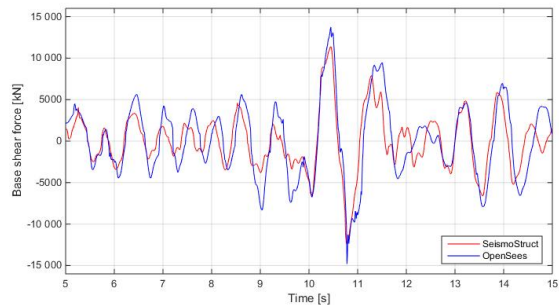
(a) San Fernando



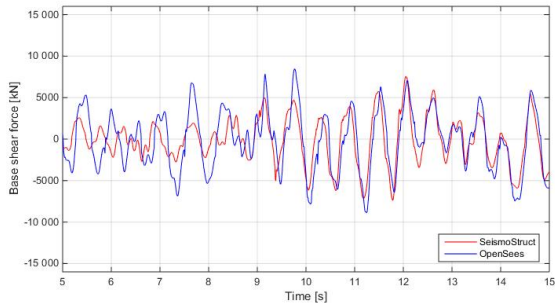
(b) Imperial Valley



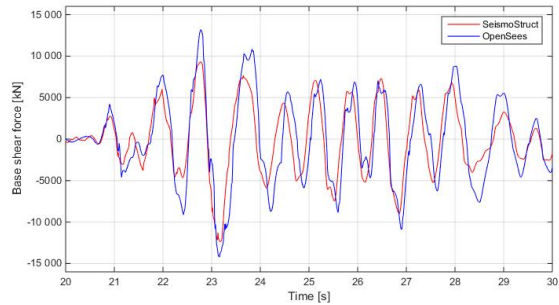
(c) Superstition Hills-02



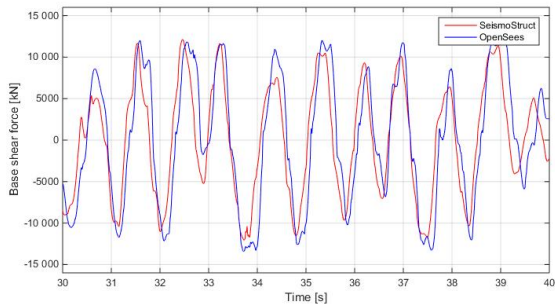
(d) Spitak Armenia



(e) Manjil Iran

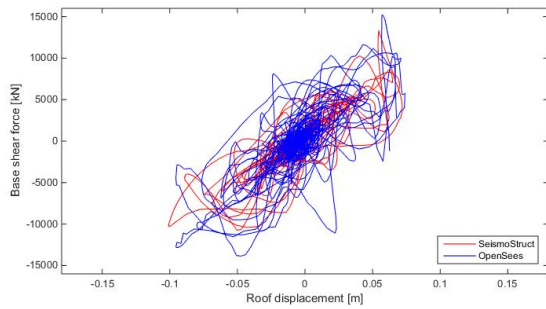


(f) Joetsu City

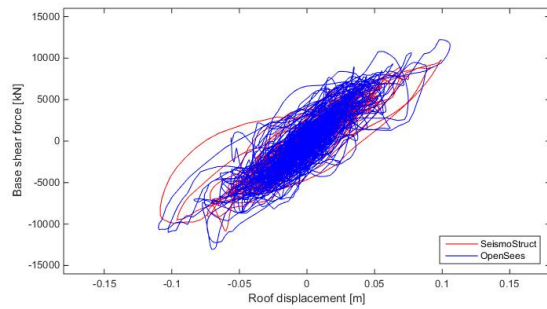


(g) Iwate Japan

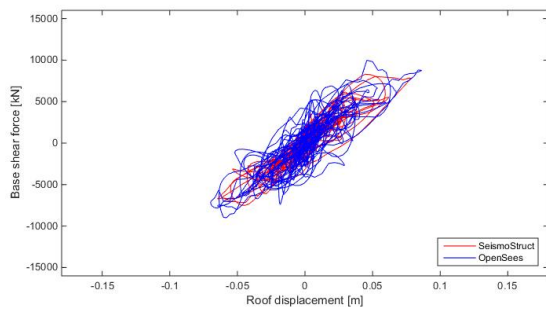
Figure 6.6: Base shear-time history relationships. Individual time ranges are selected to reveal possible discrepancies between SeismoStruct and OpenSees.



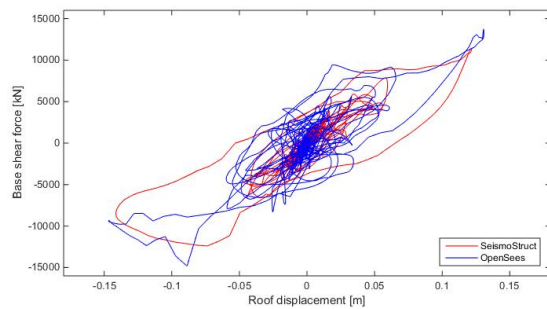
(a) San Fernando



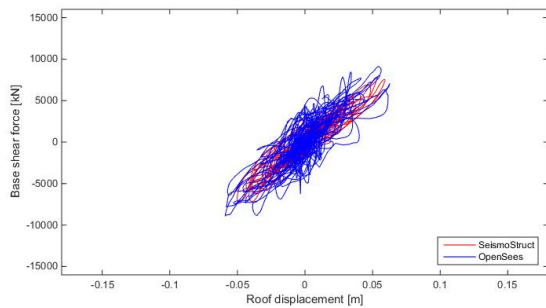
(b) Imperial Valley



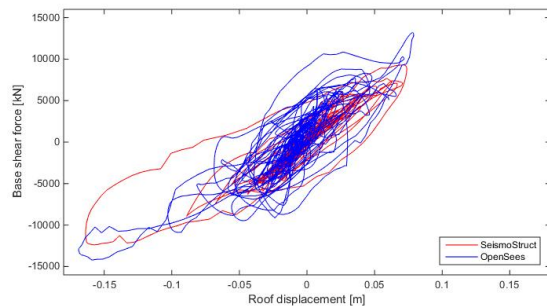
(c) Superstition Hills-02



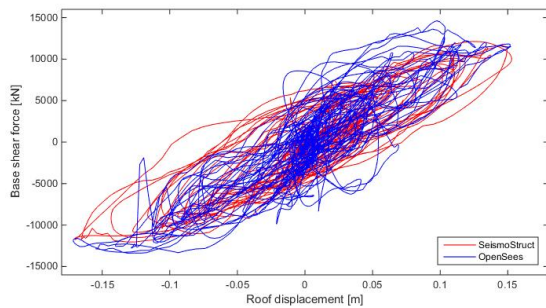
(d) Spitak Armenia



(e) Manjil Iran

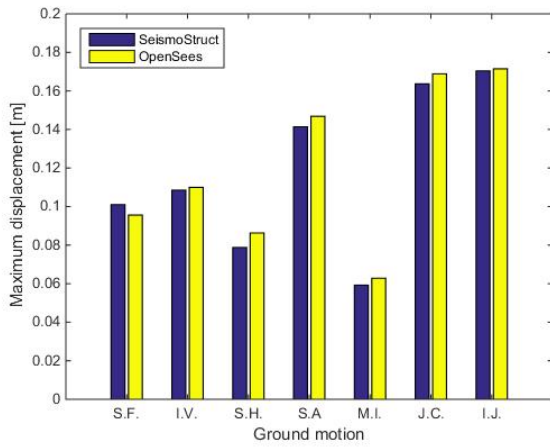


(f) Joetsu City

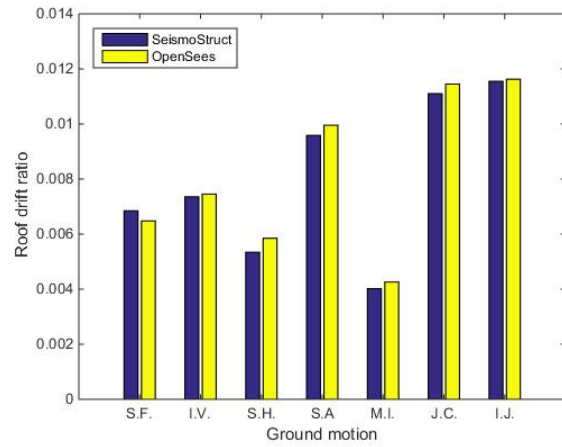


(g) Iwate Japan

Figure 6.7: Hysteric base shear - roof displacement relationship.



(a) Maximum roof displacements.



(b) Roof drift ratios.

Figure 6.8: Maximum roof displacements and drift ratios from the non-linear time history analysis.

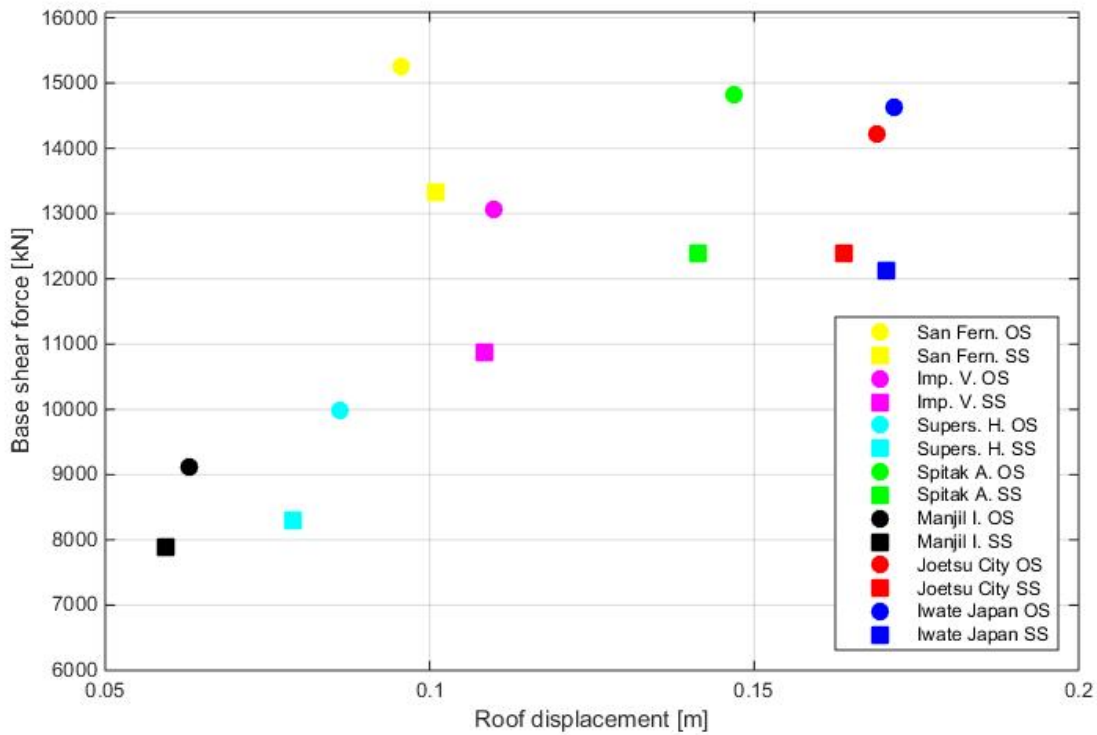
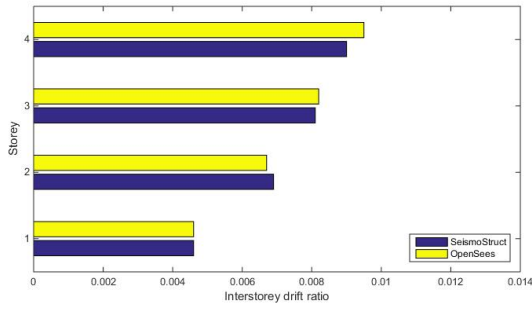
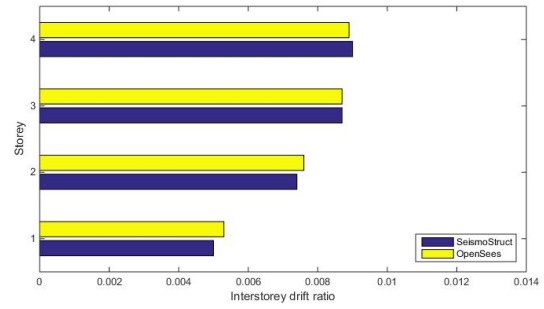


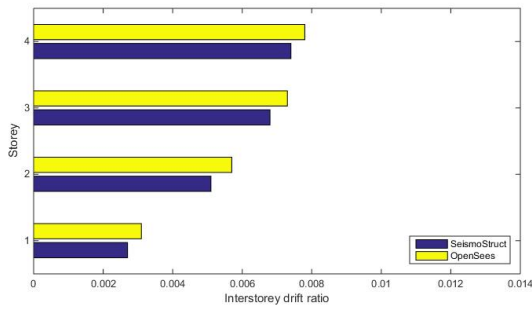
Figure 6.9: Maximum base shear forces plotted against maximum displacements for the individual non-linear dynamic analyses.



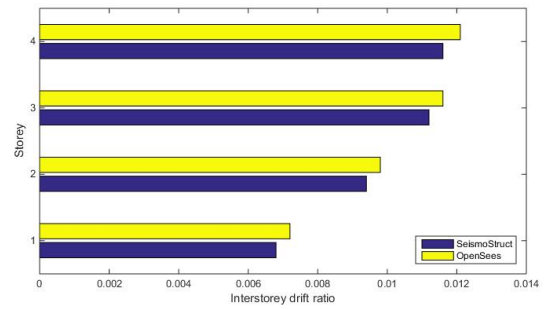
(a) San Fernando



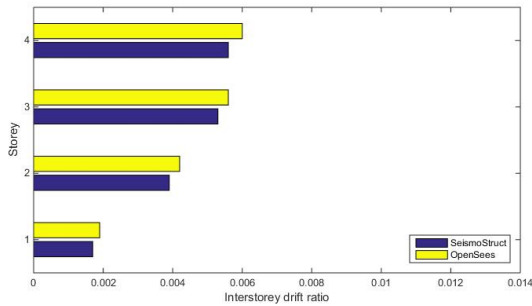
(b) Imperial Valley



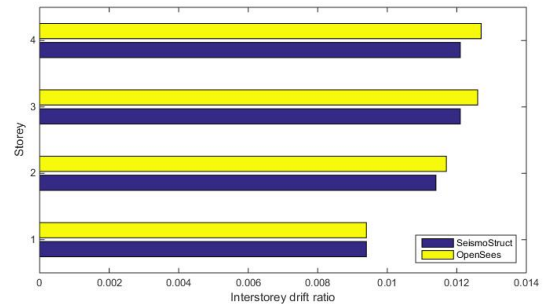
(c) Superstition Hills-02



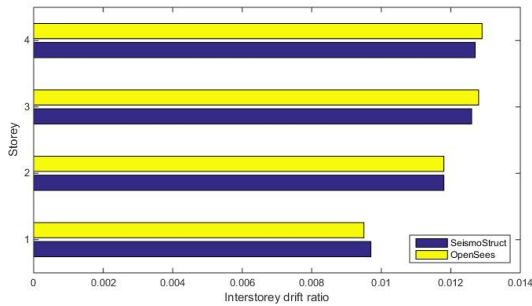
(d) Spitak Armenia



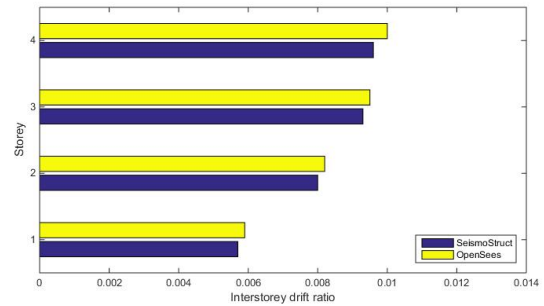
(e) Manjil Iran



(f) Joetsu City



(g) Iwate Japan



(h) Average interstorey drift ratios from NTHA.

Figure 6.10: Interstorey drift ratios from the non-linear time history analyses.

Chapter 7

Discussion of the results

7.1 Introduction

This chapter discusses the results from the static and dynamic non-linear analyses assessed in Chapters 5 and 6. Section 7.2 compares the results from OpenSees with those obtained in SeismoStruct, Section 7.3 evaluates and compares the static and dynamic procedures and Section 7.4 reviews the requirements in EN 1998-1 in relation to the acquired results.

7.2 SeismoStruct versus OpenSees

7.2.1 Non-linear static response

Apart from the sudden drop around 0.22 m, the only significant difference between the pushover curves is that SeismoStruct [2] exhibits an abrupt decrease in initial stiffness while the curve from OpenSees [3] decreases rather smoothly. See Figure 5.1a. The latter is explained by the formulation of the concrete material model applied outside the confined area. As mentioned in Section 4.2.2, the unconfined concrete material model in OpenSees includes tension softening, while the tensile strength in SeismoStruct is abruptly lost when the maximum tensile strain is reached. There is however no obvious explanation behind why SeismoStruct experiences abrupt strength-loss while OpenSees does not. See Figure 5.1c. The time-history response is thoroughly discussed in Section 7.2.2, but it should be noted here that the maximum roof displacements presented in Table 6.3 do not exceed 0.22 m for any ground motion and that the individual time-history roof displacements presented in Figures 6.3 and 6.4 show general agreement between SeismoStruct and OpenSees. Seeking to clarify the discrepancy from the static analysis, the structure is subjected to the "Iwate Japan"-ground motion when the scaling factor is increased by 50 %. The response is presented in Figure 7.1. It is observed that there is no compliance between SeismoStruct and OpenSees after the control node reaches a displacement of approximately 0.22 m at time 25.3 s. The maximum response from SeismoStruct exceeds the one from OpenSees by a factor of $0.73 \text{ m} / 0.35 \text{ m} = 2.09$. Also, the solution in SeismoStruct diverges after 37.11 s. It is emphasized that confined material models, geometry, constraints, restraints, element type, applied loads,

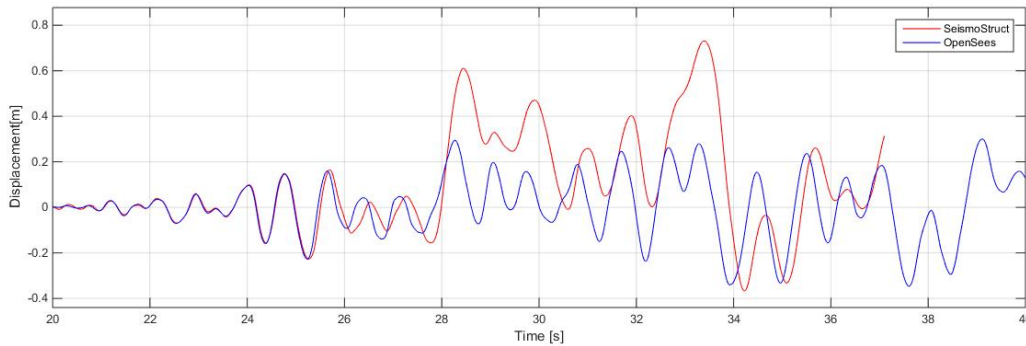


Figure 7.1: Displacement response of the control node for "Iwate Japan"-ground motion increased by 50 %.

integrators, algorithms, convergence criteria and damping is consistent throughout the models in SeismoStruct and OpenSees.

The design of walls in Section 3.3.5 revealed that for the elastic range of response, the lateral forces are primarily resisted by the walls. Due to the nature of drop in the pushover-curve from SeismoStruct, i.e. the sudden and significantly high loss of strength, it reasonable to suspect that the loss occurs in the walls. The confined concrete material models used in SeismoStruct and OpenSees exhibit smooth and gradual loss of strength as illustrated in Figure 7.2. However, similar to the *non-confined* concrete model, the steel model in SeismoStruct exhibits abrupt loss of tensile strength. This is revealed through the results from the non-linear static analysis performed in SeismoStruct. For the 1st storey wall, the tensile strength in the reinforcement at the section ends is lost at the same step as the drop occurs, i.e. 0.217 mm. At displacement 0.216 m, the maximum tensile strain in the reinforcement at the bottom of the wall is equal to 0.0992 with a corresponding stress equal to 597 N/mm^2 . At the next step, i.e. displacement 0.217 m, the strain is equal to 0.1030 while the stress is equal to 0 N/mm^2 . This limit is defined as the fracture/buckling strain in the material model. The stress-strain relationship for the steel model applied in SeismoStruct is presented in Figure 7.3a. The stress-displacement and strain-displacement relationships for the reinforcement bars in the 1st storey wall are presented in Figure 7.5, where the bars are numbered from left to right with reference to Figure 7.4. For example, the bar denoted as $\phi 32 - 7$, is the last confined bar from the left. It is observed from Figure 7.5 that the reinforcing bars in the boundary area almost simultaneously loose strength. In OpenSees, the applied steel model *Steel01* does not exhibit such behaviour. The bi-linear relationship is defined solely by the E-modulus, yielding stress and the isotropic hardening factor, i.e. no fracture strain is defined. Illustration of the stress-strain relationship for the material model *Steel01* is presented in Figure 7.3b.

The fracture limit also explains the difference between SeismoStruct and OpenSees when the structure is subjected to the amplified "Iwate Japan" ground motion. The model in SeismoStruct experiences alterations of the modal properties as the bending stiffness of the 1st storey wall decreases due to fracturing of reinforcing bars. In practice, the system becomes

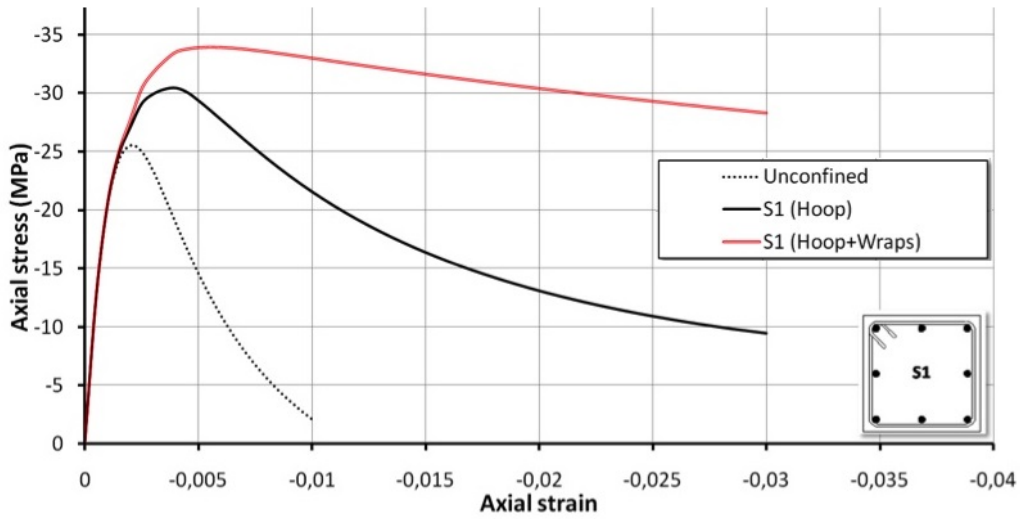
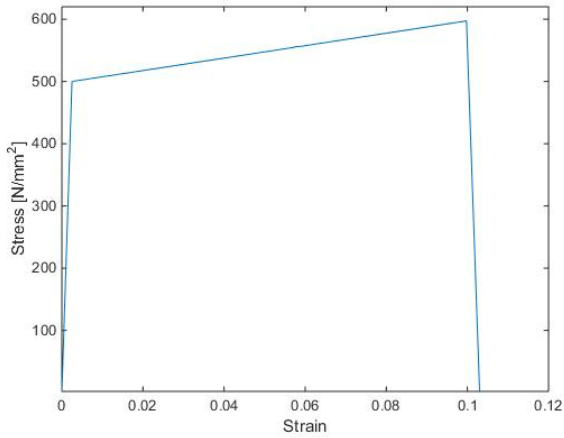
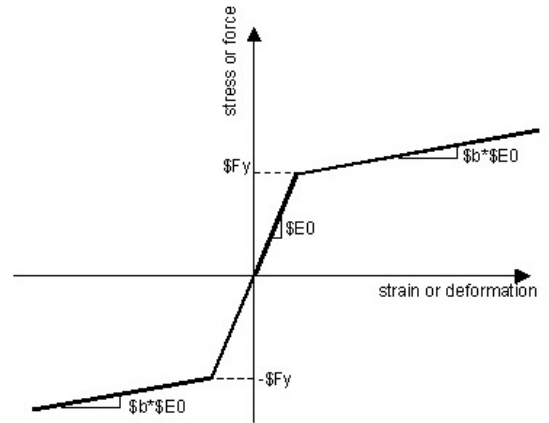


Figure 7.2: Illustration of the confined concrete model applied in SeismoStruct and OpenSees. Illustration: OpenSeesWiki.



(a) Steel model from SeismoStruct.



(b) Steel model from OpenSees. Illustration: OpenSeesWiki

Figure 7.3: The steel material models applied in SeismoStruct and OpenSees. Note that a) represents the actual steel model in SeismoStruct, while b) is an illustration of the steel model in OpenSees.

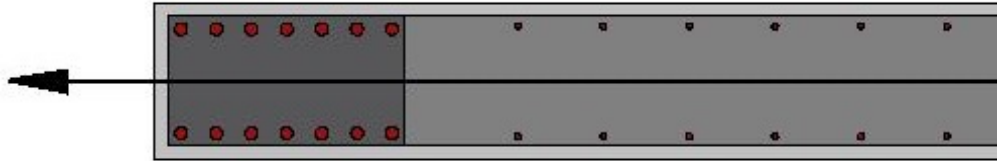
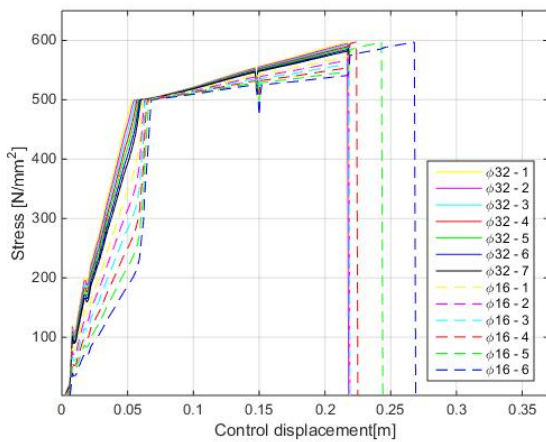
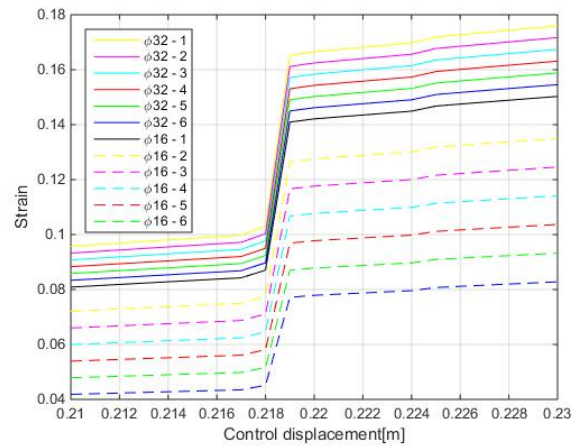


Figure 7.4: Illustration of the 1st storey wall cross section. Observe that the figure only illustrates half of the cross section.



(a) Stress-displacement relationships.

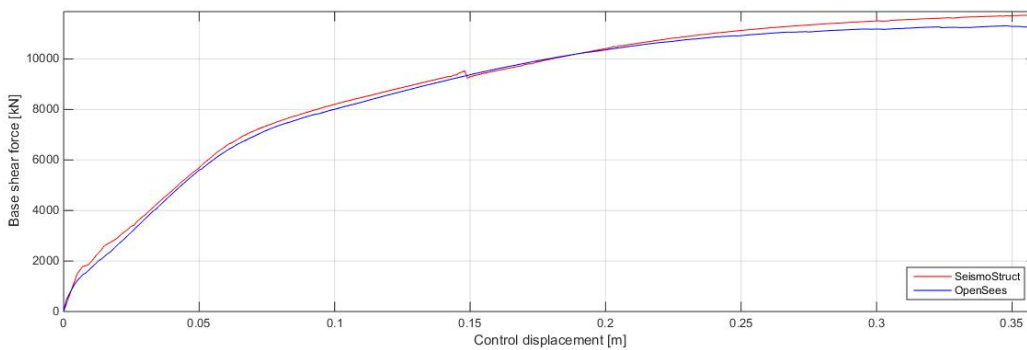


(b) Strain-displacement relationships.

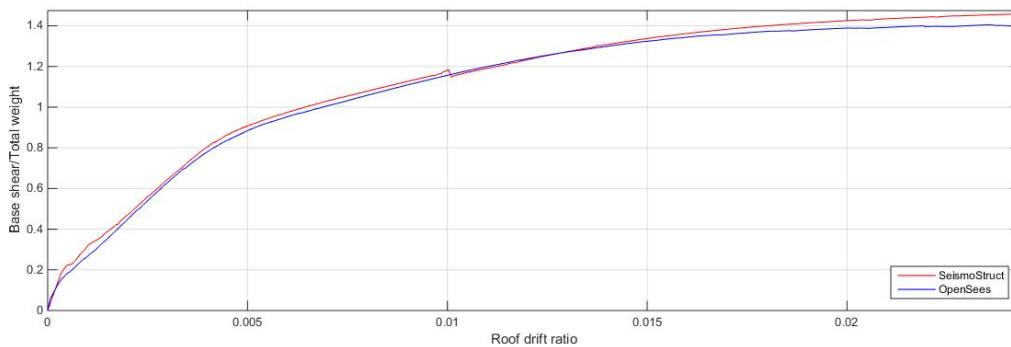
Figure 7.5: Stress and strain-displacement relationships for the reinforcement illustrated in Figure 7.4. The relationships are assessed from the static analysis. The bars are numbered from left to right. Note that the presented range of displacement differs in the two figures.

softer. In OpenSees, the reinforcement in the 1st story wall is not fractured and the modal properties are maintained throughout the response. According to EN 1992-1-1 [19], Table C.1, the minimum fracture strain for reinforcement steel in class C is equal to 0.075. Thus the fracture limit in the steel model applied SeismoStruct is not conservative, and it complies better with actual material behaviour than the steel model in OpenSees.

In order to confirm the effects of the fracture limit, a non-linear static analysis is assessed in SeismoStruct when the fracture strain of the steel model is increased to unity. The pushover-curve is presented in Figure 7.6. The responses from SeismoStruct and OpenSees are practically in perfect compliance, except for the slightly larger maximum base shear force produced by SeismoStruct. The modified model in SeismoStruct is then subjected to the amplified "Iwate Japan" ground motion and the results are presented in Figure 7.7. There are no convergence issues experienced, and SeismoStruct and OpenSees are in nearly complete agreement. The maximum roof displacement in SeismoStruct exceeds the one from OpenSees by a factor of $0.38 \text{ m}/0.35 \text{ m} = 1.08$.



(a) Base shear-control displacement relationship.



(b) Normalized base shear-roof drift ratio relationship.

Figure 7.6: Base shear-control displacement relationship. The fracture strain of reinforcement steel in SeismoStruct is set equal to unity.

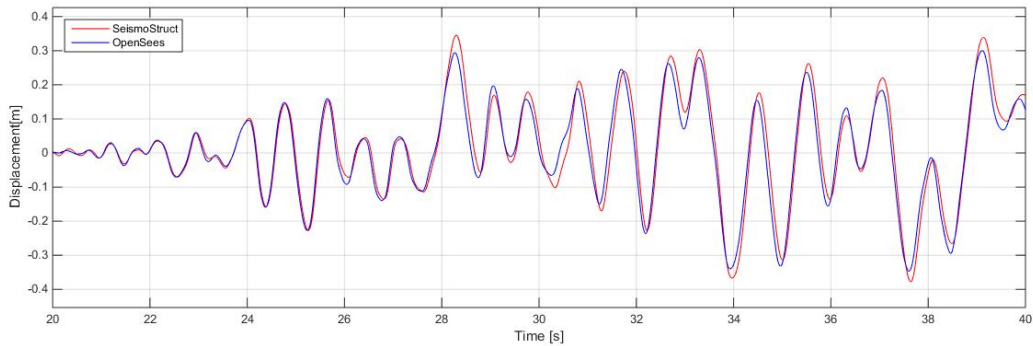


Figure 7.7: Displacement response of the control node for "Iwate Japan" ground motion increased by 50 % when the fracture strain of reinforcement steel in SeismoStruct is set equal to unity.

7.2.2 Time-history response

The individual time-history roof displacement presented in Figures 6.3 and 6.4 show agreement between SeismoStruct [2] and OpenSees [3]. There are some differences though, e.g. the permanent displacement caused by the "Joetsu City" and "Manjil Iran" ground motions. In general, OpenSees renders somewhat more conservative results, but the difference is negligible for all practical purposes. As for the roof displacements, OpenSees produces slightly larger interstorey drift ratios (See Figure 6.10). There is however a larger difference between SeismoStruct and OpenSees in terms of base shear forces. It can be observed from Figure 6.6 that base shear forces in SeismoStruct and OpenSees generally correlate less than displacements, and that for each peak, OpenSees generates larger forces. The hysteric curves presented in Figure 6.7 reveal practically no co-variation for large displacements. Also, Table 6.3 and Figure 6.9 show substantial differences between the maximum obtained shear forces. In the general finite element method, shear forces are obtained through derivatives which amplify possible errors in the displacement field. Considering force-based elements, i.e. elements where the *force field* is enforced, the displacements are obtained through integrals [28]. Integrals tend to "smooth" out errors, which explains why SeismoStruct and OpenSees agree better in terms of deformations.

7.3 NSA versus NTHA

7.3.1 Period elongation

Considering the average response from NTHA, the maximum displacements obtained from NSA and NTHA are practically identical. The target displacement from NSA is equal to 0.121 m, while the maximum displacement from NTHA is equal to 0.118 m (SeismoStruct) and 0.120 m (OpenSees). Although partly coincidental, the similarity is perhaps explained by successful selection and scaling of the ground motions in combination with the fact that the structure is dominated by the first mode. It has previously been demonstrated, e.g. by

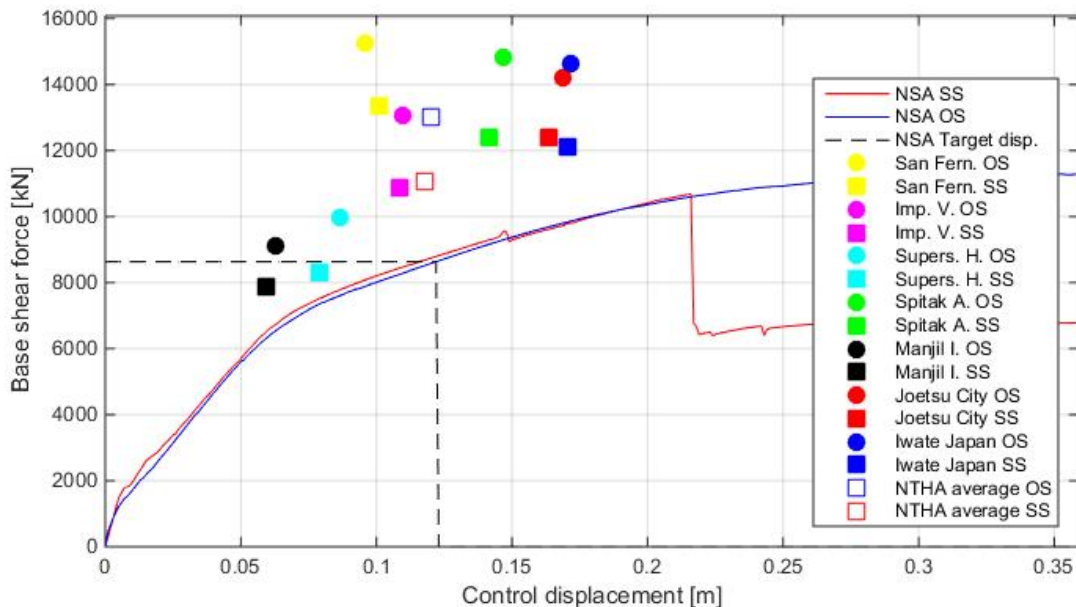


Figure 7.8: Target displacement from NSA together with maximum displacements/base shear from NTHA.

Krawinkler and Seneviratna [29], that the non-linear static analysis is likely to render reasonable results for structures that vibrate primarily in the first mode. The pushover-curve was formed by applying incremental loading based on the first modal pattern and the response spectrum was fitted around the first natural period of the structure. However, there are several uncertainties to be considered. Firstly, the results from the modal analysis computed in Robot revealed that even though the structure *primarily* vibrates in the first mode, there are significant mass contributions from higher modes. Secondly, the ground motions were scaled to fit the first natural period of the cracked system computed in Robot. The results from Chapter 4 exposed differences in modal properties between the elastic model in Robot and the inelastic models in SeismoStruct and OpenSees.

Due to these uncertainties, it is interesting to compare *individual* time-history responses with the results from NSA. The pushover-curves are plotted together with the maximum base shear-displacement values from the individual time-history analyses and presented in Figure 7.8. It should be noted that the maximum base shear forces and displacement do not necessarily occur simultaneously. This can be observed from the hysteric curves in Figure 6.7. Figure 7.8 reveals that even though the average response from NTHA is almost in perfect match with NSA considering maximum displacements, there are still large discrepancies between the individual responses. For example, the maximum displacements caused by "Manjil Iran" and "Iwate Japan" obtained from OpenSees are equal to 0.063 m and 0.172 m, respectively. Both ground motions cause displacements that differ significantly, both from each other and the target displacement from NSA. This is typical for NTHA results, and explains why EN 1998-1 [1] demands that at least three ground motions are applied in the

assessment of structural response due to seismic loading.

Figure 7.9 shows that "San Fernando" induces the highest spectral accelerations for $0 \leq T \leq 0.4$. Since the first four natural periods of the structure calculated in OpenSees, i.e.,

$$T = [0.352 \ 0.123 \ 0.111 \ 0.099] \text{ s} \quad (7.1)$$

are within that range, it is reasonable to expect that the "San Fernando" ground motion also generates the highest response values. The largest displacements are however caused by "Iwate Japan" and Joetsu City" which dominate the scaled response spectrum for periods around 0.65-0.70 s. See Figures 7.8 and 7.9b. The fact that the structure is most sensitive to these ground motions indicates global softening. The most obvious explanation is related to cracking. The natural periods of the building presented in Equation 7.1 are based on the non-cracked system. As previously mentioned, the response spectrum was fitted to match the first natural period of the structure when the stiffness of beams and columns was reduced by 50 %. Even though calculated in Robot [24], which generally gave softer systems, the reduction of stiffness was perhaps not sufficient. Moreover, the importance of the reinforcement in the 1st storey wall with regards to global stiffness has been demonstrated throughout this thesis. Figure 7.10 shows the stress and strain-time relationship caused by Joetsu City" and "Iwate Japan". In both cases, the stress exceeds the yielding limit. After first yield, the tangential modulus E of the reinforcing steel is reduced significantly. With reference to Figure 7.3a, the initial stiffness is equal to

$$E = \frac{\sigma_y}{\varepsilon_y} = \frac{500 \text{ N/mm}^2}{0.0025} = 200 \ 000 \text{ N/mm}^2 \quad (7.2)$$

and the stiffness is reduced to

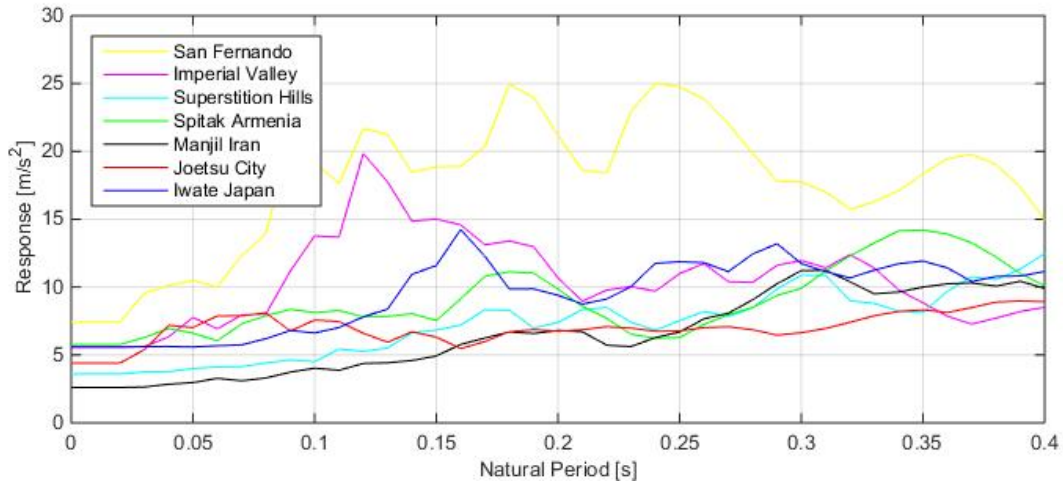
$$E_t = \frac{597 \text{ N/mm}^2 - 500 \text{ N/mm}^2}{0.1 - 0.0025} = 995 \text{ N/mm}^2 \quad (7.3)$$

after yielding. In practice, the stiffness contribution from the reinforcing bars is lost once yielding is reached, but retained when the stress is reduced later in the cycle. The results from Chapter 4 revealed that the modal properties of a building containing heavily reinforced shear walls were sensitive to the presence of reinforcement. However, the *magnitude* of the modal alterations were not in the same scale as the global softening that apparently occurs during the excitation from the time-history records. This indicates that the effects of cracking are of much greater significance than yielding of reinforcement when considering global softening.

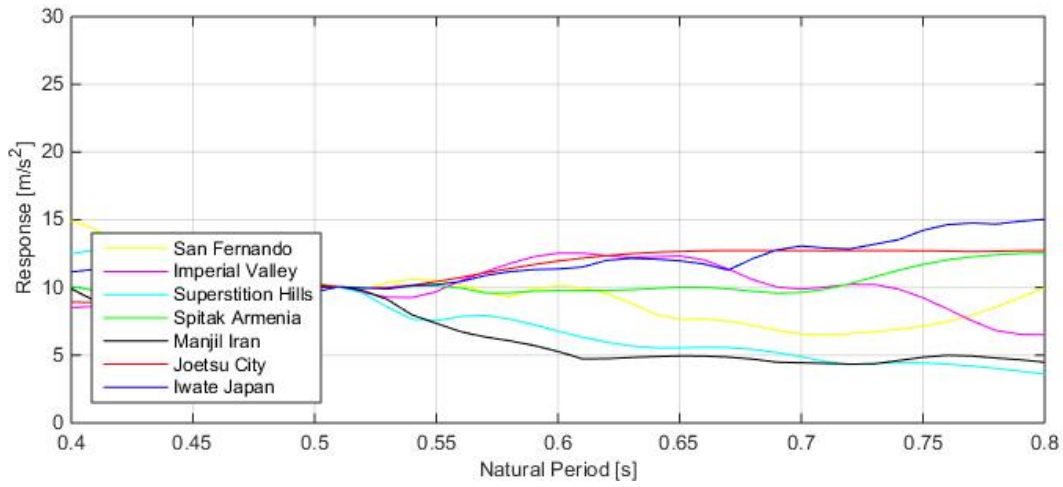
The results from NTHA suggest that the period is increased by a factor of two (approximately) during the earthquake loading. Thus, the general expression for the natural period,

$$T = 2 \times \pi \times \sqrt{\frac{m}{k}} \quad (7.4)$$

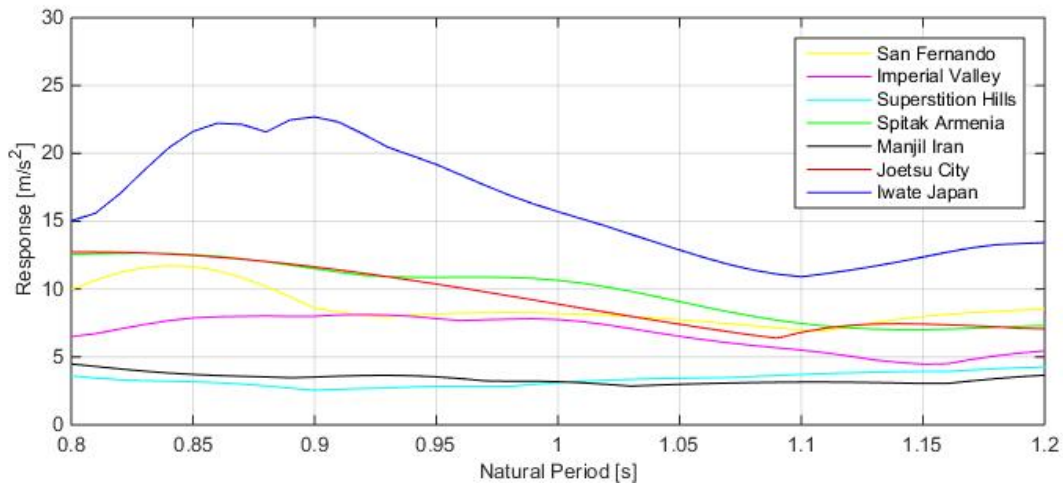
implies that the global stiffness has been reduced by a factor of 0.25. Similar results are obtained from the non-linear static analysis and will be demonstrated next. The idealized



(a) Scaled response spectrum for $0 \leq T \leq 0.4$.

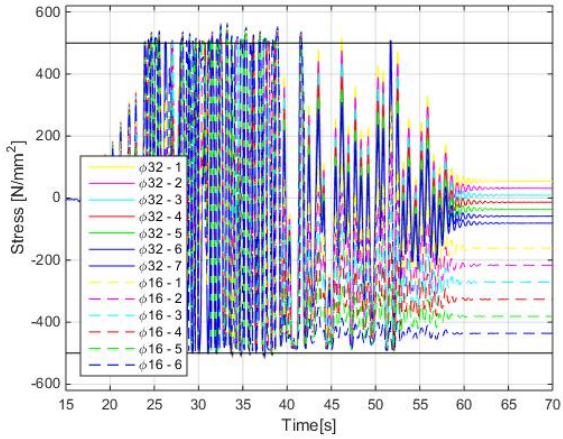


(b) Scaled response spectrum for $0.4 \leq T \leq 0.8$.

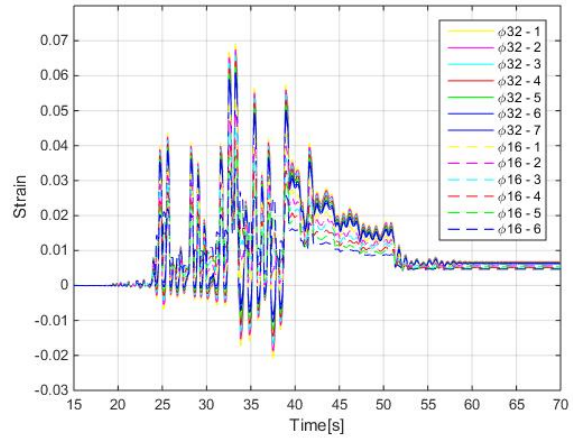


(c) Scaled response spectrum for $0.8 \leq T \leq 1.2$.

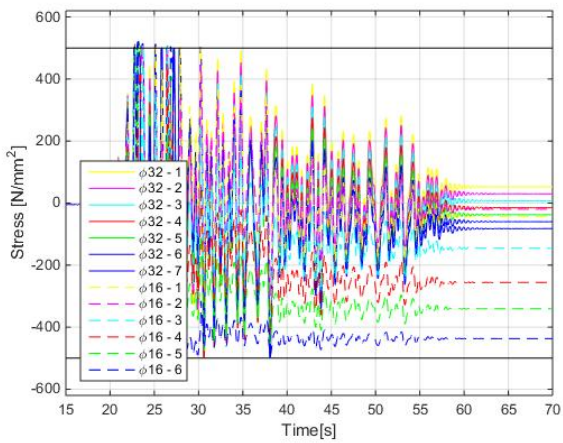
Figure 7.9: Scaled response spectrum for $0 \leq T \leq 1.2$ presented in three figures.



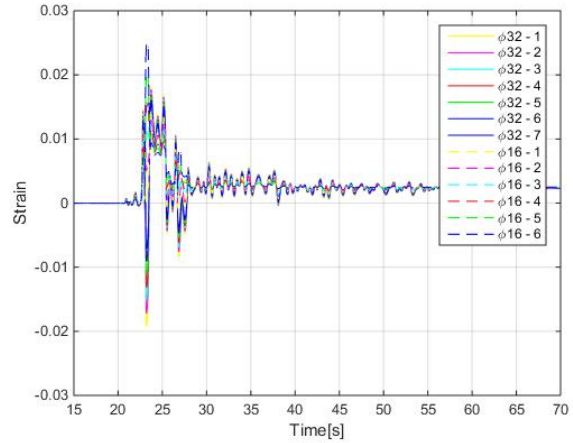
(a) Stress-time relationship, Iwate Japan



(b) Strain-time relationship, Iwate Japan



(c) Stress-time relationship, Joetsu City



(d) Strain-time relationship, Joetsu City

Figure 7.10: Stress and strain-time relationship for the reinforcement illustrated in Figure 7.4.

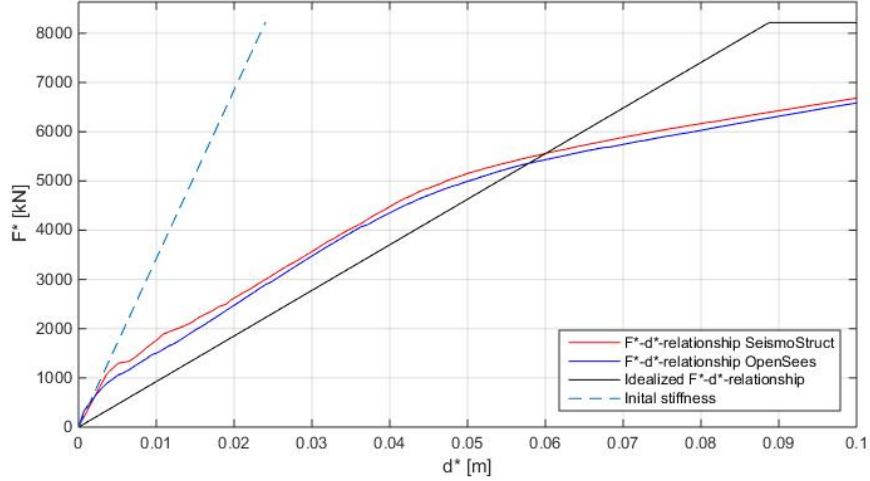


Figure 7.11: Extraction of SDOF pushover-curves together with the initial stiffness of the system.

and initial stiffness is determined in accordance with Figure 7.11, i.e.,

$$K_{idz} = \frac{F_y^*}{d_y^*} = \frac{8217\,000\text{ N}}{0.089\text{ m}} = 9.233 \times 10^7 \text{ N/m} \quad (7.5)$$

$$K_{init} = \frac{8217\,000\text{ N}}{0.024\text{ m}} = 3.424 \times 10^8 \text{ N/m} \quad (7.6)$$

Hence, the global stiffness has been reduced by a factor of $9.233 \times 10^7 \text{ N/m} / 3.424 \times 10^8 \text{ N/m} = 0.27$ during the course of loading.

It should be noted that the level of cracking varies with the various ground motion loadings, which implies that the period elongation is not consistent during different earthquakes. Individual eigenvalue analysis has therefore been performed after the structure has been exposed to the respective ground motion records, and the results are presented in Figure 7.12. The analyses are performed solely in OpenSees. To the author's knowledge, SeismoStruct offers no possibility of evaluating the eigenvalue problem post a static or dynamic analysis. The first prolonged natural periods caused by "Iwate Japan" and "Joetsu City" are equal to 0.63 s, which is slightly lower than what was approximated from the scaled response spectrum. Still, the structure experiences a first natural period prolongation by a factor of $0.63/0.35 = 1.8$, which corresponds to a global stiffness reduction factor equal to 0.30. "Manjil Iran" causes the lowest period elongation equal to 0.54 s, corresponding to a global stiffness factor of 0.42. Figure 7.12 shows that effects of cracking have the largest impact on the first mode. Generally, period prolongation correlates well with the maximum displacements obtained from the ground motions. This indicates that roof displacements are primarily affected by the first mode shape. See Figure 7.13. Altogether, the maximum displacements acquired from the non-linear time-history analysis become more sensible compared with the scaled response spectra when considering a structure with prolonged natural periods.

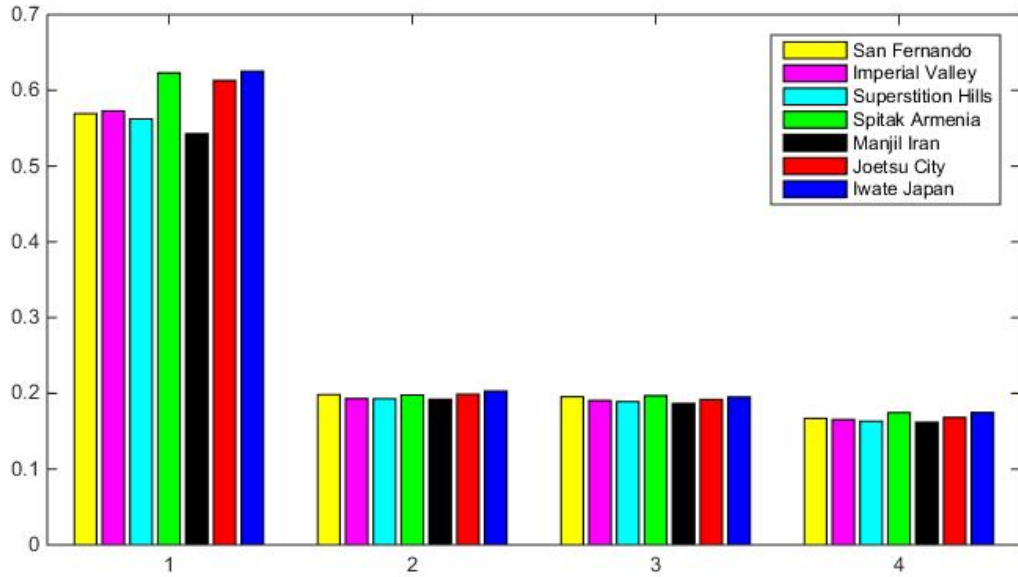


Figure 7.12: Natural periods of the cracked system. Eigenvalue analysis has been performed after the structure has been exposed to the individual ground motion.

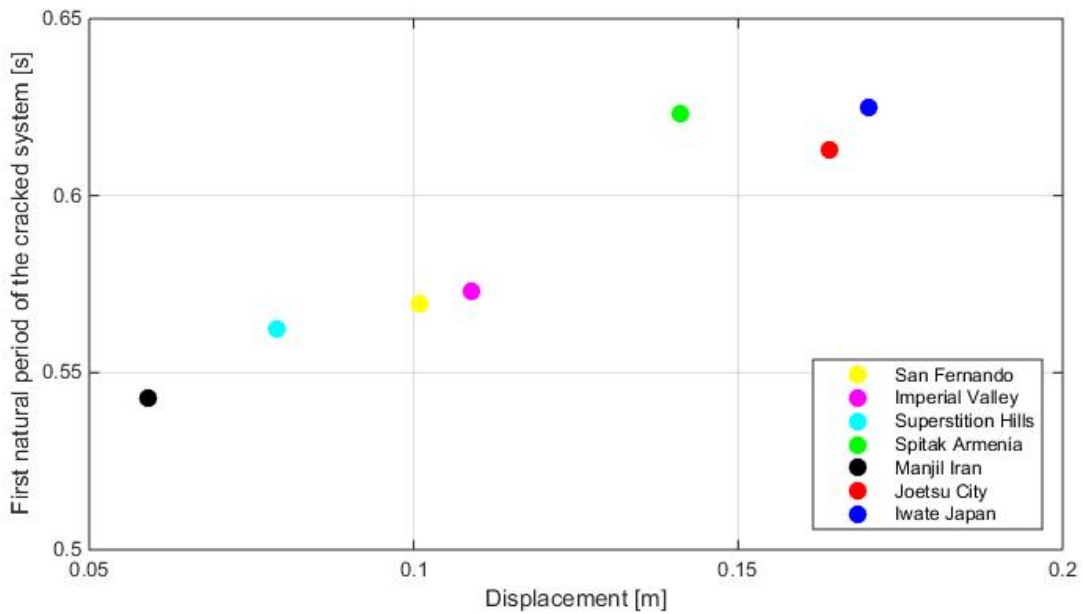


Figure 7.13: First natural periods from the cracked system plotted against the maximum displacement from the individual ground motions.

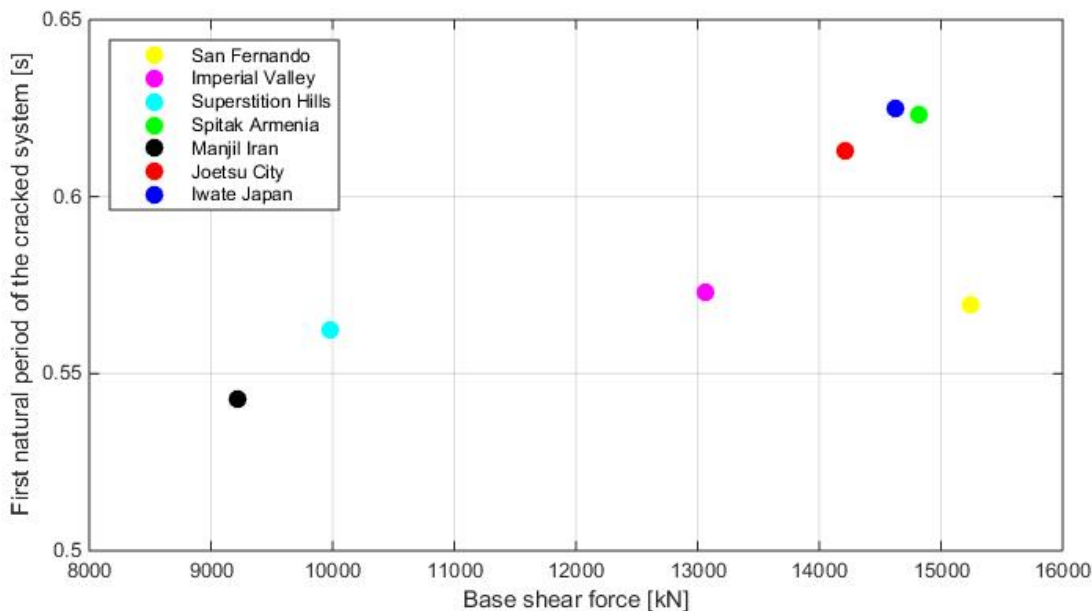


Figure 7.14: First natural periods from the cracked system plotted against the maximum base shear forces from the individual ground motions.

7.3.2 Base shear force

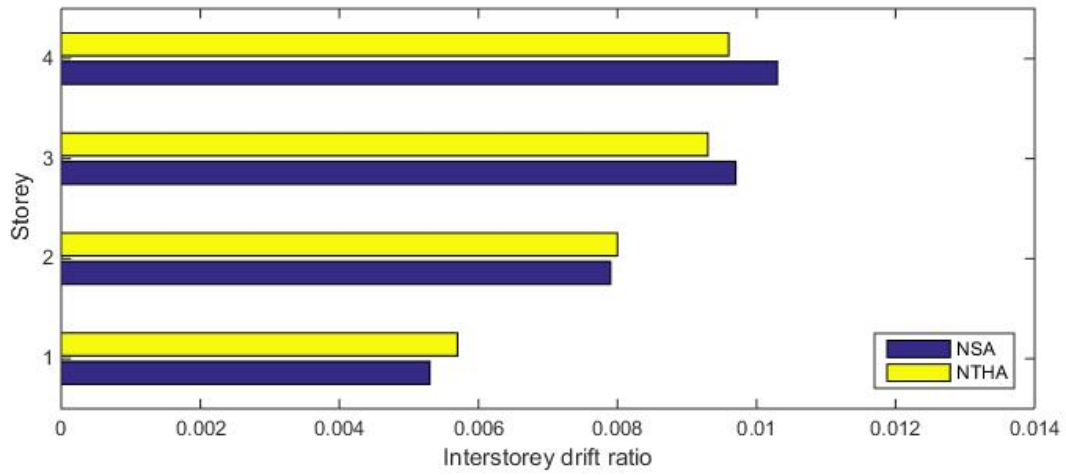
The maximum base shear forces from the individual time-histories are considerably higher than the base shear force at target displacement. Observe that the difference is larger in OpenSees [3] than in SeismoStruct [2]. See Figure 7.8. This is in compliance with a study presented in FEMA 440 [14], Appendix F, where the purpose was to expose multi-degree-of-freedom effects on structural behaviour. Five example buildings were tested, including an eight storey shear wall. Response quantities from static procedures were compared with those obtained from several non-linear dynamic analyses. In all cases, the results showed that dynamic procedures caused higher base shear forces than static procedures for roof drift ratios larger than 1 %, and that the discrepancies increased with the roof drift ratio.

As for displacement, the first natural periods of the cracked system are plotted against the maximum base shear forces obtained from the individual ground motion records and presented in Figure 7.14. Apparently, first natural periods correlate less with base shear forces than with displacements. Causing relatively low first period elongation, the "San Fernando" ground motion generates the largest base shear force. The second, third and fourth prolonged natural periods caused by "San Fernando" are between 0.17 and 0.20 s. Figure 7.9a shows that "San Fernando" dominates the response spectrum for periods within the aforementioned range. "Imperial Valley" produces approximately the same first period elongation as "Superstition Hills", but the maximum base shear force is substantially larger. Similar to "San Fernando", the ground motion induces high spectral accelerations for higher modes. This implies that base shear forces are more sensitive to multi-degree-of-freedom effects than roof

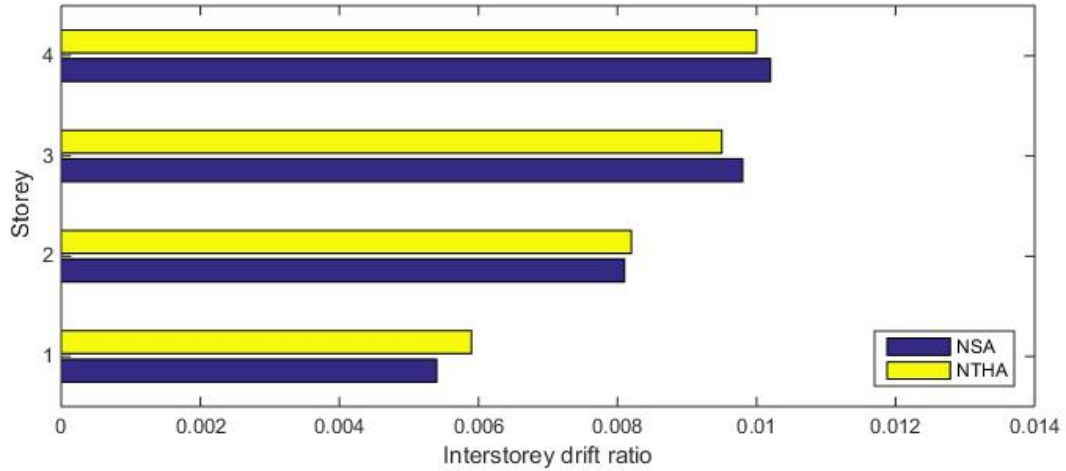
displacements, which also explains why dynamic analyses produce higher base shear forces than static procedures based on the first mode shape. This can also be observed in Figure 7.8. The base shear forces from "San Fernando" and "Imperial Valley" are substantially larger than the base shear force obtained at target displacement. The maximum displacements, however, are practically identical to the target displacement. In opposite to displacements, base shear forces are directly related to accelerations. It is clearly seen from the scaled response spectrum in Figure 7.9, that spectral accelerations are considerably higher in lower modes for "San Fernando" and "Imperial Valley".

7.3.3 Interstorey drift ratios

Figure 7.15 presents a comparison between the average interstorey drift ratios (IDR) from the seven ground motions and those obtained from NSA. It should be noticed that the maximum IDRs are not attained simultaneously during the time-history. Figure 7.15 shows that the non-linear time-history analysis renders slightly higher ratios for the 1st and 2nd storey, while the opposite is the case for the 3rd and 4th storey. Figures 7.16-7.22 compare the individual IDRs with the values from NSA, assessed at target displacement equal to the maximum roof displacement of the respective ground motion. High IDRs in upper stories imply contributions from higher modes. It is therefore interesting that "San Fernando" and "Imperial Valley" do not generate higher IDRs in the upper stories considering that the response spectrum in Figure 7.9 indicates the opposite. See Figures 7.16 and 7.17. Drift ratios caused by "Manjil Iran" and Superstition Hills are presented in Figures 7.18 and 7.20. Both ground motions induce IDRs that are in near perfect agreement with NSA. This complies Figure 7.9, which clearly shows that these records are dominated by the first mode. "Spitak Armenia" induces higher drift ratios in all stories. See Figure 7.19. It is observed from Figures 7.21 and 7.22 that "Joetsu City" and "Iwate Japan" cause lower ratios than NSA in the upper stories, which also correlate well the scaled response spectrum in Figure 7.9.



(a) SeismoStruct.



(b) OpenSees.

Figure 7.15: Interstorey drift ratio comparison between NSA and the average values from NTHA.

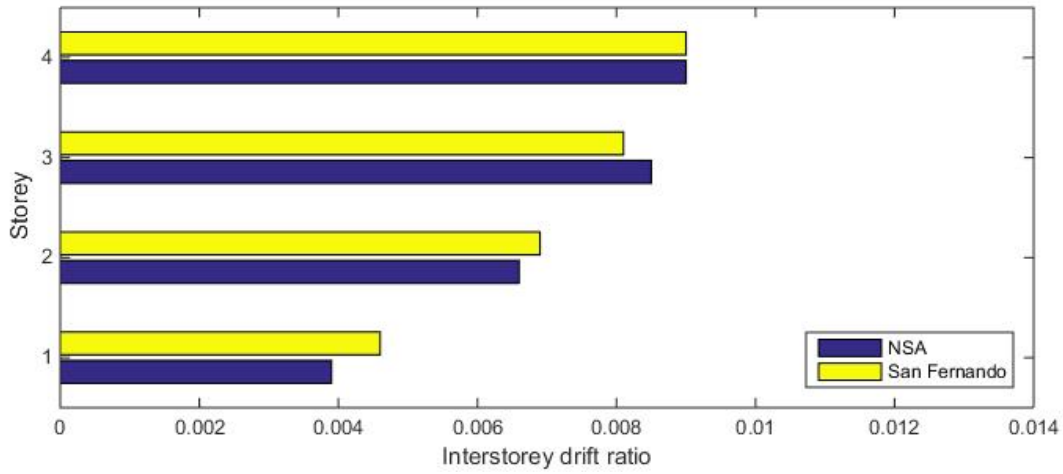


Figure 7.16: Interstorey drift ratio comparison between NSA and San Fernando. The drift ratios from NSA are assessed at target displacement equal to maximum roof displacement from San Fernando. The values are obtained from SeismoStruct.

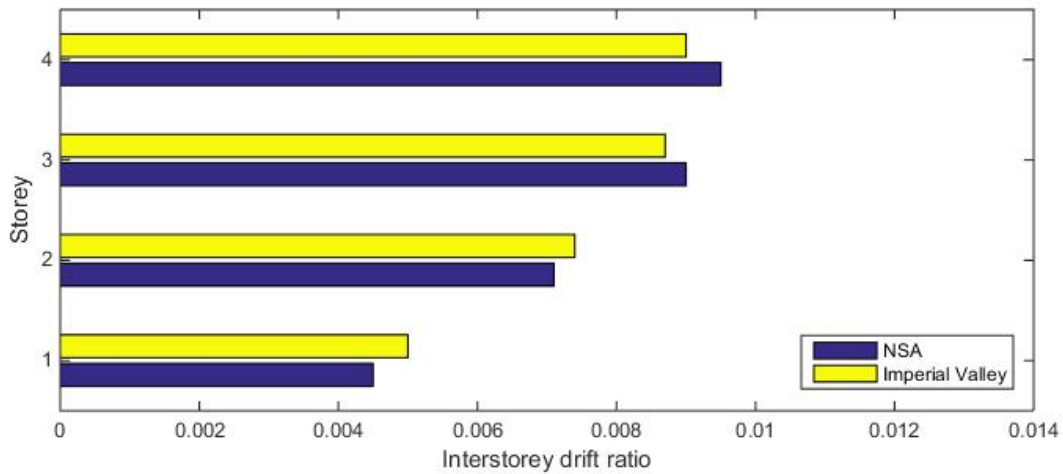


Figure 7.17: Interstorey drift ratio comparison between NSA and Imperial Valley. The drift ratios from NSA are assessed at target displacement equal to maximum roof displacement from Imperial Valley. The values are obtained from SeismoStruct.

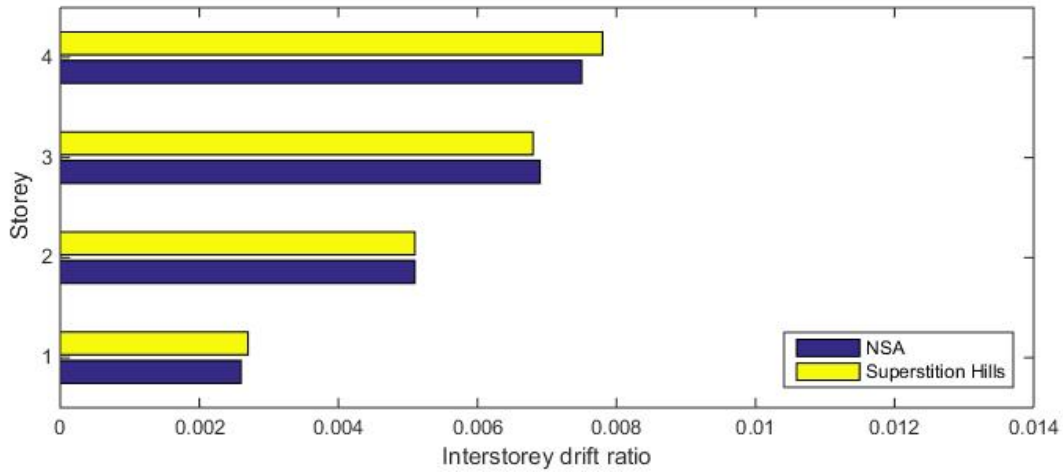


Figure 7.18: Interstorey drift ratio comparison between NSA and Superstition Hills. The drift ratios from NSA are assessed at target displacement equal to maximum roof displacement from Superstition Hills. The values are obtained from SeismoStruct.

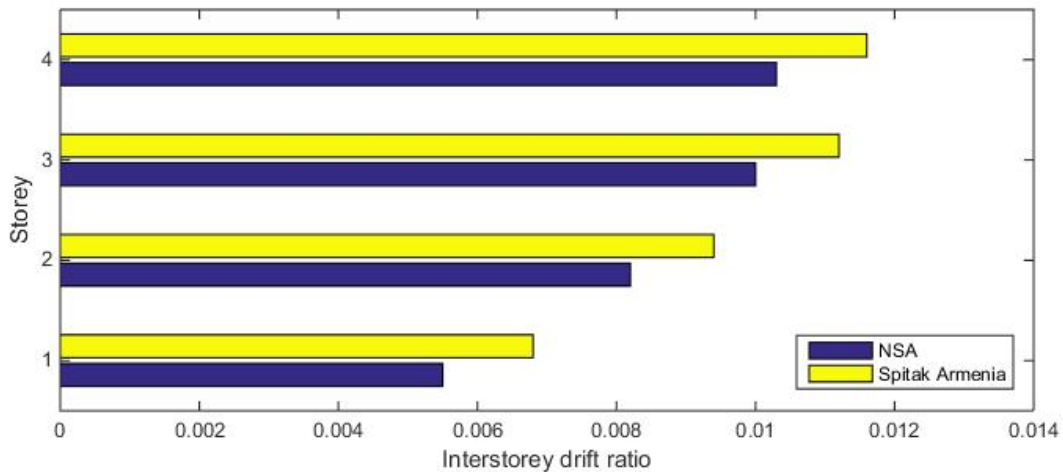


Figure 7.19: Interstorey drift ratio comparison between NSA and Spitak Armenia. The drift ratios from NSA are assessed at target displacement equal to maximum roof displacement from Spitak Armenia. The values are obtained from SeismoStruct.

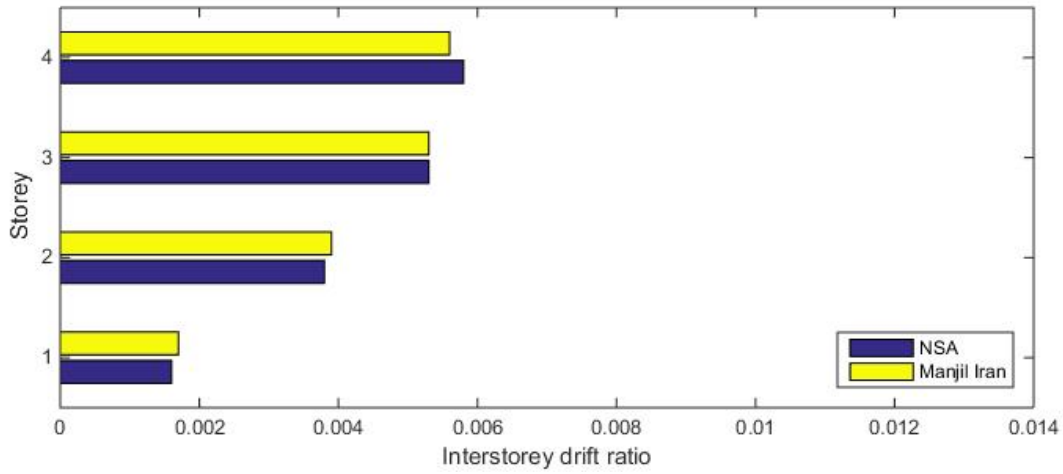


Figure 7.20: Interstorey drift ratio comparison between NSA and Manjil Iran. The drift ratios from NSA are assessed at target displacement equal to maximum roof displacement from Manjil Iran. The values are obtained from SeismoStruct.

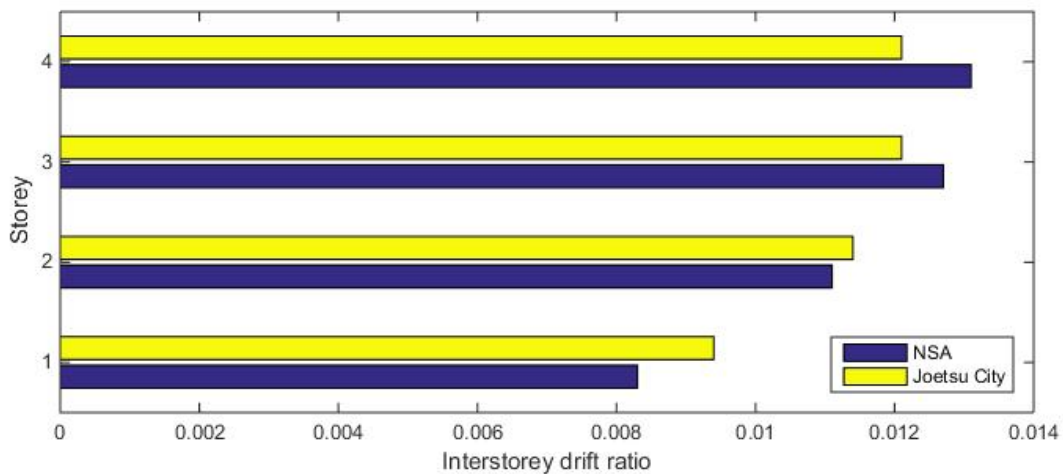


Figure 7.21: Interstorey drift ratio comparison between NSA and Joetsu City. The drift ratios from NSA are assessed at target displacement equal to maximum roof displacement from Joetsu City. The values are obtained from SeismoStruct.

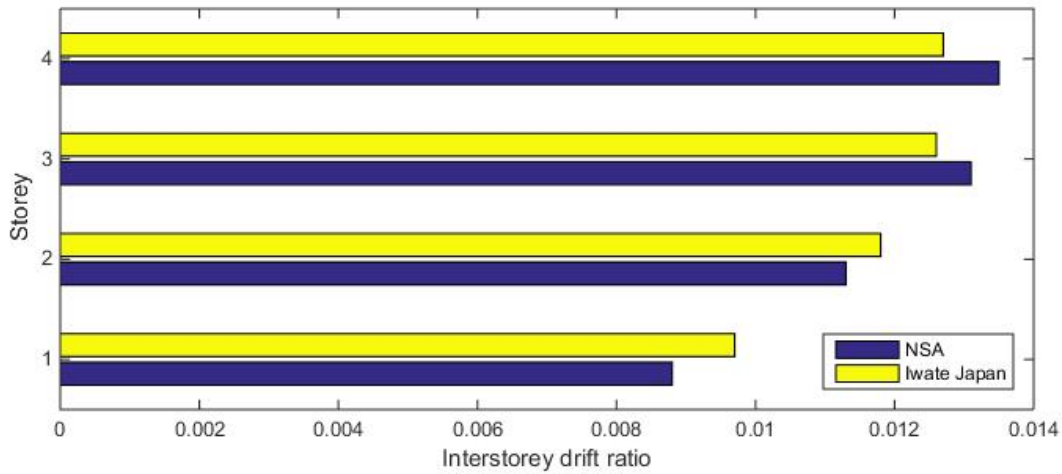


Figure 7.22: Interstorey drift ratio comparison between NSA and Iwate Japan. The drift ratios from NSA are assessed at target displacement equal to maximum roof displacement from Iwate Japan. The values are obtained from SeismoStruct.

7.4 Requirements in EN 1998-1

7.4.1 Ductility and over-strength

The structure was designed "conventionally" with the application of the linear static analysis for high ductility in accordance with guidelines given in EN 1998-1 [1]. The modification factor q was determined equal to 3.51. In accordance with the principles discussed in Section 2.1, and with reference to the non-linear static analysis procedures presented in Figures 5.1c and 7.23, the force reduction factor μ is equal to unity. This implies that even though expecting and designing for high ductility, the structural response nearly remained in the elastic range. The over-strength factor,

$$\Omega = \frac{11\,200\text{ kN}}{6\,815\text{ kN}} = 1.64 \quad (7.7)$$

and modification factor q is thus equal to 1.64. The code-based q exceeds the assessed q by a factor of $3.51/1.64 = 2.14$. In Section 3.3.2, the design base shear force was determined equal to 3 718 kN. The structure is however experiencing a base shear force equal to 8 579 kN. If the assessed q was applied in the linear static analysis, the design base shear force would be equal to

$$F_b = \frac{3\,718\text{ kN} \times 3.51}{1.64} = 7\,958\text{ kN} \quad (7.8)$$

which agrees better with the actual obtained shear force at target displacement.

7.4.2 Reduction of stiffness

EN 1998-1 [1], section 4.3.1 states that unless an evaluation of the concrete members in the *cracked* state is performed, the stiffness parameters must be set equal to half the values

in the *non-cracked* state. Both the static and dynamic analysis discussed in Section 7.3 revealed that global stiffness was reduced by a factor ranging between 0.31 and 0.42 during the course of seismic loading. The reduction was mainly caused by cracking of unconfined concrete. There is a significant difference in the prolongation of natural periods if the stiffness is reduced by a factor of 0.5 compared to 0.31. Considering a mass equal to unity, the natural periods are prolonged by a factor of

$$\frac{T_{0.5 \times k^2}}{2 \times \pi} = \sqrt{\frac{1}{0.5}} = 1.41 \quad (7.9)$$

$$\frac{T_{0.31 \times k^2}}{2 \times \pi} = \sqrt{\frac{1}{0.31}} = 1.80 \quad (7.10)$$

for stiffness reduction factors equal to 0.5 and 0.31, respectively. Structural walls are less sensitive to stiffness reduction caused by cracking due to large cross sectional heights. It therefore interesting to investigate global softening of structure when the shear walls are replaced by interior beams. The eigenvalue analysis is therefore performed (in OpenSees) after the frame structure is subjected to "Joetsu City" and "Iwate Japan". The first four natural periods prior seismic loading,

$$T = [0.809 \quad 0.260 \quad 0.144 \quad 0.116] \text{ s} \quad (7.11)$$

The prolonged natural periods are,

$$T = [1.145 \quad 0.358 \quad 0.195 \quad 0.187] \text{ s} \quad (7.12)$$

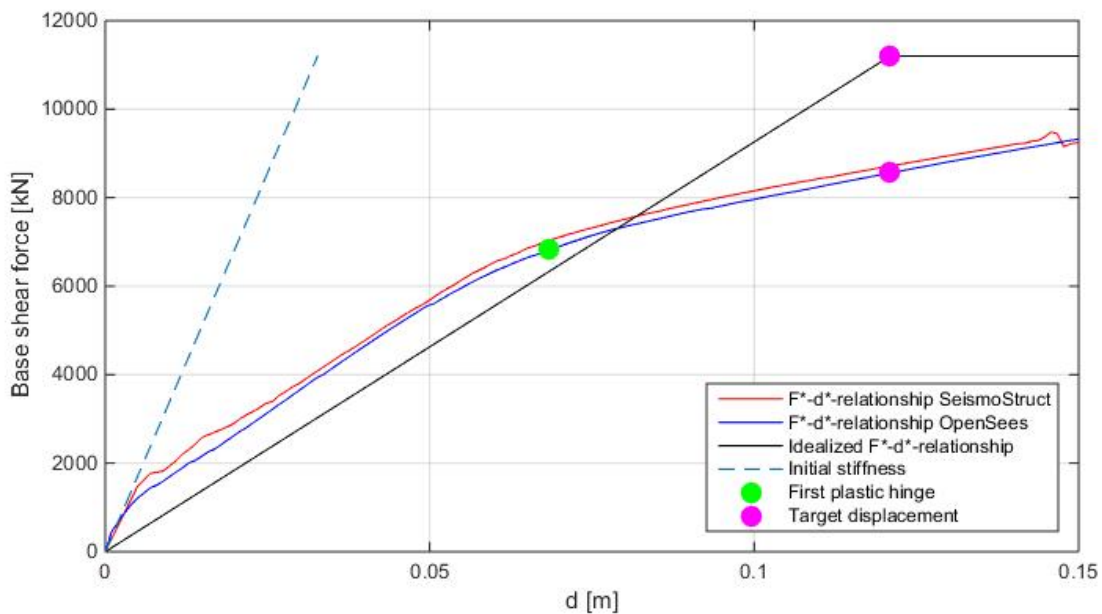


Figure 7.23: Base shear-displacement relationship, target displacement and first plastic hinge from the non-linear static analysis for $0 \text{ m} \leq d \leq 0.1 \text{ m}$.

$$T = [1.320 \quad 0.396 \quad 0.213 \quad 0.206] \text{ s} \quad (7.13)$$

caused by "Joetsu City" and "Iwate Japan", respectively. The first natural period is prolonged by a factor of $1.32/0.81 = 1.63$ for "Iwate Japan" and $1.15/0.81 = 1.42$ for "Joetsu City", which is less than for the stiff frame-wall structure. This was not expected and contradicts the results acquired by Mwafy and Elnashai [30]. It was however observed that the natural periods prior cracking are substantially longer compared to the wall-frame system. Time limitations prevent further investigation.

Throughout the guidelines in Eurocode, the natural periods of the structure influence design through the assessment of acting forces, reduction factors, detailing of members etc., and discrepancies of the magnitude presented can be of great significance in terms of structural configuration and member dimensions. Both the frame-wall and the frame structure experienced modal alterations beyond the recommendations in EN 1998-1. This indicates that the code is non-conservative since a larger reduction of stiffness results in larger displacements.

7.4.3 Shear demands in EN 1998-1

In DCH, the evaluation of acting shear forces on ductile walls primarily depends on whether the wall is slender or stump. The results from Chapter 4 exposed that the walls are responding in conjunction. This is evident from the mode shapes, together with the fact that including shear deformations did not have a significant effect on the modal properties. The latter directly indicates beam-like behaviour. Therefore, the first storey wall was designed as a slender wall, and the acting shear force was increased by the amplification factor determined by Equation 3.40, i.e. 1.75.

The shear *capacity* requirements for DCH are given in EN 1998-1 [1], sections 5.5.3.4.2 and 5.5.3.4.3. The former section evaluates compression failure due to shear, where the capacity is determined according to EN 1992-1-1 [19], section 6.2.3 and reduced by 40 % within the critical boundaries. Section 5.5.3.4.3 evaluates tension failure due to shear, and states that if α (Equation 3.42) is larger than 2.0, the wall is considered slender and expected to fail in moment. The shear capacity is determined in accordance with EN 1992-1-1 [19], section 6.2.3 without additional requirements. If α is less or equal 2.0, the wall is considered stump and expected to fail in shear. The shear capacity is therefore determined through a comprehensive and rigorous set of guidelines that increase the demands. For the 1st storey wall, the combination of acting moment, shear force and wall length resulted in α less than 2.0, thus implying a stump wall. It is paradoxical that the acting shear forces are assessed considering a slender wall, which generally gives higher amplification factors, while the capacity is determined considering a stump wall, which gives lower capacities. In practice, the acting shear forces are increased due to redistribution of forces in addition to possible dynamic effects related to slender walls. Then, the capacity is further reduced because the wall is considered stump and expected to fail in shear. It is evident that these requirements are inconsistent and self-contradictory. They are the main reason for the dimension increase of the 1st storey wall and thus primarily accountable for not achieving inelastic structural

response. Essentially, fulfilling the shear demands in DCH, i.e. a ductility class that allows for *high* ductility, resulted in a structural system that failed to exhibit ductile behaviour.

7.4.4 DCM versus DCH

The shear force demands for ductile walls given in EN 1998-1 [1] are substantially simpler and less rigorous for DCM than for DCH. The shear *capacity* demands for DCM essentially state that, in addition to the requirements in EN 1992-1-1 [19], section 6.2.3, the normalized axial force must not exceed 0.4. The *acting* shear forces on ductile walls are increased by a amplification factor of 1.5. It must be emphasized that design in accordance with DCM gives a lower q-factor. For the given structure, the q-factor in DCM is equal to 2.34. In order to compare DCH with DCM in terms of the structural behaviour, the 1st storey wall is designed according to the aforementioned guidelines for DCM. The acting base shear force, when accounting for accidental torsion,

$$V_{Ed} = V_{Ed}' \times \varepsilon = 1770 \text{ kN} \times \frac{3.51}{2.34} \times 1.5 \times 1.347 = 5\,364 \text{ kN} \quad (7.14)$$

and the acting moment,

$$M_{Ed} = 17\,637 \text{ kNm} \times \frac{3.51}{2.34} \times 1.347 = 36\,635 \text{ kNm} \quad (7.15)$$

The design forces in DCM are higher than in DCH, but the capacity requirements are less rigorous. First, the vertical bending reinforcement is determined in BtSnitt [22] and the result is $\phi 32c90 + 7\phi 40$ in the critical boundary area. Shear capacity is determined according to EN 1992-1-1 [19] and the calculations are performed in Matlab [20]. The moment capacity is equal to 36 976 kNm and the shear capacity is equal to 5 845 kN. The dimensions and reinforcement is chosen such that the ductility demands in EN 1998-1 [1], section 5.4.3.4.2 are satisfied. The 1st storey wall characteristics are presented in Table 7.1.

Next, the non-linear static analysis is assessed when the 1st storey wall is designed according to the guidelines for DCM in EN 1998-1. It is emphasized that *solely* the first storey wall is designed in DCM. The remaining walls, beams and columns are kept in DCH. In practice, designing one member in DCM and the others in DCH does not make sense due to the various demands that depend on q-factors, natural periods etc., which are all contingent on the ductility class. The purpose of this experiment is to evaluate the structural behaviour when the dominating member is designed in a lower ductility class. The pushover-curve, together

Table 7.1: The 1st storey wall designed in DCM.

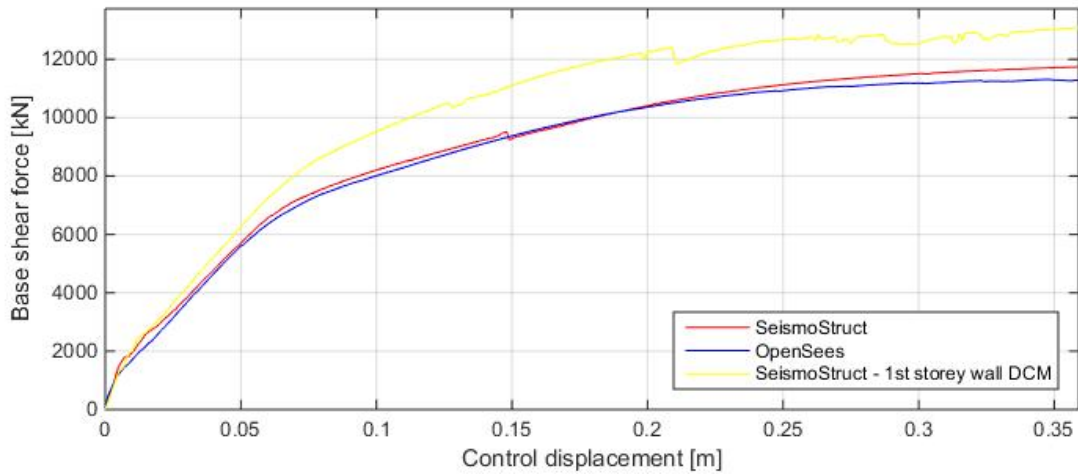
Storey	b_c (mm)	b_{wo}	l_c (mm)	Vert. reinf.	Vert. reinf. l_c	Hor. reinf.	Stirrups I_c
1st	220	220	700	$\phi 12c250$	$\phi 32c90 + 7\phi 40$	$\phi 16c100$	$\phi 12c75$

Table 7.2: Target displacement calculations according to EN 1998-1, Appendix B. Structural system with 1st storey wall designed in DCM.

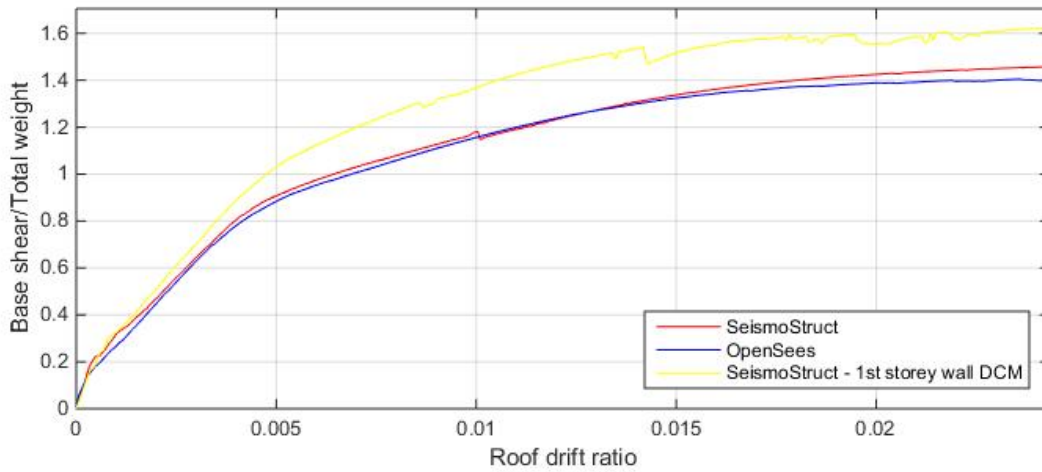
Iteration	d_m^* (m)	F_y^* (kN)	E_m (kN \times m)	d_y^* (m)	T (s)	d_t^* (m)	d_t^*/d_m^*
0	0.200	9 102	1 394	0.093	0.58	0.085	0.425
0	0.085	9 102	403	0.081	0.54	0.074	0.871
0	0.074	9 102	324	0.077	0.52	0.070	0.946
0	0.070	9 102	294	0.076	0.52	0.068	0.971
0	0.068	9 102	284	0.074	0.51	0.067	0.985
0	0.067	9 102	274	0.074	0.51	0.067	1.000

with the curves from the original system, is presented in Figures 7.24a and 7.24b. The target displacement is calculated in the same manner as in Chapter 5, and the results are presented in Figure 7.24 and in Table 7.2. The structural response is even less ductile than for the original structure, which is to be expected due to increased longitudinal reinforcement. The decrease of wall width did not impact structural response due the fact that shear deformations were not included in the model. The results from Chapter 4 revealed that shear deformations are not of importance for the respective structure. The ratio between target and yield displacement is equal to $0.067 \text{ m}/0.074 \text{ m} = 0.905$, indicating that the structure is responding well within the elastic range.

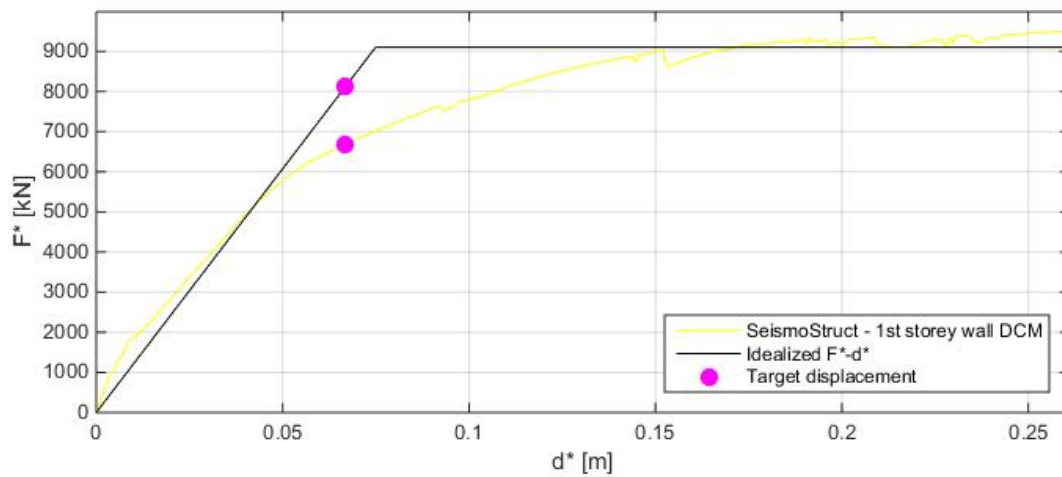
It is noteworthy that the structure does not exhibit ductility, neither in DCM nor in DCH, according to the non-linear static analysis. However, the results from the non-linear time-history procedure assessed in Chapter 6 implied that the structure does in fact respond past the elastic limit, but the magnitude of inelastic response is less than expected for a building designed in DCH. Considering the requirements in EN 1998-1, it is positive that the DCM-system indicated less ductility than the DCH-system. Nevertheless, fulfilling the requirements in EN 1998-1 generally resulted in less ductile behaviour than what was desired and expected.



(a) Base shear-control displacement relationship.



(b) Normalized base shear-roof drift ratio relationship.



(c) F^*-d^* -relationship.

Figure 7.24: Base shear-displacement relationship for the structure with 1st storey wall designed in DCM.

7.5 Effect of integration points

The motivation behind this post-analysis experiment is that prior to achieving the desired pushover curves and time-history responses, convergence issues were experienced in both SeismoStruct [2] and OpenSees [3]. Originally, force-based elements with seven integration points were applied. Even though multiple solution strategies were tried by altering integrators, algorithms, time-steps etc., the solution always diverged before the target displacement was reached or time-history analysis completed. It is therefore interesting to investigate the application of a various number of IPs in both SeismoStruct and OpenSees in terms of convergence. The analyses performed in Chapters 4, 5 and 6 were based on force-based beam-column elements with four integration points.

2 This section briefly evaluates the effects of increasing the number of integration points through the non-linear static analysis. The building is "pushed" to a displacement of 0.6 m and the pushover-curve is presented in Figure 7.25. The filled circles and squares indicate where divergence occurs. Evidently, the solution in SeismoStruct converges for 4 and 5 integration points, but diverges for every other configuration. It is observed that the displacement at which the solution diverges, decreases with increasing number of integration points. The same trend is however *not* observed in OpenSees, where convergence issues occur somewhat randomly considering the number of IPs. It is observed that the drop in SeismoStruct occurs at different displacement steps when applying 4 and 5 integration points. Thorough evaluation of force-based inelastic elements is beyond the scope of this thesis and will not be further discussed. The readers is referred to the literature [16, 28].

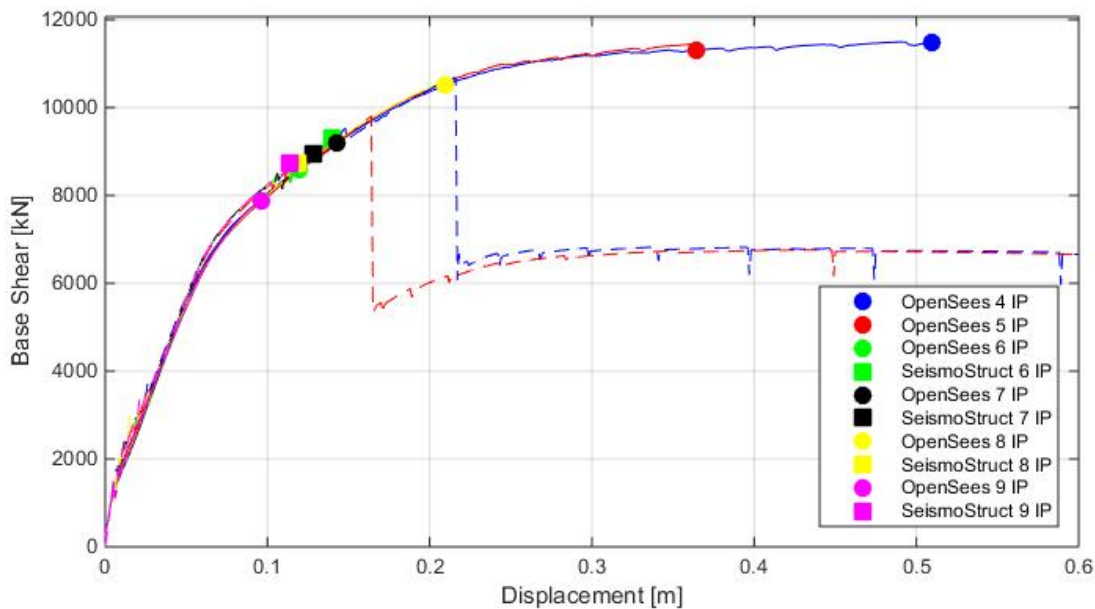


Figure 7.25: Non-linear analysis with varying number of integration points.

Chapter 8

Conclusion

8.1 EN 1998-1

During the course of design, it was observed more than often that fulfilling one requirement in the governing code resulted in the strengthening of another. The author's experience was that the several approximated and empirically estimated parameters made it difficult to exercise rational judgement when designing members. Even though expecting, and designing for, high ductility, the structural response remained nearly in the elastic range. For the structure in question, the q-factor was determined equal to 3.51 according to EN 1998-1 [1], while the non-linear static analysis implied 1.64. The elastic behaviour was a result of oversized and heavily reinforced members, with emphasis on the lower storey walls. The reduction of global stiffness caused by the selected time-history ground motions was greater than the recommendation in EN 1998-1. The stiffness reduction factor varied from 0.31 to 0.42, depending on the ground motion, while EN 1998-1 recommended 0.5. Throughout the guidelines in Eurocode, the natural periods of the structure influenced design through the assessment of acting forces, reduction factors, detailing of members etc., and were of great significance in terms of structural configuration and member dimensions. Thus, underestimating the reduction of stiffness may be highly unfortunate for the final design and should therefore be avoided by assessing modal properties in the cracked state.

8.2 Dynamic versus static procedures

The non-linear static analysis rendered reasonable results in terms of displacements for the first-mode-dominated structure. There were however significant differences between the maximum displacements obtained from individual records and the target displacement from the static analysis. This highlights the importance of applying multiple ground motions in the assessment of NTHA. The results revealed that dynamic analyses induced stronger base shear forces than static procedures due higher mode effects. The largest discrepancies were experienced for ground motions with significant high-frequency content. It has been demonstrated

that the structure's natural sensitivity to multi-degree-of-freedom effects limited the static analysis based on a single mode shape, consequently not revealing possible behaviour. However, the static analysis had the advantage of displaying a clear image of stiffness, strength and ductility, together with the ability of approximating a target displacement within reasonable time consumption. The "exact" non-linear time-history analysis was dependent on successful selection and scaling of ground motions, in addition to a sufficiently accurate finite element model. The static analysis, within its range of validity, enabled for the confirmation of results from the time-history procedures. For complete evaluation of structural response and general performance, it is therefore recommended to perform both a static and dynamic non-linear analysis when evaluating seismic problems.

8.3 SeismoStruct versus OpenSees

SeismoStruct [2] has the clear advantage of a graphical interface that allows for easy and time-efficient modelling of structures. In addition, the user is able to evaluate response parameters graphically without the use of external applications, which is of great convenience in the early stages of model establishment. Compared to OpenSees [3], SeismoStruct is limited in terms of element assortment, algorithms, integrators and output selection. It is noteworthy that the latter lacks elements that take into account shear deformations. SeismoStruct is therefore inadequate when assessing structural response of short building containing shear walls. OpenSees has the advantage of flexibility and is thus generally more robust, both in terms of equation solving and structural configuration. In addition, OpenSees allows for solving the eigenvalue problem post analysis and thus assessing the modal properties for RC-systems in the cracked state. Except for the fact that OpenSees rendered higher base shear forces, the response quantities generally matched.

Bibliography

- [1] C. E. de Normalisation, “Eurocode 8: Design of structures for earthquake resistance: Part 1: General rules, seismic actions and rules for buildings,” 2004.
- [2] SeismoStruct, *SeismoStruct is a FEM-program developed for the analytical assessment of structures subjected to earthquake strong motion*. Seismosoft Ltd, Version 7.0.2, 2015.
- [3] OpenSees, *The Open System for Earthquake Engineering Simulation (OpenSees) is a software framework for simulating the seismic response of structural and geotechnical systems*. Pacific Earthquake Engineering Research Center, Version 2.4.5, 2013.
- [4] B. Asgarian and H. Shokrgozar, “Brbf response modification factor,” *Journal of constructional steel research*, vol. 65, no. 2, pp. 290–298, 2009.
- [5] M. Priestley, G. Calvi, and M. Kowalsky, “Direct displacement-based seismic design of structures,” in *2007 NZSEE Conference*, 2007.
- [6] B. S. S. Council, “Prestandard and commentary for the seismic rehabilitation of buildings,” *Report FEMA-356, Washington, DC*, 2000.
- [7] N. Øystad-Larsen, “Dimensjonering for jordskjelv: Teorigrunnlag, regelverk og beregninger,” 2010.
- [8] A. K. Chopra, *Dynamics of structures*, vol. 4. Prentice Hall New Jersey, 1995.
- [9] C. E. de Normalisation, “Eurocode 8: Design of structures for earthquake resistance: Part 3: Assessment and retrofitting of buildings,” 2004.
- [10] R. K. Goel and A. K. Chopra, “Evaluation of modal and fema pushover analyses: Sac buildings,” *Earthquake Spectra*, vol. 20, no. 1, pp. 225–254, 2004.
- [11] P. Fajfar and M. Dolšek, “Pushover-based analysis in performance-based seismic engineering—a view from europe,” in *Performance-Based Seismic Engineering: Vision for an Earthquake Resilient Society*, pp. 265–277, Springer, 2014.
- [12] P. Fajfar and M. Fischinger, “N2-a method for non-linear seismic analysis of regular buildings,” in *Proceedings of the Ninth World Conference in Earthquake Engineering*, vol. 5, pp. 111–116, 1988.

BIBLIOGRAPHY

- [13] S. Antoniou and R. Pinho, “Advantages and limitations of adaptive and non-adaptive force-based pushover procedures,” *Journal of Earthquake Engineering*, vol. 8, no. 04, pp. 497–522, 2004.
- [14] A. T. Council, “Improvement of nonlinear static seismic analysis procedures,” *FEMA-440, Redwood City*, 2005.
- [15] J. P. Moehle, “Performance-based seismic design of tall buildings in the us,” in *14th World Conference on Earthquake Engineering (CD), Beijing, China*, 2008.
- [16] A. Calabrese, J. P. Almeida, and R. Pinho, “Numerical issues in distributed inelasticity modeling of rc frame elements for seismic analysis,” *Journal of Earthquake Engineering*, vol. 14, no. S1, pp. 38–68, 2010.
- [17] E. Weisstein, “Wolfram mathworld: The web’s most extensive mathematics resource,” 2015.
- [18] C. E. de Normalisation, “Eurocode 0: Basis of structural design,” 2008.
- [19] C. E. de Normalisation, “Eurocode 2: Design of concrete structures: Part 1: General rules and rules for buildings,” 2010.
- [20] MATLAB, *MATLAB (matrix laboratory) is a multi-paradigm numerical computing environment and programming language*. The MathWorks, Inc., Version 8.4 R2014b, 2014.
- [21] G-Prog, *G-Prog is FEM-program developed for the assessment of structural elements*. Norconsult Informasjonssystemer, Version 7.3.1, 2010.
- [22] BtSnitt, *BtSnitt program that calculates the cross sectional capacities of concrete members*. Sivilingenior Ove Sletten, Version 6.1.1, 2010.
- [23] SHARE, “European seismic hazard map 2013,” <http://www.share-eu.org/node/90>, April 2015.
- [24] Robot, *Robot Structural Analysis Professional is an BIM-integrated FEM-software developed for the assessment of structural analysis and member design*. . Autodesk, Inc., Version 2.4.5, 2013.
- [25] R. D. Cook, D. S. Malkus, P. M. E., and R. J. Witt, *Concepts and applications of finite element analysis*, vol. 4. John Wiley and Sons, INC., 2002.
- [26] OpenSeesWiki, “Openseeswiki is a wiki creation. the goal is to provide information about opensees. <http://opensees.berkeley.edu/wiki/>,” 2015.
- [27] P. E. E. R. Center, “Peer ground motion database,” <http://ngawest2.berkeley.edu/>, April 2015.
- [28] A. Gharakhanloo, “Distributed and concentrated inelasticity beam-column elements used in earthquake engineering,” 2014.

BIBLIOGRAPHY

- [29] H. Krawinkler and G. Seneviratna, “Pros and cons of a pushover analysis of seismic performance evaluation,” *Engineering structures*, vol. 20, no. 4, pp. 452–464, 1998.
- [30] A. Mwafy and A. Elnashai, “Static pushover versus dynamic collapse analysis of rc buildings,” *Engineering structures*, vol. 23, no. 5, pp. 407–424, 2001.

Appendices

Appendix A

Calculations

A.1 Loads

Gravity loads

$$Q_D = 25 \text{ kN/m}^3 \times 0.12 \text{ m} + 0.5 \text{ kN/m}^2 = \underline{3.5 \text{ kN/m}^2}$$

$$Q_{G, \text{Roof}} = 3.5 \text{ kN/m}^2 + 0.8 \times 0.2 \times 0.0 \text{ kN/m}^2 = \underline{3.5 \text{ kN/m}^2}$$

$$Q_{G, \text{Story}} = 3.5 \text{ kN/m}^2 + 0.8 \times 0.3 \times 0.0 \text{ kN/m}^2 = \underline{4.0 \text{ kN/m}^2}$$

$$Q_D = 0.7 \times 3.5 \text{ kN/m}^2 = \underline{2.5 \text{ kN/m}^2}$$

$$Q_L = 0.7 \times 2.0 \text{ kN/m}^2 = \underline{1.4 \text{ kN/m}^2}$$

$$q_{Ed, \text{bdr}} = 2.6 \text{ m} \times \max [1.35 \times 3.5 \text{ kN/m}^2 + 1.05 \times 2.0 \text{ kN/m}^2, 1.15 \times 3.5 \text{ kN/m}^2 + 1.05 \times 2.0 \text{ kN/m}^2]$$

$$= \underline{18.4 \text{ kN/m}}$$

$$q_{Ed, \text{bdr}} = (3.4 \text{ m} + 3 \text{ m}) \times \max [1.35 \times 3.5 \text{ kN/m}^2 + 1.05 \times 2.0 \text{ kN/m}^2, 1.15 \times 3.5 \text{ kN/m}^2 +$$

$$1.05 \times 2.0 \text{ kN/m}^2] = \underline{45.3 \text{ kN/m}}$$

Seismic design situation

$$\text{For the border beam, } M_{Ed, \text{Top}} = 74 \text{ kN} \times 1.6 = \underline{118 \text{ kNm}}$$

$$M_{Ed, \text{Bottom}} = 31 \text{ kN} \times 1.6 = \underline{50 \text{ kNm}}$$

For the interior beams connected to the border column,

$$M_{\text{Ed,Top}} = 122 \text{ kNm} \times 1.347 = \underline{164}$$

$$M_{\text{Ed,Bottom}} = 75 \text{ kNm} \times 1.347 = \underline{101 \text{ kNm}}$$

For the interior beams connected to the interior column,

$$M_{\text{Ed,Top}} = 200 \text{ kNm} \times 1.347 = \underline{269 \text{ kNm}}$$

$$M_{\text{Ed,Bottom}} = 107 \text{ kNm} \times 1.347 = \underline{144 \text{ kNm}}$$

$$M_{\text{Ed,wall,1st}} = (312 \text{ kN} \times 4.25 \text{ m} + 441 \text{ kN} \times 7.75 \text{ m} + 602 \text{ kN} \times 11.25 \text{ m} + 415 \text{ kN} \times 14.75 \text{ m}) \times 1.347$$

$$= \underline{23\,757 \text{ kNm}}.$$

A.2 Effective flange width of the beams

Initial effective flange width of the beams

For the border beam connected to the border column,

$$b_{\text{eff}} = 250 \text{ mm} + 2 \times 120 \text{ mm} = \underline{490 \text{ mm}}$$

For the interior connected to the border column,

$$b_{\text{eff}} = \underline{250 \text{ mm}}$$

For the interior beam connected to the interior column,

$$b_{\text{eff}} = 250 \text{ mm} + 2 \times 4 \times 120 \text{ mm} = \underline{1210 \text{ mm}}$$

Effective flange width of the beams due to increased columns

For the border beam connected to the border column $b_{\text{eff}} = 330 \text{ mm} + 2 \times 120 \text{ mm} = \underline{570 \text{ mm}}$

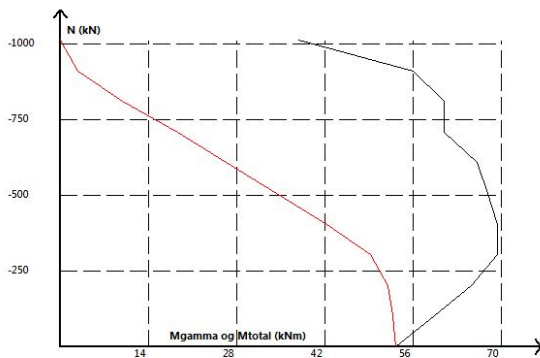
For the interior connected to the border column,

$$b_{\text{eff}} = \underline{330 \text{ mm}}$$

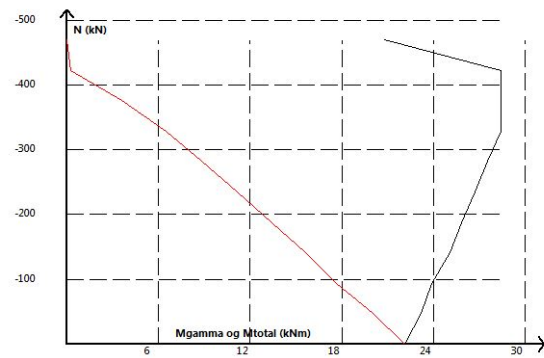
For the interior beam connected to the interior column,

$$b_{\text{eff}} = 440 \text{ mm} + 2 \times 4 \times 120 \text{ mm} = \underline{1400 \text{ mm}}$$

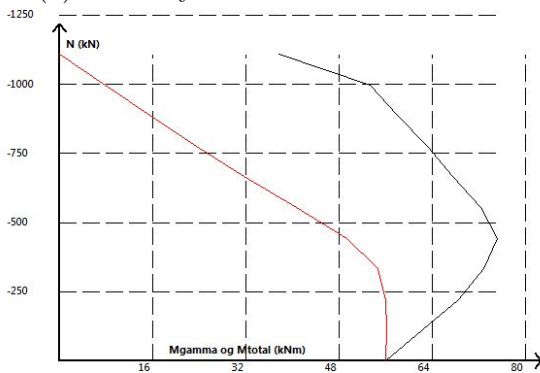
A.3 Moment capacities of initial columns



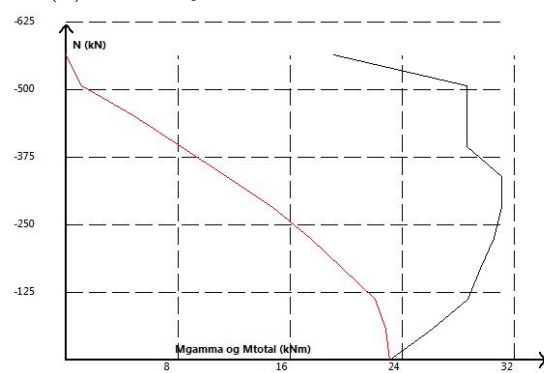
(a) 1st story 280 mm interior column.



(b) 1st story 230 mm border column.



(c) 2nd, 3rd, 4th story 280 mm interior column.



(d) 2nd, 3rd, 4th story 230 mm border column.

Figure A.1: M/N-diagrams for the 280 mm interior and border 230 mm border columns.

Table A.1: Axial loads and moment capacities of the 280 mm and 230 mm columns.

Column	Storey	Axial force (kN)	M_{RC} (kNm)
Interior 280 × 280 mm	4th	153	56
	3rd	237	54
	2nd	500	45
	1st	675	20
Interior 230 × 230 mm	4th	69	23
	3rd	149	20
	2nd	228	17
	1st	307	8

A.4 General calculations and equations from Eurocode

$$b_{wo,1st} = \max \{150 \text{ mm}; 3500 \text{ mm}/20\} = \underline{220 \text{ mm}}$$

$$b_{wo, 2nd, 3rd, 4th} = \max \{150 \text{ mm}; 3500 \text{ mm}/20\} = \underline{175 \text{ mm}}$$

$$A_{s,min} = 0.002 \times 1000 \text{ mm} \times 220 \text{ mm} = \underline{440 \text{ mm}^2}$$

$$h_{cr,wall,1st} = \max \{4500 \text{ mm}; 14750 \text{ mm}/6\} \leq (4250 \text{ mm} - 120 \text{ mm}) = \underline{4130 \text{ mm}}$$

$$q_0 = 4.5 \times 1.2 = \underline{5.4}$$

$$\alpha_0 = (4 \times 4250 \text{ mm}) / (4 \times 4500 \text{ mm}) = \underline{0.94}$$

$$k_w = (1 + 0.94) / 3 = \underline{0.65}$$

$$q = 5.4 \times 0.65 = \underline{3.51}$$

$$F_b = 2.87 \text{ m/s}^2 \times 1\,524\,100 \text{ kg} \times 0.85 = \underline{3\,178 \text{ kN}}$$

For axes 1, 6, A and F

$$\delta = 1 + 1.2 \times (14.25 \text{ m}/28.5 \text{ m}) = \underline{1.600}$$

For axes 2, 5, B and E,

$$\delta = 1 + 1.2 \times (8.25 \text{ m}/28.5 \text{ m}) = \underline{1.347}$$

For axes 3, 4, C and D,

$$\delta = 1 + 1.2 \times (2.25 \text{ m}/28.5 \text{ m}) = \underline{1.094}$$

$$\mu_{\phi} = 1 + 2 \times (5.4 - 1) \times (0.6/0.51) = \underline{11.35}$$

$$S_{\text{int}} = (440 \text{ mm} - 4 \times (32 \text{ mm} + 10 \text{ mm}) - 2 \times (35 \text{ mm} + 8 \text{ mm}))/3 = \underline{62 \text{ mm}}$$

For the border column,

$$v_d = 307\,000 \text{ N}/(330 \text{ mm} \times 330 \text{ mm} \times 16.7 \text{ N/mm}^2) = \underline{0.17}$$

For the interior column,

$$v_d = 675\,000 \text{ N}/(440 \text{ mm} \times 440 \text{ mm} \times 16.7 \text{ N/mm}^2) = \underline{0.21}$$

For the first storey wall,

$$\alpha_s = 23\,757 \text{ kNm}/(4\,148 \text{ kN} \times 4.5 \text{ m}) = \underline{1.27}$$

A.5 Equivalent spacing of shear reinforcement for walls

Since the shear reinforcement is different in the confined boundary elements and between, an equivalent spacing must be calculated. Total cross sectional area from the stirrups is equal to

$$101 \text{ mm}^2 \times (675 \text{ mm}/90 \text{ mm}) \times 2 = 1\,515 \text{ mm}^2$$

Total area from the horizontal reinforcement is equal to

$$226 \text{ mm}^2 \times (4500 \text{ mm}/250 \text{ mm}) = 4\,068 \text{ mm}^2$$

Thus,

$$s_{\text{eqv},\phi 12} = (226 \text{ mm}^2 \times 4500 \text{ mm})/(4\,068 \text{ mm}^2 + 1\,515 \text{ mm}^2) = \underline{182 \text{ mm}}$$

A.6 Ductility demands for beams in the seismic situation

Calculations prior increase of reinforcement

For border beams,

$$\rho = (2 \times \pi \times ((5 \text{ mm})^2 + (10 \text{ mm})^2))/(200 \text{ mm} \times 294 \text{ mm}) = \underline{0.0134}$$

$$\rho_{\max} = (2 \times \pi \times (10 \text{ mm})^2)/(200 \text{ mm} \times 294 \text{ mm}) + ((0.0018/(11.35 \times 0.00217)) \times 16.7 \text{ N/mm}^2)/435 \text{ N/mm}^2$$

$$= \underline{0.0134}$$

$$A_s = 2 \times \pi \times ((10 \text{ mm})^2 + (5 \text{ mm})^2) = \underline{785 \text{ mm}^2}$$

$$A_s' = 2 \times \pi \times (10 \text{ mm})^2 = \underline{628 \text{ mm}^2}$$

For the interior beams connecting to border columns,

$$\rho = (2 \times \pi \times (12.5 \text{ mm})^2)/(250 \text{ mm} \times 338 \text{ mm}) = \underline{0.0116}$$

$$\rho_{\max} = (2 \times \pi \times (12.5 \text{ mm})^2)/(250 \text{ mm} \times 338 \text{ mm}) + ((0.0018/(11.35 \text{ times } 0.00217)) \times 16.7 \text{ N/mm}^2)/435 \text{ N/mm}^2$$

$$= \underline{0.0147}$$

$$A_s = 2 \times \pi \times (12.5 \text{ mm})^2 = A_{\max} = \underline{982 \text{ mm}^2}$$

For the interior beams connecting to the interior columns,

$$\rho = (\pi \times (6 \times (5 \text{ mm})^2 + 2 \times (12.5 \text{ mm})^2))/(250 \text{ mm} \times 338 \text{ mm}) = \underline{0.0172}$$

$$\rho_{\max} = (2 \times \pi \times (12.5 \text{ mm})^2)/(250 \text{ mm} \times 238 \text{ mm}) + ((0.0018/(11.35 \times 0.00217)) \times 16.7 \text{ N/mm}^2)/435 \text{ N/mm}^2$$

$$= \underline{0.0147}$$

$$A_s = \pi \times (6 \times (5 \text{ mm})^2 + 2 \times (12.5 \text{ mm})^2) = \underline{1453 \text{ N/mm}^2}$$

$$A_s' = 2 \times \pi \times (12.5 \text{ mm})^2 = \underline{982 \text{ N/mm}^2}$$

Calculations post increase of reinforcement

For border beams,

$$\rho = (2 \times \pi \times ((5 \text{ mm})^2 + (12.5 \text{ mm})^2))/(200 \text{ mm} \times 294 \text{ mm}) = \underline{0.0194}$$

$$\begin{aligned} \rho_{\max} &= (2 \times \pi \times (12.5 \text{ mm})^2)/(200 \text{ mm} \times 294 \text{ mm}) + ((0.0018/(11.35 \times 0.00217)) \times \\ &16.7 \text{ N/mm}^2)/435 \text{ N/mm}^2 \\ &= \underline{0.0198} \end{aligned}$$

$$A_s = 2 \times \pi \times ((12.5 \text{ mm})^2 + (5 \text{ mm})^2) = \underline{1\,184 \text{ mm}^2}$$

$$A_s' = 2 \times \pi \times (12.5 \text{ mm})^2 = \underline{982 \text{ mm}^2}$$

For the interior beams connecting to border columns,

$$\rho = (3 \times \pi \times (16 \text{ mm})^2)/(250 \text{ mm} \times 338 \text{ mm}) = \underline{0.0286}$$

$$\begin{aligned} \rho_{\max} &= (3 \times \pi \times (12.5 \text{ mm})^2)/(250 \text{ mm} \times 338 \text{ mm}) + ((0.0018/(11.35 \times 0.00217)) \times \\ &16.7 \text{ N/mm}^2)/435 \text{ N/mm}^2 \\ &= \underline{0.0317} \end{aligned}$$

$$A_s = 3 \times \pi \times (16 \text{ mm})^2 = A_s' = \underline{2\,413 \text{ mm}^2}$$

For the interior beams connecting to the interior columns,

$$\rho = (\pi \times (6 \times (5 \text{ mm})^2 + 3 \times (16 \text{ mm})^2))/(250 \text{ mm} \times 338 \text{ mm}) = \underline{0.0341}$$

$$\begin{aligned} \rho_{\max} &= (3 \times \pi \times (16 \text{ mm})^2)/(250 \text{ mm} \times 238 \text{ mm}) + ((0.0018/(11.35 \times 0.00217)) \times \\ &16.7 \text{ N/mm}^2)/435 \text{ N/mm}^2 \\ &= \underline{0.0317} \end{aligned}$$

$$A_s = \pi \times (6 \times (5 \text{ mm})^2 + 3 \times (16 \text{ mm})^2) = \underline{2\,884 \text{ N/mm}^2}$$

$$A_s' = 3 \times \pi \times (16 \text{ mm})^2 = \underline{2\,413 \text{ N/mm}^2}$$

Calculations post increase of reinforcement due to seismic loading

For the interior beams connecting to border columns,

$$\rho = (3 \times \pi \times (16 \text{ mm})^2)/(250 \text{ mm} \times 338 \text{ mm}) = \underline{0.0286}$$

$$\rho_{\max} = (3 \times \pi \times (16 \text{ mm})^2 + 3 \times \pi \times (6 \text{ mm})^2)/(250 \text{ mm} \times 238 \text{ mm}) + ((0.0018/(11.35 \times 0.00217)) \times$$

$$16.7 \text{ N/mm}^2)/435 \text{ N/mm}^2 = \underline{0.0343}$$

$$A_s = 3 \times \pi \times (16 \text{ mm})^2 = \underline{2\,413 \text{ N/mm}^2}$$

$$A_s' = \pi \times (3 \times (16 \text{ mm})^2 + 2 \times (6 \text{ mm})^2) = \underline{2\,639 \text{ N/mm}^2}$$

For the interior beams connecting to the interior columns,

$$\rho = (\pi \times (6 \times (5 \text{ mm})^2 + 3 \times (16 \text{ mm})^2))/(250 \text{ mm} \times 338 \text{ mm}) = \underline{0.0341}$$

$$\rho_{\max} = (3 \times \pi \times (16 \text{ mm})^2 + 3 \times \pi \times (6 \text{ mm})^2)/(250 \text{ mm} \times 238 \text{ mm}) + ((0.0018/(11.35 \times 0.00217)) \times$$

$$16.7 \text{ N/mm}^2)/435 \text{ N/mm}^2 = \underline{0.0343}$$

$$A_s = \pi \times (6 \times (5 \text{ mm})^2 + 3 \times (16 \text{ mm})^2) = \underline{2\,884 \text{ N/mm}^2}$$

$$A_s' = \pi \times (3 \times (16 \text{ mm})^2 + 2 \times (6 \text{ mm})^2) = \underline{2\,639 \text{ N/mm}^2}$$

A.7 Shear capacities in the seismic design situation

Shear capacities of beams designed for seismic loading

For the border beams,

$$V_{\text{Ed,max}} = (10.3 \text{ kN/m} \times 6 \text{ m})/2 + 1.2 \times (120 \text{ kNm} + 114 \text{ kNm})/6 \text{ m} = \underline{78 \text{ kN}}$$

$$V_{\text{Ed,min}} = (10.3 \text{ kN/m} \times 6 \text{ m})/2 - 1.2 \times (120 \text{ kNm} + 114 \text{ kNm})/6 \text{ m} = \underline{-16 \text{ kN}}$$

$$\zeta = -16 \text{ kN}/78 \text{ kN} = \underline{-0.21}$$

For the interior beams connecting to the border columns,

$$V_{\text{Ed,max}} = (23.8 \text{ kN/m} \times 6 \text{ m})/2 + 1.2 \times (290 \text{ kNm} + 304 \text{ kNm})/6 \text{ m} = \underline{204 \text{ kN}}$$

$$V_{\text{Ed,min}} = (28.3 \text{ kN/m} \times 6 \text{ m})/2 - 1.2 \times (290 \text{ kNm} + 304 \text{ kNm})/6 \text{ m} = \underline{-34 \text{ kN}}$$

$$\zeta = -34 \text{ kN}/204 \text{ kN} = \underline{-0.17}$$

For the interior beams connecting to the interior columns,

$$V_{Ed,max} = (23.8 \text{ kN/m} \times 6 \text{ m})/2 + 1.2 \times (336 \text{ kNm} + 336 \text{ kNm})/6 \text{ m} = \underline{219 \text{ kN}}$$

$$V_{Ed,min} = (28.3 \text{ kN/m} \times 6 \text{ m})/2 - 1.2 \times (336 \text{ kNm} + 336 \text{ kNm})/6 \text{ m} = \underline{-50 \text{ kN}}$$

$$\zeta = -50 \text{ kN}/219 \text{ kN} = \underline{-0.23}$$

The shear capacity can be evaluated in accordance with EN 1992-1-1, i.e. Equation 3.23 and Equation 3.24. In addition, EN 1998-1, section 5.5.3.1.2, demands that $\Theta = 45^\circ$ within the critical areas. First, the acting shear force outside the critical area is determined. For border beams,

$$V_{Ed,red} = 78 \text{ kN} - 0.525 \text{ m} \times 10.3 \text{ kN/m} = \underline{73 \text{ kN}}$$

For interior beams,

$$V_{Ed,red} = 219 \text{ kN} - 0.525 \text{ m} \times 28.3 \text{ kN/m} = \underline{204 \text{ kN}}$$

The shear capacities are calculated in Matlab and the script is shown in Appendix B.

Shear capacities of columns designed for seismic loading

For the interior column,

$$M_{bottom,d} = 1.3 \times 580 \text{ kNm} \times (672 \text{ kNm}/160 \text{ kNm}) = \underline{437 \text{ kNm}}$$

$$M_{top,d} = 1.3 \times 595 \text{ kNm} \times 1 = \underline{774 \text{ kNm}}$$

$$V_{Ed} = (437 \text{ kNm} + 774 \text{ kNm})/3.5 \text{ m} = \underline{346 \text{ kN}}$$

The border beam is evaluated in the same manner.

Moment diagram in the seismic design situation

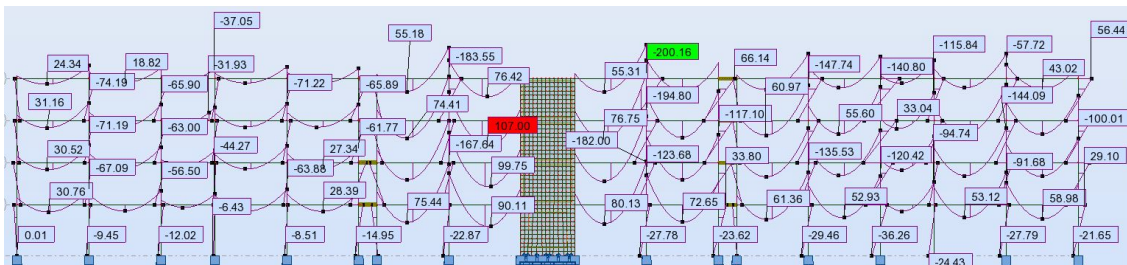


Figure A.2: Moment diagram from the seismic design situation.

A.8 Moment and shear capacity of walls in the seismic design situation

General

All calculations of acting forces are calculated in Robot [24]. The calculations according to Eurocode are performed in Matlab.

2nd storey wall

$$V_{Ed}' = \underline{1\,458\text{ kN}}$$

$$M_{Ed} = (441\text{ kN} \times 3.5\text{ m} + 602 \times 7\text{ m} + 415\text{ kN} \times 10.5\text{ m}) \times 1.347 = \underline{13\,625\text{ kNm}}$$

The wall is checked is BtSnitt [22] and does not have sufficient capacity. Therefore, the critical area is increased to 900 mm and the vertical reinforcement within the critical area is increased to $\phi 32c125$. This gives

$$M_{Rd} = \underline{15\,675\text{ kNm}}$$

The reinforcement factor is calculated in Matlab equal to 1.77

$$V_{Ed} = 1.347 \times 1.77 \times 1\,458\text{ kN} = \underline{3\,476\text{ kN}}$$

$$\text{This gives } \alpha = 13\,625\text{ kNm} / (3\,476\text{ kN} \times 4.5\text{ m}) = \underline{0.87}$$

The wall width in the 2nd storey is increased to 220 mm between the confined length, the horizontal reinforcement is increased to $\phi 16c150$ and the shear stirrups are increased to $\phi 16c250$.

This gives

$$V_{Rd} = \underline{3\,564\text{ kN}}$$

3rd storey wall

$$V_{Ed}' = \underline{1\,017\text{ kN}}$$

$$M_{Ed} = (602\text{ kN} \times 3.5\text{ m} + 415 \times 7\text{ m}) \times 1.347 = \underline{6\,751\text{ kNm}}$$

The wall is checked is BtSnitt [22] and does not have sufficient capacity. Therefore, there is added $6\phi 25$ is at each wall end. This gives

$$M_{Rd} = \underline{8\,360\text{ kNm}}$$

The reinforcement factor is calculated in Matlab equal to 1.85.

$$V_{Ed} = 1.347 \times 1.85 \times 1\,017 \text{ kN} = \underline{2\,534 \text{ kN}}$$

This gives

$$\alpha = 6\,751 \text{ kNm} / (2\,534 \text{ kN} \times 4.5 \text{ m}) = \underline{0.59}$$

The horizontal reinforcement are increased to $\phi 16c150$. This gives

$$V_{Rd} = \underline{2\,656 \text{ kN}}$$

4th storey wall

$$V_{Ed}' = \underline{415 \text{ kN}}$$

$$M_{Ed} = 415 \text{ kN} \times 3.5 \text{ m} \times 1.347 = \underline{1\,956 \text{ kNm}}$$

The wall is checked is BtSnitt [22].

$$M_{Rd} = \underline{3135 \text{ kNm}}$$

The reinforcement factor is equal to 2.22.

$$V_{Ed} = 1.347 \times 2.22 \times 415 \text{ kN} = \underline{1\,241 \text{ kN}}$$

This gives

$$\alpha = 3\,135 \text{ kNm} / (1\,241 \text{ kN} \times 4.5 \text{ m}) = \underline{0.56}$$

The horizontal reinforcement is increased to $\phi 16c200$.

$$V_{Rd} = \underline{1\,945 \text{ kN}}$$

Capacity check after analysis with increased elements

For the 1st storey wall,

$$M_{Ed}/M_{Rd} = 24\,607 \text{ kNm} / 26\,600 \text{ kNm} = \underline{0.97}$$

$$V_{Ed}/V_{Rd} = 4\,131 \text{ kN} / 4\,250 \text{ kN} = \underline{0.97}$$

For the 2nd storey wall,

$$M_{Ed}/M_{Rd} = 14\,285 \text{ kNm} / 15\,675 \text{ kNm} = \underline{0.97}$$

$$V_{Ed}/V_{Rd} = 3\,492 \text{ kN}/3\,564 \text{ kN} = \underline{0.98}$$

For the 3rd storey wall,

$$M_{Ed}/M_{Rd} = 7\,185 \text{ kNm}/8\,360 \text{ kNm} = \underline{0.86}$$

$$V_{Ed}/V_{Rd} = 2\,546 \text{ kN}/2\,835 \text{ kN} = \underline{0.90}$$

For the 4th storey wall,

$$M_{Ed}/M_{Rd} = 2\,178 \text{ kNm}/3\,135 \text{ kNm} = \underline{0.69}$$

$$V_{Ed}/V_{Rd} = 1\,276 \text{ kN}/1\,414 \text{ kN} = \underline{0.89}$$

Table A.2: Capacity check of walls after increased forces.

Story	M_{Ed} (kNm)	M_{Rd} (kNm)	M_{Ed}/M_{Rd}	V_{Ed} (kN)	V_{rd} (kN)	V_{Ed}/V_{Rd}
4th	2 178	3 135	0.69	1 276	1 440	0.89
3rd	7 185	8 360	0.86	2 546	2 835	0.90
2nd	14 285	15 675	0.97	3 492	3 564	0.98
1st	24 607	26 600	0.97	4 131	4 250	0.97

Appendix B

Matlab scripts

B.1 Response spectrum

```
%% Ground Motions
% *****

%% Clear all
clear all;close all;clc;

%% Find maximum PGA and PGV
% *****

% Acceleraion in g, velocity in cm/s
clear all;close all;clc;

% Load data
% *****

load RSN730_SPITAK_GUK090V.VT2
VelSPI90=max(abs(RSN730_SPITAK_GUK090V(:)))
load RSN730_SPITAK_GUK090A.AT2
AccSPI90=max(abs(RSN730_SPITAK_GUK090A(:)))
load RSN730_SPITAK_GUK000V.VT2
VelSPI100=max(abs(RSN730_SPITAK_GUK000V(:)))
load RSN730_SPITAK_GUK000A.AT2
AccSPI100=max(abs(RSN730_SPITAK_GUK000A(:)))

load RSN724_SUPER_B_B_PLS135V.VT2
VelSH135=max(abs(RSN724_SUPER_B_B_PLS135V(:)))
load RSN724_SUPER_B_B_PLS135A.AT2
AccSH135=max(abs(RSN724_SUPER_B_B_PLS135A(:)))
```

Response spectrum

```
load RSN724_SUPER_B_B_PLS045A.AT2
AccSH045=max(abs(RSN724_SUPER_B_B_PLS045A(:)))
load RSN724_SUPER_B_B_PLS045V.VT2
VelSH045=max(abs(RSN724_SUPER_B_B_PLS045V(:)))

load RSN169_IMPVALL_H_H_DLT352A.AT2
AccIMPV352=max(abs(RSN169_IMPVALL_H_H_DLT352A(:)))
load RSN169_IMPVALL_H_H_DLT352V.VT2
VelIMPV352=max(abs(RSN169_IMPVALL_H_H_DLT352V(:)))
load RSN169_IMPVALL_H_H_DLT262A.AT2
AccIMPV262=max(abs(RSN169_IMPVALL_H_H_DLT262A(:)))
load RSN169_IMPVALL_H_H_DLT262V.VT2
VelIMPV262=max(abs(RSN169_IMPVALL_H_H_DLT262V(:)))

load RSN68_SFERN_PEL180V.VT2
VelSFERN180=max(abs(RSN68_SFERN_PEL180V(:)))
load RSN68_SFERN_PEL180A.AT2
AccSFERN180=max(abs(RSN68_SFERN_PEL180A(:)))
load RSN68_SFERN_PEL090V.VT2
VelSFERN90=max(abs(RSN68_SFERN_PEL090V(:)))
load RSN68_SFERN_PEL090A.AT2
AccSFERN90=max(abs(RSN68_SFERN_PEL090A(:)))

load RSN1634_MANJIL_184057V.VT2
VelMANJIL000=max(abs(RSN1634_MANJIL_184057V(:)))
load RSN1634_MANJIL_184057A.AT2
AccMANJIL000=max(abs(RSN1634_MANJIL_184057A(:)))
load RSN1634_MANJIL_184327V.VT2
VelMANJIL090=max(abs(RSN1634_MANJIL_184327V(:)))
load RSN1634_MANJIL_184327A.AT2
AccMANJIL090=max(abs(RSN1634_MANJIL_184327A(:)))

load RSN4853_CHUETSU_65019EWV.VT2
VelCHUETSU000=max(abs(RSN4853_CHUETSU_65019EWV(:)))
load RSN4853_CHUETSU_65019EWA.AT2
AccCHUETSU000=max(abs(RSN4853_CHUETSU_65019EWA(:)))
load RSN4853_CHUETSU_65019NSV.VT2
VelCHUETSU090=max(abs(RSN4853_CHUETSU_65019NSV(:)))
load RSN4853_CHUETSU_65019NSA.AT2
AccCHUETSU090=max(abs(RSN4853_CHUETSU_65019NSA(:)))

load RSN5786_IWATE_54038EWV.VT2
VelIWATE000=max(abs(RSN5786_IWATE_54038EWV(:)))
load RSN5786_IWATE_54038EWA.AT2
```


Response spectrum

```
AccIWATE000=max(abs(RSN5786_IWATE_54038EWA(:)))
load RSN5786_IWATE_54038NSV.VT2
VelIWATE090=max(abs(RSN5786_IWATE_54038NSV(:)))
load RSN5786_IWATE_54038NSA.AT2
AccIWATE090=max(abs(RSN5786_IWATE_54038NSA(:)))

% Format data
% *****

% Maximum ground motion time length
Maxlength=max([length(RSN68_SFERN_PEL090A(:))
length(RSN169_IMPVALL_H_H_DLT352A(:))
length(RSN724_SUPER_B_B_PLS135A(:))
length(RSN730_SPITAK_GUK000A(:))
length(RSN1634_MANJIL_184327A(:))
length(RSN4853_CHUETSU_65019EWA(:))
length(RSN5786_IWATE_54038NSA(:))])

% Formatting SAN FERNANDO, 09.02.1971
SFERNDATA=RSN68_SFERN_PEL090A;

Trans_SFERNDATA=transpose(SFERNDATA); %<-- Format Acceleration data
ORGaccSFERN=9.81*Trans_SFERNDATA(:);
TimeSFERN=zeros(Maxlength,1);
AccSFERN=zeros(Maxlength,1);

for i=1:length(ORGaccSFERN);
    AccSFERN(i)=ORGaccSFERN(i);
end
for i=2:Maxlength;
    TimeSFERN(i)=TimeSFERN(i-1)+0.01;
end

% Formatting Imperial Valley-06, 15.10.1979
IMPVDATA=RSN169_IMPVALL_H_H_DLT352A;

Trans_IMPVDATA=transpose(IMPVDATA); %<-- Format Acceleration data
ORGaccIMPV=9.81*Trans_IMPVDATA(:);
TimeIMPV=zeros(Maxlength,1);
AccIMPV=zeros(Maxlength,1);

for i=1:length(ORGaccIMPV);
    AccIMPV(i)=ORGaccIMPV(i);
end
```

Response spectrum

```
for i=2:Maxlength;
    TimeIMPV(i)=TimeIMPV(i-1)+0.01;
end

% Formatting Superstition Hills-02, 24.11.1987
SHDATA=RSN724_SUPER_B_B_PLS135A;

Trans_SHDATA=transpose(SHDATA); %<-- Format Acceleration data
ORGAccSH=9.81*Trans_SHDATA(:);
TimeSH=zeros(Maxlength,1);
AccSH=zeros(Maxlength,1);

for i=1:length(ORGAccSH);
    AccSH(i)=ORGAccSH(i);
end
for i=2:Maxlength;
    TimeSH(i)=TimeSH(i-1)+0.01;
end

% Formatting Spitak Armenia, 07.12.1988
SADATA=RSN730_SPITAK_GUK000A;
Trans_SADATA=transpose(SADATA); %<-- Format Acceleration data
ORGAccSA=9.81*Trans_SADATA(:);
TimeSA=zeros(Maxlength,1);
AccSA=zeros(Maxlength,1);

for i=1:length(ORGAccSA);
    AccSA(i)=ORGAccSA(i);
end
for i=2:Maxlength;
    TimeSA(i)=TimeSA(i-1)+0.01;
end

% Formatting Manjil Iran, 20.06.1990
MADATA=RSN1634_MANJIL_184327A;
Trans_MADATA=transpose(MADATA); %<-- Format Acceleration data
ORGAccMA=9.81*Trans_MADATA(:);
TimeMA=zeros(Maxlength,1);
AccMA=zeros(Maxlength,1);

for i=1:length(ORGAccMA);
    AccMA(i)=ORGAccMA(i);
end
for i=2:Maxlength;
```

Response spectrum

```
    TimeMA(i)=TimeMA(i-1)+0.01;
end

% Formatting Joetsu City Japan, 16.07.2007
JCdata=RSN4853_CHUETSU_65019EWA;
Trans_JCdata=transpose(JCdata); %<-- Format Acceleration data
ORGAccJC=9.81*Trans_JCdata(:);
TimeJC=zeros(Maxlength,1);
AccJC=zeros(Maxlength,1);

for i=1:length(ORGAccJC);
    AccJC(i)=ORGAccJC(i);
end
for i=2:Maxlength;
    TimeJC(i)=TimeJC(i-1)+0.01;
end

% Formatting Iwate, Japan , 13.06.2008
IWDATA=RSN5786_IWATE_54038NSA;
Trans_IWDATA=transpose(IWDATA); %<-- Format Acceleration data
ORGAccIW=9.81*Trans_IWDATA(:);
TimeIW=zeros(Maxlength,1);
AccIW=zeros(Maxlength,1);

for i=1:length(ORGAccIW);
    AccIW(i)=ORGAccIW(i);
end
for i=2:Maxlength;
    TimeIW(i)=TimeIW(i-1)+0.01;
end

% Plots ground motions
% *****

figure('position', [0, 0, 2000, 200]) % San Fernando, 09.02.1971
plot(TimeSFERN,AccSFERN);
xlabel('Time [s]');ylabel('Acceleration [m/s^2]');
xlim([0,max(TimeSFERN)]);ylim([1.2*min(AccSFERN),1.2*max(AccSFERN)]);grid;

figure('position', [0, 0, 2000, 200]) % Imperial Valley, 15.10.1979
plot(TimeIMPV,AccIMPV);
xlabel('Time [s]');ylabel('Acceleration [m/s^2]');
xlim([0,max(TimeIMPV)]);ylim([1.2*min(AccIMPV),1.2*max(AccIMPV)]);grid;
```

Response spectrum

```
figure('position', [0, 0, 2000, 200]) % Superstition Hills-02, 24.11.1987
plot(TimeSH,AccSH);
xlabel('Time [s]');ylabel('Acceleration [m/s^2]');
xlim([0,max(TimeSH)]);ylim([1.2*min(AccSH),1.2*max(AccSH)]);grid;

figure('position', [0, 0, 2000, 200]) % Spitak Armenia, 07.12.1988
plot(TimeSA,AccSA);
xlabel('Time [s]');ylabel('Acceleration [m/s^2]');
xlim([0,max(TimeSA)]);ylim([1.2*min(AccSA),1.2*max(AccSA)]);grid;

figure('position', [0, 0, 2000, 200]) % Manjil Iran, 20.06.1990
plot(TimeMA,AccMA);
xlabel('Time [s]');ylabel('Acceleration [m/s^2]');
xlim([0,max(TimeMA)]);ylim([1.2*min(AccMA),1.2*max(AccMA)]);grid;

figure('position', [0, 0, 2000, 200]) % Joetsu City, 16.07.2007
plot(TimeJC,AccJC);
xlabel('Time [s]');ylabel('Acceleration [m/s^2]');
xlim([0,max(TimeJC)]);ylim([1.2*min(AccJC),1.2*max(AccJC)]);grid;

figure('position', [0, 0, 2000, 200]) % Iwate, Japan , 13.06.2008
plot(TimeIW,AccIW);
xlabel('Time [s]');ylabel('Acceleration [m/s^2]');
xlim([0,max(TimeIW)]);ylim([1.2*min(AccIW),1.2*max(AccIW)]);grid;

%% Computation of reponse spectrum by
%% Newmarks linear method
%% Constant average acceleration method (gamma=1/2, beta=1/4)
%% Linear acceleration method (gamma=1/2, beta=1/6)
% *****
% *****

gamma=0.5; beta=1/6; % <-- For a stable solution, 2*beta > gamma > 0.5
m=1; % Mass is set equal to one and the stiffness is varied.
psi=0.05; % Determine damping.
Tmax=4; % Determine maximum period

% San Fernando Valley, 09.02.1971
dt=TimeSFERN(2,1)-TimeSFERN(1,1);
u=zeros(size(AccSFERN));v=u;a=u;
m=1;
T(1,1)=0;
for j=1:round(Tmax/dt)
```

Response spectrum

```
    omega(j,1)=2*pi*(1/T(j,1));
    k=(omega(j))^2*m;
    c=2*psi*omega(j)*m;
    a1=(gamma/(beta*dt))*c+(1/(beta*dt^2))*m;
    a2=(1/(beta*dt))*m+((gamma/beta)-1)*c;
    a3=((gamma/(2*beta))-1)*c*dt+((1/(2*beta))-1)*m;
    keff=k+a1;
for i=1:length(u)-1
    Ph=-AccSFERN(i+1)*m+a1*u(i,1)+a2*v(i,1)+a3*a(i,1);
    u(i+1,1)=Ph/keff;
    v(i+1,1)=(gamma/(beta*dt))*(u(i+1,1)-u(i,1))+(1-(gamma/beta))*v(i,1)
    +dt*(1-(gamma/(2*beta)))*a(i,1);
    a(i+1,1)=(1/(beta*dt^2))*(u(i+1,1)-u(i,1))-(1/(beta*dt))*v(i,1)-
    ((1/(2*beta))-1)*a(i,1);
end
SFERNPSd(j,1)=max(abs(u));
SFERNPSv(j,1)=max(abs(v));
SFERNPSa(j,1)=SFERNPSd(j,1)*(omega(j))^2;
T(j+1,1)=T(j)+dt;
end
T(end)=[];
SFERNPSd(1:2,1)=0;SFERNPSv(1:2,1)=0;SFERNPSa(1:3,1)=max(abs(AccSFERN));
These manual values ensure continuity in the spectru

% Imperial Valley-06, 15.10.1979
dt=TimeIMPV(2,1)-TimeIMPV(1,1);
u=zeros(size(AccIMPV));
v=u;
a=u;
m=1;
T(1,1)=0;
for j=1:round(Tmax/dt)
    omega(j,1)=2*pi*(1/T(j,1));
    k=(omega(j))^2*m;
    c=2*psi*omega(j)*m;
    a1=(gamma/(beta*dt))*c+(1/(beta*dt^2))*m;
    a2=(1/(beta*dt))*m+((gamma/beta)-1)*c;
    a3=((gamma/(2*beta))-1)*c*dt+((1/(2*beta))-1)*m;
    keff=k+a1;
for i=1:length(u)-1
    Ph=-AccIMPV(i+1)*m+a1*u(i,1)+a2*v(i,1)+a3*a(i,1);
    u(i+1,1)=Ph/keff;
    v(i+1,1)=(gamma/(beta*dt))*(u(i+1,1)-u(i,1))+(1-
    (gamma/beta))*v(i,1)+dt*(1-(gamma/(2*beta)))*a(i,1);
```

Response spectrum

```

        a(i+1,1)=(1/(beta*dt^2))*(u(i+1,1)-u(i,1))-(1/(beta*dt))*v(i,1)-
        ((1/(2*beta))-1)*a(i,1);
    end
    IMPVPSd(j,1)=max(abs(u));
    IMPVPSv(j,1)=max(abs(v));
    IMPVPSa(j,1)=IMPVPSd(j,1)*(omega(j))^2;
    T(j+1,1)=T(j)+dt;
    end
    T(end)=[];
    IMPVPSd(1:2,1)=0;IMPVPSv(1:2,1)=0;IMPVPSa(1:3,1)=max(abs(AccIMPV));
    % These manual values ensure continuity in the spectrum

% Superstition Hills-02, 24.11.1987
dt=TimeSH(2,1)-TimeSH(1,1);
u=zeros(size(AccSH));
v=u;
a=u;
m=1;
T(1,1)=0;
for j=1:round(Tmax/dt)
    omega(j,1)=2*pi*(1/T(j,1));
    k=(omega(j))^2*m;
    c=2*psi*omega(j)*m;
    a1=(gamma/(beta*dt))*c+(1/(beta*dt^2))*m;
    a2=(1/(beta*dt))*m+((gamma/beta)-1)*c;
    a3=((gamma/(2*beta))-1)*c*dt+((1/(2*beta))-1)*m;
    keff=k+a1;
    for i=1:length(u)-1
        Ph=-AccSH(i+1)*m+a1*u(i,1)+a2*v(i,1)+a3*a(i,1);
        u(i+1,1)=Ph/keff;
        v(i+1,1)=(gamma/(beta*dt))*(u(i+1,1)-u(i,1))+
        (1-(gamma/beta))*v(i,1)+dt*(1-(gamma/(2*beta)))*a(i,1);
        a(i+1,1)=(1/(beta*dt^2))*(u(i+1,1)-u(i,1))-(1/(beta*dt))*v(i,1)-
        ((1/(2*beta))-1)*a(i,1);
    end
    SHPSd(j,1)=max(abs(u));
    SHPSv(j,1)=max(abs(v));
    SHPSa(j,1)=SHPSd(j,1)*(omega(j))^2;
    T(j+1,1)=T(j)+dt;
    end
    T(end)=[];
    SHPSd(1:2,1)=0;SHPSv(1:2,1)=0;SHPSa(1:3,1)=max(abs(AccSH));
    % These manual values ensure continuity in the spectrum

```

Response spectrum

```
% Spitak Armenia, 7.12.1988
dt=TimeSA(2,1)-TimeSA(1,1);
u=zeros(size(AccSA));
v=u;
a=u;
m=1;
T(1,1)=0;
for j=1:round(Tmax/dt)
    omega(j,1)=2*pi*(1/T(j,1));
    k=(omega(j))^2*m;
    c=2*psi*omega(j)*m;
    a1=(gamma/(beta*dt))*c+(1/(beta*dt^2))*m;
    a2=(1/(beta*dt))*m+((gamma/beta)-1)*c;
    a3=((gamma/(2*beta))-1)*c*dt+((1/(2*beta))-1)*m;
    keff=k+a1;
for i=1:length(u)-1
    Ph=-AccSA(i+1)*m+a1*u(i,1)+a2*v(i,1)+a3*a(i,1);
    u(i+1,1)=Ph/keff;
    v(i+1,1)=(gamma/(beta*dt))*(u(i+1,1)-u(i,1))+
        (1-(gamma/beta))*v(i,1)+dt*(1-(gamma/(2*beta)))*a(i,1);
    a(i+1,1)=(1/(beta*dt^2))*(u(i+1,1)-u(i,1))-
        (1/(beta*dt))*v(i,1)-((1/(2*beta))-1)*a(i,1);
end
SAPSD(j,1)=max(abs(u));
SAPSV(j,1)=max(abs(v));
SAPSA(j,1)=SAPSD(j,1)*(omega(j))^2;
T(j+1,1)=T(j)+dt;
end
T(end)=[];
SAPSD(1:2,1)=0;SAPSV(1:2,1)=0;SAPSA(1:3,1)=max(abs(AccSA));
% These manual values ensure continuity in the spectrum

% Manjil Iran, 20.06.1990
dt=TimeMA(2,1)-TimeMA(1,1);
u=zeros(size(AccMA));
v=u;
a=u;
m=1;
T(1,1)=0;
for j=1:round(Tmax/dt)
    omega(j,1)=2*pi*(1/T(j,1));
    k=(omega(j))^2*m;
    c=2*psi*omega(j)*m;
    a1=(gamma/(beta*dt))*c+(1/(beta*dt^2))*m;
```

```

a2=(1/(beta*dt))*m+((gamma/beta)-1)*c;
a3=((gamma/(2*beta))-1)*c*dt+((1/(2*beta))-1)*m;
keff=k+a1;
for i=1:length(u)-1
    Ph=-AccMA(i+1)*m+a1*u(i,1)+a2*v(i,1)+a3*a(i,1);
    u(i+1,1)=Ph/keff;
    v(i+1,1)=(gamma/(beta*dt))*(u(i+1,1)-u(i,1))+
        (1-(gamma/beta))*v(i,1)+dt*(1-(gamma/(2*beta)))*a(i,1);
    a(i+1,1)=(1/(beta*dt^2))*(u(i+1,1)-u(i,1))-
        (1/(beta*dt))*v(i,1)-((1/(2*beta))-1)*a(i,1);
end
MAPSd(j,1)=max(abs(u));
MAPSv(j,1)=max(abs(v));
MAPSa(j,1)=MAPSd(j,1)*(omega(j))^2;
T(j+1,1)=T(j)+dt;
end
T(end)=[];
MAPSd(1:2,1)=0;MAPSv(1:2,1)=0;MAPSa(1:3,1)=max(abs(AccMA));
% These manual values ensure continuity in the spectrum

% Joetsu City, 16.07.2007
dt=TimeJC(2,1)-TimeJC(1,1);
u=zeros(size(AccJC));
v=u;
a=u;
m=1;
T(1,1)=0;
for j=1:round(Tmax/dt)
    omega(j,1)=2*pi*(1/T(j,1));
    k=(omega(j))^2*m;
    c=2*psi*omega(j)*m;
    a1=(gamma/(beta*dt))*c+(1/(beta*dt^2))*m;
    a2=(1/(beta*dt))*m+((gamma/beta)-1)*c;
    a3=((gamma/(2*beta))-1)*c*dt+((1/(2*beta))-1)*m;
    keff=k+a1;
for i=1:length(u)-1
    Ph=-AccJC(i+1)*m+a1*u(i,1)+a2*v(i,1)+a3*a(i,1);
    u(i+1,1)=Ph/keff;
    v(i+1,1)=(gamma/(beta*dt))*(u(i+1,1)-u(i,1))+
        (1-(gamma/beta))*v(i,1)+dt*(1-(gamma/(2*beta)))*a(i,1);
    a(i+1,1)=(1/(beta*dt^2))*(u(i+1,1)-u(i,1))-
        (1/(beta*dt))*v(i,1)-((1/(2*beta))-1)*a(i,1);
end
JCPSd(j,1)=max(abs(u));

```


Response spectrum

```
JCPsV(j,1)=max(abs(v));
JCPsA(j,1)=JCPsD(j,1)*(omega(j))^2;
T(j+1,1)=T(j)+dt;
end
T(end)=[];
JCPsD(1:2,1)=0;JCPsV(1:2,1)=0;JCPsA(1:3,1)=max(abs(AccJC));
% These manual values ensure continuity in the spectrum

% Iwate Japan , 13.06.2008
dt=TimeIW(2,1)-TimeIW(1,1);
u=zeros(size(AccIW));
v=u;
a=u;
m=1;
T(1,1)=0;
for j=1:round(Tmax/dt)
    omega(j,1)=2*pi*(1/T(j,1));
    k=(omega(j))^2*m;
    c=2*psi*omega(j)*m;
    a1=(gamma/(beta*dt))*c+(1/(beta*dt^2))*m;
    a2=(1/(beta*dt))*m+((gamma/beta)-1)*c;
    a3=((gamma/(2*beta))-1)*c*dt+((1/(2*beta))-1)*m;
    keff=k+a1;
for i=1:length(u)-1
    Ph=-AccIW(i+1)*m+a1*u(i,1)+a2*v(i,1)+a3*a(i,1);
    u(i+1,1)=Ph/keff;
    v(i+1,1)=(gamma/(beta*dt))*(u(i+1,1)-u(i,1))+
    (1-(gamma/beta))*v(i,1)+dt*(1-(gamma/(2*beta)))*a(i,1);
    a(i+1,1)=(1/(beta*dt^2))*(u(i+1,1)-u(i,1))-
    (1/(beta*dt))*v(i,1)-((1/(2*beta))-1)*a(i,1);
end
IWPSD(j,1)=max(abs(u));
IWPSV(j,1)=max(abs(v));
IWPSA(j,1)=IWPSD(j,1)*(omega(j))^2;
T(j+1,1)=T(j)+dt;
end
T(end)=[];
IWPSD(1:2,1)=0;IWPSV(1:2,1)=0;IWPSA(1:3,1)=max(abs(AccIW));
% These manual values ensure continuity in the spectrum

%% Scaled Response acceleration to PGA
% *****

PGAEC8=3.5;
```

Response spectrum

```
SSFERNPSa=SFERNPSa*(PGAEC8/SFERNPSa(1,1));
SIMPVPSa=IMPVPSa*(PGAEC8/IMPVPSa(1,1));
SSHPSa=SHPSa*(PGAEC8/SHPSa(1,1));
SSAPSa=SAPSa*(PGAEC8/SAPSa(1,1));
SMAPSa=MAPSa*(PGAEC8/MAPSa(1,1));
SJCPsa=JCPSa*(PGAEC8/JCPSa(1,1));
SIWPSa=IWPSa*(PGAEC8/IWPSa(1,1));

%% Scaled Response acceleration to T
% *****

PSaEC8=10.06;
TSSFERNPSa=SFERNPSa*(PSaEC8/SFERNPSa(48,1));
TSIMPVPSa=IMPVPSa*(PSaEC8/IMPVPSa(48,1));
TSSHPSa=SHPSa*(PSaEC8/SHPSa(52,1));
TSSAPSa=SAPSa*(PSaEC8/SAPSa(52,1));
TSMAPSa=MAPSa*(PSaEC8/MAPSa(52,1));
TSJCPSa=JCPSa*(PSaEC8/JCPSa(52,1));
TSIWPSa=IWPSa*(PSaEC8/IWPSa(52,1));

%% Plot Response Spectrum
% *****

figure('position', [0, 0, 800, 400]) % Response spectrum
plot(T,IMPVPSa);hold on;
plot(T,SFERNPSa);hold on;
plot(T,SHPSa);hold on;
plot(T,SAPSa);hold on;
plot(T,MAPSa);hold on;
plot(T,JCPSa);hold on;
plot(T,IWPSa);hold on;grid;
legend('Imperial Valley','San Fernando','Superstition Hills',
'Spitak Armenia','Manjil Iran','Joetsu City','Iwate Japan')
xlabel('Natural Period [s]','FontSize',10);ylabel('Response [m/s^2]','FontSize',10)

figure('position', [0, 0, 800, 400]) % Scaled response spectrum, PGA
plot(T,SIMPVPSa);hold on;
plot(T,SSFERNPSa);hold on;
plot(T,SSHPSa);hold on;
plot(T,SSAPSa);hold on;
plot(T,SMAPSa);hold on;
plot(T,SJCPSa);hold on;
plot(T,SIWPSa);hold on;grid;
legend('Imperial Valley','San Fernando','Superstition Hills',
```

Response spectrum

```
'Spitak Armenia','Manjil Iran','Joetsu City','Iwate Japan')
xlabel('Natural Period [s]','FontSize',10');ylabel('Response [m/s^2]','FontSize',10')

figure('position', [0, 0, 800, 400]) % Scaled response spectrum, T1
plot(T,TSIMPVPSa);hold on;
plot(T,TSSFERNPSa);hold on;
plot(T,TSSHPSa);hold on;
plot(T,TSSAPSa);hold on;
plot(T,TSMAPSa);hold on;
plot(T,TSJCPSa);hold on;
plot(T,TSIWPSa);hold on;grid;
legend('Imperial Valley','San Fernando','Superstition Hills',
'Spitak Armenia','Manjil Iran','Joetsu City','Iwate Japan')
xlabel('Natural Period [s]','FontSize',10');ylabel('Response [m/s^2]','FontSize',10')
```

Appendix C

OpenSees scripts

C.1 Main file

```
# Master thesis - Four storey RC building
# Miran Cemalovic - 22.04.2015
# metric units m, kg, N, sec

# Delete previous objects.
#*****
wipe;

# Define model
#*****
model BasicBuilder -ndm 2 -ndf 3; set numModes 6;

# Run model
#*****
source Structure_material.tcl
source Structure_sections.tcl
source Structure_geometry.tcl
source Structure_constraints.tcl
source Structure_gravity_loads.tcl
source Structure_records.tcl
source Structure_NSA.tcl
source Structure_NTHA.tcl
```

C.2 Material

```
# **** Material ****
#*****
#*****
```

Material

```
# Material Concrete - B25
#*****
# Material Concrete 01 - B25 <<-- Does not accounts for confinement
set B25 2500;
set fpc25 [expr -25000000.*1.];
set epsc025 [expr -0.002*1.];
set fpcu25 [expr -(25000000./6)*0.];
set epsu225 -0.035;
#uniaxialMaterial Concrete01 $B25 $fpc25 $epsc025 $fpcu25 $epsu225;

# Material Concrete 07 - B25 <<-- Accounts for confinement
set fc25 [expr 1.2*$fpc25];
set ec25 [expr 1.2*$epsc025];
set Ec25 [expr 2.*($fc25/$ec25)];
set ft25 2600000;
set et25 0.000104;
set xp25 [expr 2.]
set xn25 [expr 2.3]
set r25 [expr ($fc25/5.2)-1.9]
# uniaxialMaterial Concrete07 $B25 $fc25 $ec25 $Ec25
$ft25 $et25 $xp25 $xn25 $r25

# Material Concrete 02 - B25
set lambda 1;
set ft25 2600000.0;
set Ets25 [expr $Ec25];
# uniaxialMaterial Concrete02 $B25 $fpc25
$epsc025 $fpcu25 $epsu225 $lambda $ft25 $Ets25;

# Material Concrete 04 - B25
uniaxialMaterial Concrete04 $B25 $fpc25 $epsc025
$epsu225 $Ec25 $ft25 $et25

# Material ConfinedConcrete 01 - B25 <<-- Accounts for confinement
#****Reinforcement tags****
set kam6 0.006;set Akam6 [expr 3.14159*($kam6/2)*($kam6/2)];
set kam8 0.008;set Akam8 [expr 3.14159*($kam8/2)*($kam8/2)];
set kam10 0.010;set Akam10 [expr 3.14159*($kam10/2)*($kam10/2)];
set kam12 0.012;set Akam12 [expr 3.14159*($kam12/2)*($kam12/2)];
set kam16 0.016;set Akam16 [expr 3.14159*($kam16/2)*($kam16/2)];
set kam20 0.020;set Akam20 [expr 3.14159*($kam20/2)*($kam20/2)];
set kam25 0.025;set Akam25 [expr 3.14159*($kam25/2)*($kam25/2)];
set kam32 0.032;set Akam32 [expr 3.14159*($kam32/2)*($kam32/2)];
```

Material

```
set kam40 0.040;set Akam40 [expr 3.14159*($kam40/2)*($kam40/2)];
set cover 0.035;
```

```
set nu 0.1;
set fyh 500000000.;
set Es0 200000000000.;
set haRatio 0.005;
set mu 10;
```

#Border Beam

```
set B25bb 2501;
set L1bb 0.268;
set L2bb 0.118;
set Sbb 0.085;
set phisbb $kam6;
set phiLonbb $kam25;
uniaxialMaterial ConfinedConcrete01 $B25bb R $fpc25 $Ec25
-eps cu [expr $epsu225*10] -nu $nu $L1bb $L2bb $phisbb
$Sbb $fyh $Es0 $haRatio $mu $phiLonbb;
```

#Interior Beam

```
set B25ib 2502;
set L1ib 0.310;
set L2ib 0.160;
set Sib 0.10;
set phisib $kam10;
set phiLonib $kam32;
uniaxialMaterial ConfinedConcrete01 $B25ib R $fpc25 $Ec25
-eps cu [expr $epsu225*10] -nu $nu $L1ib $L2ib $phisib
$Sib $fyh $Es0 $haRatio $mu $phiLonib;
```

#Border Column

```
set B25bc 2503;
set L1bc 0.24;
set phisbc $kam10;
set Sbc 0.120;
set phiLonbc $kam25;
uniaxialMaterial ConfinedConcrete01 $B25bc S1 $fpc25 $Ec25
-eps cu [expr $epsu225*10] -nu $nu $L1bc $phisbc
$Sbc $fyh $Es0 $haRatio $mu $phiLonbc;
```

#Interior Column

```
set B25ic 2504;
set L1ic 0.338;
```

Material

```
set phisic $kam16;
set Sic 0.125;
set phiLonic $kam32;
uniaxialMaterial ConfinedConcrete01 $B25ic S1 $fpc25 $Ec25
-epsu [expr $epsu225*10] -nu $nu $L1ic $phisic
$Sic $fyh $Es0 $haRatio $mu $phiLonic;

# Wall 2nd storey
set B25w2 2506;
set L1w2 0.608;
set L2w2 0.142;
set Sw2 0.250;
set phisw2 $kam16;
set phiLonw2 $kam32;
uniaxialMaterial ConfinedConcrete01 $B25w2 R $fpc25 $Ec25
-epsu [expr $epsu225*10] -nu $nu $L1w2 $L2w2 $phisw2
$Sw2 $fyh $Es0 $haRatio $mu $phiLonw2;

# Material Concrete Elastic - B25
#uniaxialMaterial Elastic $B25 250000000000.

# Material Concrete - B45
#*****
# Material Concrete 01 - B45 <<-- Does not accounts for confinement
set B45 4500;
set fpc45 [expr -29800000.*1.];
set epsc045 [expr -0.002*1.];
set fpcu45 [expr (-29800000./6.)*0.];
set epsu245 -0.035;
#uniaxialMaterial Concrete01 $B45 $fpc45 $epsc045 $fpcu45 $epsu245;

# Material Concrete 07 - B45 <<-- Accounts for confinement
set fc45 [expr 1*$fpc45];
set ec45 [expr 1*$epsc045];
set Ec45 [expr 2.*($fc45/$ec45)];
set ft45 3800000;
set et45 0.000128;
set xp45 [expr 2.]
set xn45 [expr 2.3]
set r45 [expr ($fc45/5.2)-1.9]
# uniaxialMaterial Concrete07 $B45 $fc45
$ec45 $Ec45 $ft45 $et45 $xp45 $xn45 $r45

# Material Concrete 02 - B45 <<-- Does not accounts for confinement
```

Material

```
set lambda 1;
set ft45 3800000.0;
set Ets45 [expr $Ec45*1];
# uniaxialMaterial Concrete02 $B45 $fpc45
$epsc045 $fpcu45 $epsu245 $lambda $ft45 $Ets45;

# Material Concrete 04 - B45
uniaxialMaterial Concrete04 $B45 $fpc45
$epsc045 $epsu245 $Ec45 $ft45 $et45;

# Wall 1st storey
set B45w1 2505;
set L1w1 0.608;
set L2w1 0.298;
set Sw1 0.125;
set phisw1 $kam16;
set phiLonw1 $kam32;
uniaxialMaterial ConfinedConcrete01 $B45w1 R $fpc45 $Ec45
-epsu [expr $epsu245*10] -nu $nu $L1w1 $L2w1 $phisw1
$Sw1 $fyh $Es0 $haRatio $mu $phiLonw1;

# Material Concrete Elastic - B45
#uniaxialMaterial Elastic $B45 29800000000.

#Material Steel - B500NC
#*****
set B500NC 5000;
set Fy 500000000.;
set E0 200000000000.;
set b 0.005;
uniaxialMaterial Steel01 $B500NC $Fy $E0 $b;
#uniaxialMaterial Elastic $B500NC 200000000000.
# ****Set mass density [kg/m^3]****
set m 2500.;

#**** Include shear deformations ****
#*****
#*****
set nu 0.1;

#Walls
#*****
set Kw1 [expr (5.*2.*($fpc45/$epsc045)*0.4*4.5)/(6.*2.*(1.+$nu))];
set Kw2 [expr (5.*2.*($fpc25/$epsc025)*0.244*4.5)/(6.*2.*(1.+$nu))];
```



```

set Kw3 [expr (5.*2.*($fpc25/$epsc025)*0.175*4.5)/(6.*2.*(1.+$nu))];
set Kw4 $Kw3;
set Kw1mat 7500;
set Kw2mat 8500;
set Kw3mat 9500;
set Kw4mat 10500;
uniaxialMaterial Elastic $Kw1mat $Kw1;
uniaxialMaterial Elastic $Kw2mat $Kw2;
uniaxialMaterial Elastic $Kw3mat $Kw3;
uniaxialMaterial Elastic $Kw4mat $Kw4;

# Beams
#*****
set Kbb5 [expr (5.*2.*($fpc25/$epsc025)*(0.2*0.23+0.57*0.12))/(6.*2.*(1.+$nu))];
set Kbis6 [expr (5.*2.*($fpc25/$epsc025)*(0.25*0.28+0.865*0.12))/(6.*2.*(1.+$nu))];
set Kbil7 [expr (5.*2.*($fpc25/$epsc025)*(0.25*0.28+1.4*0.12))/(6.*2.*(1.+$nu))];
set K5mat 11500;
set K6mat 12500;
set K7mat 13500;
uniaxialMaterial Elastic $K5mat $Kbb5;
uniaxialMaterial Elastic $K6mat $Kbis6;
uniaxialMaterial Elastic $K7mat $Kbil7;

# Columns
#*****
set Kcb8 [expr (5.*2.*($fpc25/$epsc025)*0.33*0.33)/(6.*2.*(1.+$nu))];
set Kci9 [expr (5.*2.*($fpc25/$epsc025)*0.44*0.44)/(6.*2.*(1.+$nu))];
set K8mat 14500;
set K9mat 15500;
uniaxialMaterial Elastic $K8mat $Kcb8;
uniaxialMaterial Elastic $K9mat $Kci9;

```

C.3 Sections

```

#**** Define cross sections ****
#*****
#*****

# Border beam
#*****
set BBbf 0.57;
set BBh 0.35;
set BBbw 0.2;

```

Sections

```
set BBtf 0.12;
set BBnftw 7;
set BBnfdw 8;
set BBnfbf 25;
set BBnftf 4;

# Web
set BBWyI [expr 0.];
set BBWzI [expr -$BBbw/2];
set BBWyJ [expr $BBh-$BBtf];
set BBWzJ [expr -$BBbw/2];
set BBWyK [expr $BBh-$BBtf];
set BBWzK [expr $BBbw/2];
set BBWyL [expr 0.];
set BBWzL [expr $BBbw/2];
# Flange
set BBFyI [expr $BBh-$BBtf];
set BBFzI [expr -$BBbf/2];
set BBFyJ [expr $BBh];
set BBFzJ [expr -$BBbf/2];
set BBFyK [expr $BBh];
set BBFzK [expr $BBbf/2];
set BBFyL [expr $BBh-$BBtf];
set BBFzL [expr $BBbf/2];

set BorderBeam 10000;
section Fiber $BorderBeam {
# Define section 1
patch rect $B25 5 9 $BBWyK [expr $BBWzK-$cover-$kam6]
$BBFyK $BBFzK;
# Define Section 2
patch rect $B25 5 9 $BBFyI $BBFzI
$BBFyJ [expr $BBWzJ+$cover+$kam6];
# Define Section 3
patch rect $B25 1 6 $BBWyI $BBWzI
[expr $BBWyL+$cover+$kam6] $BBWzL;
# Define Section 4
patch rect $B25 13 1 [expr $BBWyL+$cover+$kam6]
[expr $BBWzL-$cover-$kam6] $BBWyK $BBWzK;
# Define section 5
patch rect $B25 13 1 [expr $BBWyI+$cover+$kam6]
$BBWzI $BBWyJ [expr $BBWzJ+$cover+$kam6];
# Define section 6
patch rect $B25 1 4 [expr $BBFyK-$cover-$kam6]
```

```

[expr $BBWzJ+$cover+$kam6] $BBFyK
[expr $BBWzK-$cover-$kam6];
#Define section 7
patch rect $B25bb 18 6 [expr $BBWyI+$cover+$kam6]
[expr$BBWzI+$cover+$kam6]
[expr $BBFyK-$cover-$kam6]
[expr $BBWzK-$cover-$kam6];
# Define Reinforcing Steel
layer straight $B500NC 2 $Akam25
[expr $cover+$kam6] [expr -$BBbw/2+$cover+$kam6]
[expr $cover+$kam6] [expr $BBbw/2-$cover-$kam6];
# bottom reinforcement
layer straight $B500NC 2 $Akam25 [
expr $BBh-$cover-$kam6] [expr -$BBbw/2+$cover+$kam6]
[expr $BBh-$cover-$kam6] [expr $BBbw/2-$cover-$kam6];
# top reinforcement
}
#section Elastic $BorderBeam 25000000000
[expr 0.35*0.2+(2*0.12*0.185)] 0.001127038;

# Small interior beam*
#*****
set IBSbf 0.865;
set IBSb 0.4;
set IBSbw 0.25;
set IBStf 0.12;
set IBSnftw 7;
set IBSnfdw 8;
set IBSnfbf 25;
set IBSnftf 4;

# Web
set IBSWyI [expr 0.];
set IBSWzI [expr -$IBSbw/2];
set IBSWyJ [expr $IBSh-$IBStf];
set IBSWzJ [expr -$IBSbw/2];
set IBSWyK [expr $IBSh-$IBStf];
set IBSWzK [expr $IBSbw/2];
set IBSWyL [expr 0.];
set IBSWzL [expr $IBSbw/2];
# Flange
set IBSFyI [expr $IBSh-$IBStf];
set IBSFzI [expr -$IBSbf/2];
set IBSFyJ [expr $IBSh];

```

```

set IBSFzJ [expr - $\text{\$IBSbf}/2$ ];
set IBSFyK [expr  $\text{\$IBSh}$ ];
set IBSFzK [expr  $\text{\$IBSbf}/2$ ];
set IBSFyL [expr  $\text{\$IBSh}-\text{\$IBStf}$ ];
set IBSFzL [expr  $\text{\$IBSbf}/2$ ];

set InteriorBeamSmall 11000;
section Fiber  $\text{\$InteriorBeamSmall}$  {
# Define section 1
patch rect  $\text{\$B25}$  5 9  $\text{\$IBSWyK}$  [expr  $\text{\$IBSWzK}-\text{\$cover}-\text{\$kam10}$ ]
 $\text{\$IBSFyK}$   $\text{\$IBSFzK}$ ;
# Define Section 2
patch rect  $\text{\$B25}$  5 9  $\text{\$IBSFyI}$   $\text{\$IBSFzI}$   $\text{\$IBSFyJ}$ 
[expr  $\text{\$IBSWzJ}+\text{\$cover}+\text{\$kam10}$ ];
# Define Section 3
patch rect  $\text{\$B25}$  1 6  $\text{\$IBSWyI}$   $\text{\$IBSWzI}$ 
[expr  $\text{\$IBSWyL}+\text{\$cover}+\text{\$kam10}$ ]  $\text{\$IBSWzL}$ ;
# Define Section 4
patch rect  $\text{\$B25}$  13 1 [expr  $\text{\$IBSWyL}+\text{\$cover}+\text{\$kam10}$ ]
[expr  $\text{\$IBSWzL}-\text{\$cover}-\text{\$kam10}$ ]  $\text{\$IBSWyK}$   $\text{\$IBSWzK}$ ;
# Define section 5
patch rect  $\text{\$B25}$  13 1 [expr  $\text{\$IBSWyI}+\text{\$cover}+\text{\$kam10}$ ]
 $\text{\$IBSWzI}$   $\text{\$IBSWyJ}$  [expr  $\text{\$IBSWzJ}+\text{\$cover}+\text{\$kam10}$ ];
# Define section 6
patch rect  $\text{\$B25}$  1 4 [expr  $\text{\$IBSFyK}-\text{\$cover}-\text{\$kam10}$ ]
[expr  $\text{\$IBSWzJ}+\text{\$cover}+\text{\$kam10}$ ]  $\text{\$IBSFyK}$ 
[expr  $\text{\$IBSWzK}-\text{\$cover}-\text{\$kam10}$ ];
#Define section 7
patch rect  $\text{\$B25ib}$  18 6
[expr  $\text{\$IBSWyI}+\text{\$cover}+\text{\$kam10}$ ]
[expr  $\text{\$IBSWzI}+\text{\$cover}+\text{\$kam10}$ ]
[expr  $\text{\$IBSFyK}-\text{\$cover}-\text{\$kam10}$ ]
[expr  $\text{\$IBSWzK}-\text{\$cover}-\text{\$kam10}$ ];
#Define reinforcement
layer straight  $\text{\$B500NC}$  3  $\text{\$Akam32}$ 
[expr  $\text{\$cover}+\text{\$kam10}$ ]
[expr  $-\text{\$IBSbw}/2+\text{\$cover}+\text{\$kam10}$ ]
[expr  $\text{\$cover}+\text{\$kam10}$ ] [expr  $\text{\$IBSbw}/2-\text{\$cover}-\text{\$kam10}$ ];
# bottom reinforcement
layer straight  $\text{\$B500NC}$  3  $\text{\$Akam32}$ 
[expr  $\text{\$IBSh}-\text{\$cover}-\text{\$kam10}$ ]
[expr  $-\text{\$IBSbw}/2+\text{\$cover}+\text{\$kam10}$ ]
[expr  $\text{\$IBSh}-\text{\$cover}-\text{\$kam10}$ ]
[expr  $\text{\$IBSbw}/2-\text{\$cover}-\text{\$kam10}$ ];

```

Sections

```
# top reinforcement
}

#section Elastic $InteriorBeamSmall
25000000000 [expr 0.4*0.25+(2*0.12*0.3075)]
0.00225416048;

# Large interior beam
#*****
set IBLbf 1.400;
set IBLh 0.4;
set IBLbw 0.25;
set IBLtf 0.12;
set IBLnftw 7;
set IBLnfdw 8;
set IBLnfbf 25;
set IBLnftf 4;
# Web
set IBLWyI [expr 0.];
set IBLWzI [expr -$IBLbw/2];
set IBLWyJ [expr $IBLh-$IBLtf];
set IBLWzJ [expr -$IBLbw/2];
set IBLWyK [expr $IBLh-$IBLtf];
set IBLWzK [expr $IBLbw/2];
set IBLWyL [expr 0.];
set IBLWzL [expr $IBLbw/2];
# Flange
set IBLFyI [expr $IBLh-$IBLtf];
set IBLFzI [expr -$IBLbf/2];
set IBLFyJ [expr $IBLh];
set IBLFzJ [expr -$IBLbf/2];
set IBLFyK [expr $IBLh];
set IBLFzK [expr $IBLbf/2];
set IBLFyL [expr $IBLh-$IBLtf];
set IBLFzL [expr $IBLbf/2];

set InteriorBeamLarge 12000;
section Fiber $InteriorBeamLarge {
# Define section 1
patch rect $B25 5 9 $IBLWyK
[expr $IBLWzK-$cover-$kam10] $IBLFyK $IBLFzK;
# Define Section 2
patch rect $B25 5 9 $IBLFyI $IBLFzI $IBLFyJ
[expr $IBLWzJ+$cover+$kam10];
```

```

# Define Section 3
patch rect $B25 1 6 $IBLWyI $IBLWzI
[expr $IBLWyL+$cover+$kam10] $IBLWzL;
# Define Section 4
patch rect $B25 13 1 [expr $IBLWyL+$cover+$kam10]
[expr $IBLWzL-$cover-$kam10] $IBLWyK $IBLWzK;
# Define section 5
patch rect $B25 13 1 [expr $IBLWyI+$cover+$kam10]
$IBLWzI $IBLWyJ [expr $IBLWzJ+$cover+$kam10];
# Define section 6
patch rect $B25 1 4 [expr $IBLFyK-$cover-$kam10]
[expr $IBLWzJ+$cover+$kam10] $IBLFyK
[expr $IBLWzK-$cover-$kam10];
#Define section 7
patch rect $B25ib 18 6 [expr $IBLWyI+$cover+$kam10]
[expr $IBLWzI+$cover+$kam10]
[expr $IBLFyK-$cover-$kam10] [expr $IBLWzK-$cover-$kam10];
# Define reinforcement
layer straight $B500NC 3 $Akam32 [expr $cover+$kam10]
[expr -$IBLbw/2+$cover+$kam10] [expr $cover+$kam10]
[expr $IBLbw/2-$cover-$kam10];
# bottom reinforcement
layer straight $B500NC 3 $Akam32 [expr $IBLh-$cover-$kam10]
[expr -$IBLbw/2+$cover+$kam10]
[expr $IBLh-$cover-$kam10] [expr $IBLbw/2-$cover-$kam10];
# top reinforcement
}
#section Elastic $InteriorBeamLarge 25000000000
[expr 0.4*0.25+(2*0.12*0.575)] 0.00263540412;

****Border column****
*****
set BCbc 0.33;
set BChc $BCbc;
set BCnftc 13;
set BCnfdc 13;
set BCyI [expr -$BChc/2];
set BCzI [expr -$BCbc/2];
set BCyJ [expr $BChc/2];
set BCzJ [expr -$BCbc/2];
set BCyK [expr $BChc/2];
set BCzK [expr $BCbc/2];
set BCyL [expr -$BChc/2];
set BCzL [expr $BCbc/2];

```

```

set BorderColumn 20000;
section Fiber $BorderColumn {
# Define section 1
patch rect $B25 4 8 $BCyI $BCzI
[expr $BCyL+$cover+$kam10] $BCzL;
# Define section 2
patch rect $B25 4 8 [expr $BCyJ-$cover-$kam10]
$BCzJ $BCyK $BCzK;
# Define section 3
patch rect $B25 6 4 [expr $BCyL+$cover+$kam10]
[expr $BCzL-$cover-$kam10]
[expr $BCyK-$cover-$kam10] $BCzK;
# Define section 4
patch rect $B25 6 4 [expr $BCyI+$cover+$kam10] $BCzI
[expr $BCyJ-$cover-$kam10]
[expr $BCzJ+$cover+$kam10];
# Define section 5
patch rect $B25bc 6 6 [expr $BCyI+$cover+$kam10]
[expr $BCzI+$cover+$kam10]
[expr $BCyK-$cover-$kam10]
[expr $BCzK-$cover-$kam10];
# Define reinforcement
layer straight $B500NC 3 $Akam25 [expr -$BChc/2+$cover+$kam10]
[expr -$BCbc/2+$cover+$kam10]
[expr -$BChc/2+$cover+$kam10]
[expr $BCbc/2-$cover-$kam10];
layer straight $B500NC 3 $Akam25
[expr $BChc/2-$cover-$kam10] [expr -$BCbc/2+$cover+$kam10]
[expr $BChc/2-$cover-$kam10] [expr $BCbc/2-$cover-$kam10];
layer straight $B500NC 1 $Akam25 [expr -$BChc/6]
[expr -$BCbc/2+$cover+$kam10]
[expr $BChc/6] [expr -$BCbc/2+$cover+$kam10];
layer straight $B500NC 1 $Akam25 [expr -$BChc/6]
[expr $BCbc/2-$cover-$kam10]
[expr $BChc/6] [expr $BCbc/2-$cover-$kam10];
}

#section Elastic $BorderColumn 25000000000
[expr 0.33*0.33] 0.0009882675;
# Interior column
#*****
set ICbc 0.44;
set IChc $ICbc;

```

```

set ICnftc 13;
set ICnfdc 13;
set ICyI [expr - $\text{IChc}/2$ ];
set ICzI [expr - $\text{ICbc}/2$ ];
set ICyJ [expr  $\text{IChc}/2$ ];
set ICzJ [expr - $\text{ICbc}/2$ ];
set ICyK [expr  $\text{IChc}/2$ ];
set ICzK [expr  $\text{ICbc}/2$ ];
set ICyL [expr - $\text{IChc}/2$ ];
set ICzL [expr  $\text{ICbc}/2$ ];

set InteriorColumn 21000;
section Fiber $InteriorColumn {
# Define section 1
patch rect $B25 4 8 $ICyI $ICzI
[expr $ICyL+$cover+$kam16] $ICzL;
# Define section 2
patch rect $B25 4 8 [expr $ICyJ-$cover-$kam16]
$ICzJ $ICyK $ICzK;
# Define section 3
patch rect $B25 6 4 [expr $ICyL+$cover+$kam16]
[expr $ICzL-$cover-$kam16]
[expr $ICyK-$cover-$kam16] $ICzK;
# Define section 4
patch rect $B25 6 4 [expr $ICyI+$cover+$kam16]
$ICzI [expr $ICyJ-$cover-$kam16]
[expr $ICzJ+$cover+$kam16];
# Define section 5
patch rect $B25ic 6 6 [expr $ICyI+$cover+$kam16]
[expr $ICzI+$cover+$kam16]
[expr $ICyK-$cover-$kam16] [expr $ICzK-$cover-$kam16];
# Define reinforcement
layer straight $B500NC 4 $Akam32
[expr - $\text{IChc}/2$ +$cover+$kam16]
[expr - $\text{ICbc}/2$ +$cover+$kam16]
[expr - $\text{IChc}/2$ +$cover+$kam16]
[expr  $\text{ICbc}/2$ -$cover-$kam16];
layer straight $B500NC 4 $Akam32
[expr  $\text{IChc}/2$ -$cover-$kam16]
[expr - $\text{ICbc}/2$ +$cover+$kam16]
[expr  $\text{IChc}/2$ -$cover-$kam16]
[expr  $\text{ICbc}/2$ -$cover-$kam16];
layer straight $B500NC 2 $Akam32
[expr - $\text{IChc}/4$ ] [expr - $\text{ICbc}/2$ +$cover+$kam16]

```


Sections

```
[expr $IChc/4] [expr -$ICbc/2+$cover+$kam16];
layer straight $B500NC 2 $Akam32 [expr -$IChc/4]
[expr $ICbc/2-$cover-$kam16]
[expr $IChc/4] [expr $ICbc/2-$cover-$kam16];
}
#section Elastic $InteriorColumn 25000000000
[expr 0.44*0.44] 0.00312341333;

# Wall 4th storey
#*****
set W4bc 0.175;
set W4hc 4.5;
set W4nftc 40;
set W4nfdc 4;
set W4yI [expr -$W4hc/2];
set W4zI [expr -$W4bc/2];
set W4yJ [expr $W4hc/2];
set W4zJ [expr -$W4bc/2];
set W4yK [expr $W4hc/2];
set W4zK [expr $W4bc/2];
set W4yL [expr -$W4hc/2];
set W4zL [expr $W4bc/2];

set Wall4 34000;
section Fiber $Wall4 {
# Define section
patch quad $B25 $W4nftc $W4nfdc $W4yI
$W4zI $W4yJ $W4zJ $W4yK $W4zK $W4yL $W4zL;
# Define reinforcement
layer straight $B500NC 18 $Akam12
[expr -$W4hc/2+$cover+$kam16] [expr -$W4bc/2+$cover+$kam16]
[expr $W4hc/2-$cover-$kam16] [expr -$W4bc/2+$cover+$kam16];
layer straight $B500NC 18 $Akam12
[expr -$W4hc/2+$cover+$kam16] [expr $W4bc/2-$cover-$kam16]
[expr $W4hc/2-$cover-$kam16] [expr $W4bc/2-$cover-$kam16];
}
#section Elastic $Wall4 25000000000
[expr 4.5*0.175] 1.32890635792;

# Wall 3rd storey
#*****
set W3bc 0.175;
set W3hc 4.5;
set W3lcr 0.675;
```

Sections

```
set W3nftc 40;
set W3nfdc 4;
set W3yI [expr -$W3hc/2];
set W3zI [expr -$W3bc/2];
set W3yJ [expr $W3hc/2];
set W3zJ [expr -$W3bc/2];
set W3yK [expr $W3hc/2];
set W3zK [expr $W3bc/2];
set W3yL [expr -$W3hc/2];
set W3zL [expr $W3bc/2];

set Wall3 33000;
section Fiber $Wall3 {
# Define section
patch quad $B25 $W3nftc $W3nfdc $W3yI
$W3zI $W3yJ $W3zJ $W3yK $W3zK $W3yL $W3zL;
# Define reinforcement
layer straight $B500NC 12 $Akam12
[expr -$W3hc/2+$W3lcr] [expr -$W3bc/2+$cover+$kam16]
[expr $W3hc/2-$W3lcr] [expr -$W3bc/2+$cover+$kam16];
layer straight $B500NC 12 $Akam12
[expr -$W3hc/2+$W3lcr] [expr $W3bc/2-$cover-$kam16]
[expr $W3hc/2-$W3lcr] [expr $W3bc/2-$cover-$kam16];

layer straight $B500NC 3 $Akam25
[expr -$W3hc/2+$cover+$kam16] [expr -$W3bc/2+$cover+$kam16]
[expr -$W3hc/2+$W3lcr] [expr -$W3bc/2+$cover+$kam16];
layer straight $B500NC 3 $Akam25
[expr $W3hc/2-$W3lcr] [expr -$W3bc/2+$cover+$kam16]
[expr $W3hc/2-$cover-$kam16] [expr -$W3bc/2+$cover+$kam16];
layer straight $B500NC 3 $Akam25
[expr -$W3hc/2+$cover+$kam16] [expr $W3bc/2-$cover-$kam16]
[expr -$W3hc/2+$W3lcr] [expr $W3bc/2-$cover-$kam16];
layer straight $B500NC 3 $Akam25 [expr $W3hc/2-$W3lcr]
[expr $W3bc/2-$cover-$kam16]
[expr $W3hc/2-$cover-$kam16]
[expr $W3bc/2-$cover-$kam16];
}
#section Elastic $Wall3 25000000000
[expr 4.5*0.175] 1.32890635792;

# Wall 2nd storey
#*****
set W2bc 0.244;
```

```

set W2hc 4.5;
set W2lcr 0.675;
set W2nftc 40;
set W2nfdc 4;
set W2yI [expr -$W2hc/2];
set W2zI [expr -$W2bc/2];
set W2yJ [expr $W2hc/2];
set W2zJ [expr -$W2bc/2];
set W2yK [expr $W2hc/2];
set W2zK [expr $W2bc/2];
set W2yL [expr -$W2hc/2];
set W2zL [expr $W2bc/2];

set Wall2 32000;
section Fiber $Wall2 {
# Define section 1
patch rect $B25 2 5 $W2yI [expr $W2zI+$cover+$kam16]
[expr $W2yL+$cover+$kam16]
[expr $W2zL-$cover-$kam16];
# Define section 2
patch rect $B25 2 5 [expr $W2yJ-$cover-$kam16]
[expr $W2zJ+$cover+$kam16] $W2yK
[expr $W2zK-$cover-$kam16];
# Define section 3
patch rect $B25 60 2 $W2yL [expr $W2zL-$cover-$kam16]
$W2yK $W2zK;
# Define section 4
patch rect $B25 60 2 $W2yI $W2zI $W2yJ
[expr $W2zJ+$cover+$kam16];
# Define section 5
patch rect $B25 40 10 [expr $W2yI+$W2lcr]
[expr $W2zI+$cover+$kam16]
[expr $W2yK-$W2lcr] [expr $W2zK-$cover-$kam16];
# Define section 6
patch rect $B25w2 20 10 [expr $W2yI+$cover+$kam16]
[expr $W2zI+$cover+$kam16]
[expr $W2yL+$W2lcr] [expr $W2zL-$cover-$kam16];
# Define section 7
patch rect $B25w2 20 10 [expr $W2yJ-$W2lcr]
[expr $W2zJ+$cover+$kam16]
[expr $W2yK-$cover-$kam16] [expr $W2zK-$cover-$kam16];
# Define reinforcement
layer straight $B500NC 12 $Akam12
[expr -$W2hc/2+$W2lcr] [expr -$W2bc/2+$cover+$kam16]

```

Sections

```
[expr $W2hc/2-$W2lcr] [expr -$W2bc/2+$cover+$kam16];
layer straight $B500NC 12 $Akam12
[expr -$W2hc/2+$W2lcr] [expr $W2bc/2-$cover-$kam16]
[expr $W2hc/2-$W2lcr] [expr $W2bc/2-$cover-$kam16];
layer straight $B500NC 5 $Akam32
  [expr -$W2hc/2+$cover+$kam16]
  [expr -$W2bc/2+$cover+$kam16]
[expr -$W2hc/2+$W2lcr] [expr -$W2bc/2+$cover+$kam16];
layer straight $B500NC 5 $Akam32 [expr $W2hc/2-$W2lcr]
[expr -$W2bc/2+$cover+$kam16]
[expr $W2hc/2-$cover-$kam16]
[expr -$W2bc/2+$cover+$kam16];
layer straight $B500NC 5 $Akam32
[expr -$W2hc/2+$cover+$kam16] [expr $W2bc/2-$cover-$kam16]
[expr -$W2hc/2+$W2lcr] [expr $W2bc/2-$cover-$kam16];
layer straight $B500NC 5 $Akam32 [expr $W2hc/2-$W2lcr]
[expr $W2bc/2-$cover-$kam16]
[expr $W2hc/2-$cover-$kam16] [expr $W2bc/2-$cover-$kam16];
}
#section Elastic $Wall2 25000000000
[expr 4.5*0.244] 1.852875;

# Wall 1st storey
#*****
set W1bc 0.400;
set W1hc 4.5;
set W1lcr 0.675;
set W1nftc 40;
set W1nfdc 4;
set W1yI [expr -$W1hc/2];
set W1zI [expr -$W1bc/2];
set W1yJ [expr $W1hc/2];
set W1zJ [expr -$W1bc/2];
set W1yK [expr $W1hc/2];
set W1zK [expr $W1bc/2];
set W1yL [expr -$W1hc/2];
set W1zL [expr $W1bc/2];

set Wall1 31000;
section Fiber $Wall1 {
# Define section 1
patch rect $B45 2 5 $W1yI [expr $W1zI+$cover+$kam16]
[expr $W1yL+$cover+$kam16]
[expr $W1zL-$cover-$kam16];
```

Sections

```
# Define section 2
patch rect $B45 2 5 [expr $W1yJ-$cover-$kam16]
[expr $W1zJ+$cover+$kam16] $W1yK
[expr $W1zK-$cover-$kam16];
# Define section 3
patch rect $B45 60 2 $W1yL
[expr $W1zL-$cover-$kam16] $W1yK $W1zK;
# Define section 4
patch rect $B45 60 2 $W1yI $W1zI $W1yJ
[expr $W1zJ+$cover+$kam16];
# Define section 5
patch rect $B45 40 10 [expr $W1yI+$W1lcr]
[expr $W1zI+$cover+$kam16]
[expr $W1yK-$W1lcr] [expr $W1zK-$cover-$kam16];
# Define section 6
patch rect $B45w1 20 10 [expr $W1yI+$cover+$kam16]
[expr $W1zI+$cover+$kam16]
[expr $W1yL+$W1lcr] [expr $W1zL-$cover-$kam16];
# Define section 7
patch rect $B45w1 20 10 [expr $W1yJ-$W1lcr]
[expr $W1zJ+$cover+$kam16]
[expr $W1yK-$cover-$kam16] [expr $W1zK-$cover-$kam16];
# Define reinforcement
layer straight $B500NC 13 $Akam16 [expr -$W1hc/2+$W1lcr]
[expr -$W1bc/2+$cover+$kam16]
[expr $W1hc/2-$W1lcr] [expr -$W1bc/2+$cover+$kam16];
layer straight $B500NC 13 $Akam16 [expr -$W1hc/2+$W1lcr]
[expr $W1bc/2-$cover-$kam16]
[expr $W1hc/2-$W1lcr] [expr $W1bc/2-$cover-$kam16];
layer straight $B500NC 7 $Akam32
[expr -$W1hc/2+$cover+$kam16] [expr -$W1bc/2+$cover+$kam16]
[expr -$W1hc/2+$W1lcr] [expr -$W1bc/2+$cover+$kam16];
layer straight $B500NC 7 $Akam32 [expr $W1hc/2-$W1lcr] [expr -$W1bc/2+$cover+$kam16]
[expr $W1hc/2-$cover-$kam16] [expr -$W1bc/2+$cover+$kam16];
layer straight $B500NC 7 $Akam32 [expr -$W1hc/2+$cover+$kam16]
[expr $W1bc/2-$cover-$kam16]
[expr -$W1hc/2+$W1lcr] [expr $W1bc/2-$cover-$kam16];
layer straight $B500NC 7 $Akam32 [expr $W1hc/2-$W1lcr]
[expr $W1bc/2-$cover-$kam16]
[expr $W1hc/2-$cover-$kam16]
[expr $W1bc/2-$cover-$kam16];
}
#section Elastic $Wall1 25000000000 [expr 4.5*0.4] 3.0375;
```

```

#Add shear deformations
#*****
#*****

# Walls
#*****
set Wall1ws 310000;
set Wall2ws 320000;
set Wall3ws 330000;
set Wall4ws 340000;
section Aggregator $Wall1ws $Kw1mat Vy -section $Wall1;
section Aggregator $Wall2ws $Kw2mat Vy -section $Wall2;
section Aggregator $Wall3ws $Kw3mat Vy -section $Wall3;
section Aggregator $Wall4ws $Kw4mat Vy -section $Wall4;

# Beams
#*****
set BorderBeamws 350000;
set InteriorBeamSmallws 360000;
set InteriorBeamLargews 370000;
section Aggregator $BorderBeamws $K5mat Vy -section $BorderBeam;
section Aggregator $InteriorBeamSmallws $K6mat Vy -section $InteriorBeamSmall;
section Aggregator $InteriorBeamLargews $K7mat Vy -section $InteriorBeamLarge;

# Columns
#*****
set BorderColumnws 380000;
set InteriorColumnws 390000;
section Aggregator $BorderColumnws $K8mat Vy -section $BorderColumn;
section Aggregator $InteriorColumnws $K9mat Vy -section $InteriorColumn;

```

C.4 Geometry

```

# **** Define geometry ****
#*****
#*****

# Define lengts, sectional areas and gravity
#*****
set L1 6.;
set L2 4.5;
set h1 4.250;
set h2 3.500;

```

```

set Acb [expr 0.33*0.33];
set Abb [expr 0.35*0.2+(2*0.12*0.185)];
set Aci [expr 0.44*0.44];
set Abl [expr 0.4*0.25+(2*0.12*0.575)];
set Abs [expr 0.4*0.25+(2*0.12*0.3075)];
set Aw4 [expr 4.5*0.175];
set Aw3 [expr 4.5*0.175];
set Aw2 [expr 4.5*0.244];
set Aw1 [expr 4.5*0.4];
set g 9.81;

# Geometry transformation
#*****
set GeoTranPdelta 100001;
geomTransf PDelta $GeoTranPdelta;

# Set number of intgration point for FB - members
#*****
set N 4;

# Frame A
#*****

# 4th storey
#*****
node 141 0. [expr $h1+3*$h2];
mass 141 [expr (($h2/2)*$Acb*$m)+(($L1/2)*$Abb*$m)+(9100.*$L1)/2./$g] 0. 0.;
node 142 $L1 [expr $h1+3*$h2];
mass 142 [expr (($h2/2)*$Acb*$m)+($L1*$Abb*$m)+(9100.*$L1)/$g] 0. 0.
node 143 [expr 2*$L1] [expr $h1+3*$h2];
mass 143 [expr (($h2/2)*$Acb*$m)+(($L1/2)*$Abb*$m)+(($L2/2)*$Abb*$m)
          +(9100.*$L1)/2/$g+(9100.*$L2)/2/$g] 0. 0.;
node 144 [expr 2*$L1+$L2] [expr $h1+3*$h2];
mass 144 [expr (($h2/2)*$Acb*$m)+(($L1/2)*$Abb*$m)+(($L2/2)*$Abb*$m)
          +(9100.*$L1)/2/$g+(9100.*$L2)/2/$g] 0. 0.;
node 145 [expr 3*$L1+$L2] [expr $h1+3*$h2];
mass 145 [expr (($h2/2)*$Acb*$m)+($L1*$Abb*$m)+(9100.*$L1)/$g] 0. 0.;
node 146 [expr 4*$L1+$L2] [expr $h1+3*$h2];
mass 146 [expr (($h2/2)*$Acb*$m)+(($L1/2)*$Abb*$m)+(9100.*$L1)/2/$g] 0. 0.;

# 3rd storey
#*****
node 131 0. [expr $h1+2*$h2];
mass 131 [expr ($h2*$Acb*$m)+(($L1/2)*$Abb*$m)+(14300.*$L1)/2./$g] 0. 0.;

```

```

node 132 $L1 [expr $h1+2*$h2];
mass 132 [expr ($h2*$Acb*$m)+($L1*$Abb*$m)+(14300.*$L1)/$g] 0. 0.;
node 133 [expr 2*$L1] [expr $h1+2*$h2];
mass 133 [expr ($h2*$Acb*$m)+(($L1/2)*$Abb*$m)+(($L2/2)*$Abb*$m)
          +(14300.*$L1)/2/$g+(14300.*$L2)/2/$g] 0. 0.;
node 134 [expr 2*$L1+$L2] [expr $h1+2*$h2];
mass 134 [expr ($h2*$Acb*$m)+(($L1/2)*$Abb*$m)+(($L2/2)*$Abb*$m)
          +(14300.*$L1)/2/$g+(14300.*$L2)/2/$g] 0. 0.;
node 135 [expr 3*$L1+$L2] [expr $h1+2*$h2];
mass 135 [expr ($h2*$Acb*$m)+($L1*$Abb*$m)+(14300.*$L1)/$g] 0. 0.;
node 136 [expr 4*$L1+$L2] [expr $h1+2*$h2];
mass 136 [expr ($h2*$Acb*$m)+(($L1/2)*$Abb*$m)+(14300.*$L1)/2./$g] 0. 0.;

# 2nd storey
#*****
node 121 0. [expr $h1+$h2];
mass 121 [expr ($h2*$Acb*$m)+(($L1/2)*$Abb*$m)+(14300.*$L1)/2./$g] 0. 0.;
node 122 $L1 [expr $h1+$h2];
mass 122 [expr ($h2*$Acb*$m)+($L1*$Abb*$m)+(14300.*$L1)/$g] 0. 0.;
node 123 [expr 2*$L1] [expr $h1+$h2];
mass 123 [expr ($h2*$Acb*$m)+(($L1/2)*$Abb*$m)+(($L2/2)*$Abb*$m)
          +(14300.*$L1)/2/$g+(14300.*$L2)/2/$g] 0. 0.;
node 124 [expr 2*$L1+$L2] [expr $h1+$h2];
mass 124 [expr ($h2*$Acb*$m)+(($L1/2)*$Abb*$m)+(($L2/2)*$Abb*$m)
          +(14300.*$L1)/2/$g+(14300.*$L2)/2/$g] 0. 0.;
node 125 [expr 3*$L1+$L2] [expr $h1+$h2];
mass 125 [expr ($h2*$Acb*$m)+($L1*$Abb*$m)+(14300.*$L1)/$g] 0. 0.;
node 126 [expr 4*$L1+$L2] [expr $h1+$h2];
mass 126 [expr ($h2*$Acb*$m)+(($L1/2)*$Abb*$m)+(14300.*$L1)/2./$g] 0. 0.;

# 1st storey
#*****
node 111 0. $h1;
mass 111
[expr ((($h1/2)*$Acb*$m)+(($h2/2)*$Acb*$m)+(($L1/2)*$Abb*$m)
          +(14300.*$L1)/2./$g] 0. 0.;
node 112 $L1 $h1
mass 112
[expr ((($h1/2)*$Acb*$m)+(($h2/2)*$Acb*$m)+($L1*$Abb*$m)
          +(14300.*$L1)/$g] 0. 0.;
node 113 [expr 2*$L1] $h1
mass 113
[expr((($h1/2)*$Acb*$m)+(($h2/2)*$Acb*$m)+(($L1/2)*$Abb*$m)+
          (($L2/2)*$Abb*$m)+(14300.*$L1)/2/$g+(14300.*$L2)/2/$g] 0. 0.;

```



```

node 114 [expr 2*$L1+$L2] $h1
mass 114
[expr(($h1/2)*$Acb*$m)+(($h2/2)*$Acb*$m)+(($L1/2)*$Abb*$m)+
(($L2/2)*$Abb*$m)+(14300.*$L1)/2/$g+(14300.*$L2)/2/$g] 0. 0.;
node 115 [expr 3*$L1+$L2] $h1;
mass 115 [expr (($h1/2)*$Acb*$m)+(($h2/2)*$Acb*$m)+($L1*$Abb*$m)
+(14300.*$L1)/$g] 0. 0.;
node 116 [expr 4*$L1+$L2] $h1;
mass 116 [expr (($h1/2)*$Acb*$m)+(($h2/2)*$Acb*$m)+(($L1/2)*$Abb*$m)
+(14300.*$L1)/2./$g] 0. 0.;

```

Ground floor

```

node 101 0. 0.;
mass 101 0. 0. 0.;
node 102 $L1 0.;
mass 102 0. 0. 0.;
node 103 [expr 2*$L1] 0.;
mass 103 0. 0. 0.;
node 104 [expr 2*$L1+$L2] 0.;
mass 104 0. 0. 0.;
node 105 [expr 3*$L1+$L2] 0.
mass 105 0. 0. 0.;
node 106 [expr 4*$L1+$L2] 0.;
mass 106 0. 0. 0.;

```

Define restraints

```

fix 101 1 1 1;
fix 102 1 1 1;
fix 103 1 1 1;
fix 104 1 1 1;
fix 105 1 1 1;
fix 106 1 1 1;

```

Define columns

```

element forceBeamColumn 1 101 111 $N $BorderColumn $GeoTranPdelta;
element forceBeamColumn 2 102 112 $N $BorderColumn $GeoTranPdelta;
element forceBeamColumn 3 103 113 $N $BorderColumn $GeoTranPdelta;
element forceBeamColumn 4 104 114 $N $BorderColumn $GeoTranPdelta;
element forceBeamColumn 5 105 115 $N $BorderColumn $GeoTranPdelta;
element forceBeamColumn 6 106 116 $N $BorderColumn $GeoTranPdelta;
element forceBeamColumn 7 111 121 $N $BorderColumn $GeoTranPdelta;

```

```

element forceBeamColumn 8 112 122 $N $BorderColumn $GeoTranPdelta;
element forceBeamColumn 9 113 123 $N $BorderColumn $GeoTranPdelta;
element forceBeamColumn 10 114 124 $N $BorderColumn $GeoTranPdelta;
element forceBeamColumn 11 115 125 $N $BorderColumn $GeoTranPdelta;
element forceBeamColumn 12 116 126 $N $BorderColumn $GeoTranPdelta;
element forceBeamColumn 13 121 131 $N $BorderColumn $GeoTranPdelta;
element forceBeamColumn 14 122 132 $N $BorderColumn $GeoTranPdelta;
element forceBeamColumn 15 123 133 $N $BorderColumn $GeoTranPdelta;
element forceBeamColumn 16 124 134 $N $BorderColumn $GeoTranPdelta;
element forceBeamColumn 17 125 135 $N $BorderColumn $GeoTranPdelta;
element forceBeamColumn 18 126 136 $N $BorderColumn $GeoTranPdelta;
element forceBeamColumn 19 131 141 $N $BorderColumn $GeoTranPdelta;
element forceBeamColumn 20 132 142 $N $BorderColumn $GeoTranPdelta;
element forceBeamColumn 21 133 143 $N $BorderColumn $GeoTranPdelta;
element forceBeamColumn 22 134 144 $N $BorderColumn $GeoTranPdelta;
element forceBeamColumn 23 135 145 $N $BorderColumn $GeoTranPdelta;
element forceBeamColumn 24 136 146 $N $BorderColumn $GeoTranPdelta;

```

Define beams

```

element forceBeamColumn 25 111 112 $N $BorderBeam $GeoTranPdelta;
element forceBeamColumn 26 112 113 $N $BorderBeam $GeoTranPdelta;
element forceBeamColumn 27 113 114 $N $BorderBeam $GeoTranPdelta;
element forceBeamColumn 28 114 115 $N $BorderBeam $GeoTranPdelta;
element forceBeamColumn 29 115 116 $N $BorderBeam $GeoTranPdelta;
element forceBeamColumn 30 121 122 $N $BorderBeam $GeoTranPdelta;
element forceBeamColumn 31 122 123 $N $BorderBeam $GeoTranPdelta;
element forceBeamColumn 32 123 124 $N $BorderBeam $GeoTranPdelta;
element forceBeamColumn 33 124 125 $N $BorderBeam $GeoTranPdelta;
element forceBeamColumn 34 125 126 $N $BorderBeam $GeoTranPdelta;
element forceBeamColumn 35 131 132 $N $BorderBeam $GeoTranPdelta;
element forceBeamColumn 36 132 133 $N $BorderBeam $GeoTranPdelta;
element forceBeamColumn 37 133 134 $N $BorderBeam $GeoTranPdelta;
element forceBeamColumn 38 134 135 $N $BorderBeam $GeoTranPdelta;
element forceBeamColumn 39 135 136 $N $BorderBeam $GeoTranPdelta;
element forceBeamColumn 40 141 142 $N $BorderBeam $GeoTranPdelta;
element forceBeamColumn 41 142 143 $N $BorderBeam $GeoTranPdelta;
element forceBeamColumn 42 143 144 $N $BorderBeam $GeoTranPdelta;
element forceBeamColumn 43 144 145 $N $BorderBeam $GeoTranPdelta;
element forceBeamColumn 44 145 146 $N $BorderBeam $GeoTranPdelta;

```

Frame B

```

# 4th storey
#*****
node 241 30. [expr $h1+3*$h2];
mass 241 [expr (($h2/2)*$Acb*$m)+(($L1/2)*$Abs*$m)+(23100.*$L1)/2/$g] 0. 0.;
node 242 [expr 30.+$L1] [expr $h1+3*$h2];
mass 242 [expr (($h2/2)*$Aci*$m)+(($L1/2)*$Abl*$m)+(($L1/2)*$Abs*$m)
          +(23100.*$L1)/$g] 0. 0.
node 243 [expr 30.+2*$L1] [expr $h1+3*$h2];
mass 243 [expr (($L1/2)*$Abl*$m)+(23100.*$L1)/2/$g] 0. 0.;
node 244 [expr 30.+2*$L1+$L2/2] [expr $h1+3*$h2];
mass 244 [expr ($h2/2)*$Aw4*$m+104000./9.81] 0. 0.;
node 245 [expr 30.+2*$L1+$L2] [expr $h1+3*$h2];
mass 245 [expr (($L1/2)*$Abl*$m)+(23100.*$L1)/2/$g] 0. 0.;
node 246 [expr 30.+3*$L1+$L2] [expr $h1+3*$h2];
mass 246 [expr (($h2/2)*$Aci*$m)+(($L1/2)*$Abl*$m)+(($L1/2)*$Abs*$m)
          +(23100.*$L1)/$g] 0. 0.
node 247 [expr 30.+4*$L1+$L2] [expr $h1+3*$h2];
mass 247 [expr (($h2/2)*$Acb*$m)+(($L1/2)*$Abs*$m)+(23100.*$L1)/2./$g] 0. 0.;

# 3rd storey
#*****
node 231 30. [expr $h1+2*$h2];
mass 231 [expr ($h2*$Acb*$m)+(($L1/2)*$Abs*$m)+(36300.*$L1)/2/$g] 0. 0.;
node 232 [expr 30.+$L1] [expr $h1+2*$h2];
mass 232 [expr (($h2*$Aci*$m)+($L1/2)*$Abs*$m)+(($L1/2)*$Abl*$m)
          +(36300.*$L1)/$g] 0. 0.;
node 233 [expr 30.+2*$L1] [expr $h1+2*$h2];
mass 233 [expr (($L1/2)*$Abl*$m)+(36300.*$L1)/2/$g] 0. 0.;
node 234 [expr 30.+2*$L1+$L2/2] [expr $h1+2*$h2];
mass 234 [expr ($h2/2)*$Aw4*$m+($h2/2)*$Aw3*$m+163400./9.81] 0. 0.;
node 235 [expr 30.+2*$L1+$L2] [expr $h1+2*$h2];
mass 235 [expr (($L1/2)*$Abl*$m)+(36300.*$L1)/2/$g] 0. 0.;
node 236 [expr 30.+3*$L1+$L2] [expr $h1+2*$h2];
mass 236 [expr (($h2*$Aci*$m)+($L1/2)*$Abs*$m)+(($L1/2)*$Abl*$m)
          +(36300.*$L1)/$g] 0. 0.;
node 237 [expr 30.+4*$L1+$L2] [expr $h1+2*$h2];
mass 237 [expr ($h2*$Acb*$m)+(($L1/2)*$Abs*$m)+(36300.*$L1)/2/$g] 0. 0.;

# 2nd storey
#*****
node 221 30.0 [expr $h1+$h2];
mass 221 [expr ($h2*$Acb*$m)+(($L1/2)*$Abs*$m)+(36300.*$L1)/2/$g] 0. 0.;
node 222 [expr 30.+$L1] [expr $h1+$h2];
mass 222 [expr ($h2*$Aci*$m)+(($L1/2)*$Abs*$m)+(($L1/2)*$Abl*$m)

```

```

        +(36300.*$L1)/$g] 0. 0.;
node 223 [expr 30.0+2*$L1] [expr $h1+$h2];
mass 223 [expr (($L1/2)*$Ab1*$m)+(36300.*$L1)/2/$g] 0. 0.;
node 224 [expr 30.+2*$L1+$L2/2] [expr $h1+$h2];
mass 224 [expr ($h2*$Aw2*$m)+($h2*$Aw3*$m)+163400./9.81] 0. 0.;
node 225 [expr 30.+2*$L1+$L2] [expr $h1+$h2];
mass 225 [expr (($L1/2)*$Ab1*$m)+(36300.*$L1)/2/$g] 0. 0.;
node 226 [expr 30.+3*$L1+$L2] [expr $h1+$h2];
mass 226 [expr ($h2*$Aci*$m)+(($L1/2)*$Abs*$m)+(($L1/2)*$Ab1*$m)
        +(36300.*$L1)/$g] 0. 0.;
node 227 [expr 30.+4*$L1+$L2] [expr $h1+$h2];
mass 227 [expr ($h2*$Acb*$m)+(($L1/2)*$Abs*$m)+(36300.*$L1)/2/$g] 0. 0.;

```

1st storey

```

node 211 30. $h1;
mass 211 [expr (($h1/2)*$Acb*$m)+(($h2/2)*$Acb*$m)+(($L1/2)*$Abs*$m)
        +(36300.*$L1)/2/$g] 0. 0.;
node 212 [expr 30.+$L1] $h1;
mass 212 [expr (($h1/2)*$Aci*$m)+(($h2/2)*$Aci*$m)+(($L1/2)*$Abs*$m)
        +(($L1/2)*$Ab1*$m)+(36300.*$L1)/$g] 0. 0.;
node 213 [expr 30.+2*$L1] $h1;
mass 213 [expr (($L1/2)*$Ab1*$m)+(36300.*$L1)/2/$g] 0. 0.;
node 214 [expr 30.+2*$L1+$L2/2] $h1;
mass 214 [expr (($h1/2)*$Aw2*$m)+(($h2/2)*$Aw1*$m)+163400./9.81] 0. 0.;
node 215 [expr 30.+2*$L1+$L2] $h1;
mass 215 [expr (($L1/2)*$Ab1*$m)+(36300.*$L1)/2/$g] 0. 0.;
node 216 [expr 30.+3*$L1+$L2] $h1;
mass 216 [expr (($h1/2)*$Aci*$m)+(($h2/2)*$Aci*$m)+(($L1/2)*$Abs*$m)
        +(($L1/2)*$Ab1*$m)+(36300.*$L1)/$g] 0. 0.;
node 217 [expr 30.+4*$L1+$L2] $h1;
mass 217 [expr (($h1/2)*$Acb*$m)+(($h2/2)*$Acb*$m)+(($L1/2)*$Abs*$m)
        +(36300.*$L1)/2/$g] 0. 0.;

```

Ground floor

```

node 201 30. 0.;
mass 201 [expr ($h1/2)*$Acb*$m] 0. 0.;
node 202 [expr 30.+$L1] 0.;
mass 202 0. 0. 0.;
node 203 [expr 30.+2*$L1] 0.;
mass 203 0. 0. 0.;
node 204 [expr 30.+2*$L1+$L2/2] 0.;
mass 204 0. 0. 0.;

```

```
node 205 [expr 30.+2*$L1+$L2] 0.;
mass 205 0. 0. 0.;
node 206 [expr 30.+3*$L1+$L2] 0.
mass 206 0. 0. 0.;
node 207 [expr 30.+4*$L1+$L2] 0.;
mass 207 0. 0. 0.;
```

Define restraints

```
*****
```

```
fix 201 1 1 1;
fix 202 1 1 1;
fix 203 1 1 1;
fix 204 1 1 1;
fix 205 1 1 1;
fix 206 1 1 1;
fix 207 1 1 1;
```

Define columns

```
*****
```

```
element forceBeamColumn 45 201 211 $N $BorderColumn $GeoTranPdelta;
element forceBeamColumn 46 202 212 $N $InteriorColumn $GeoTranPdelta;
element forceBeamColumn 47 206 216 $N $InteriorColumn $GeoTranPdelta;
element forceBeamColumn 48 207 217 $N $BorderColumn $GeoTranPdelta;
```

```
element forceBeamColumn 49 211 221 $N $BorderColumn $GeoTranPdelta;
element forceBeamColumn 50 212 222 $N $InteriorColumn $GeoTranPdelta;
element forceBeamColumn 51 216 226 $N $InteriorColumn $GeoTranPdelta;
element forceBeamColumn 52 217 227 $N $BorderColumn $GeoTranPdelta;
```

```
element forceBeamColumn 53 221 231 $N $BorderColumn $GeoTranPdelta;
element forceBeamColumn 54 222 232 $N $InteriorColumn $GeoTranPdelta;
element forceBeamColumn 55 226 236 $N $InteriorColumn $GeoTranPdelta;
element forceBeamColumn 56 227 237 $N $BorderColumn $GeoTranPdelta;
```

```
element forceBeamColumn 57 231 241 $N $BorderColumn $GeoTranPdelta;
element forceBeamColumn 58 232 242 $N $InteriorColumn $GeoTranPdelta;
element forceBeamColumn 59 236 246 $N $InteriorColumn $GeoTranPdelta;
element forceBeamColumn 60 237 247 $N $BorderColumn $GeoTranPdelta;
```

Define beams

```
*****
```

```
element forceBeamColumn 61 211 212 $N $InteriorBeamSmall $GeoTranPdelta;
element forceBeamColumn 62 212 213 $N $InteriorBeamLarge $GeoTranPdelta;
element forceBeamColumn 63 215 216 $N $InteriorBeamLarge $GeoTranPdelta;
```

Geometry

```
element forceBeamColumn 64 216 217 $N $InteriorBeamSmall $GeoTranPdelta;

element forceBeamColumn 65 221 222 $N $InteriorBeamSmall $GeoTranPdelta;
element forceBeamColumn 66 222 223 $N $InteriorBeamLarge $GeoTranPdelta;
element forceBeamColumn 67 225 226 $N $InteriorBeamLarge $GeoTranPdelta;
element forceBeamColumn 68 226 227 $N $InteriorBeamSmall $GeoTranPdelta;

element forceBeamColumn 69 231 232 $N $InteriorBeamSmall $GeoTranPdelta;
element forceBeamColumn 70 232 233 $N $InteriorBeamLarge $GeoTranPdelta;
element forceBeamColumn 71 235 236 $N $InteriorBeamLarge $GeoTranPdelta;
element forceBeamColumn 72 236 237 $N $InteriorBeamSmall $GeoTranPdelta;

element forceBeamColumn 73 241 242 $N $InteriorBeamSmall $GeoTranPdelta;
element forceBeamColumn 74 242 243 $N $InteriorBeamLarge $GeoTranPdelta;
element forceBeamColumn 75 245 246 $N $InteriorBeamLarge $GeoTranPdelta;
element forceBeamColumn 76 246 247 $N $InteriorBeamSmall $GeoTranPdelta;
```

Define walls

```
*****
```

```
element forceBeamColumn 77 204 214 $N $Wall1 $GeoTranPdelta;
element forceBeamColumn 78 214 224 $N $Wall2 $GeoTranPdelta;
element forceBeamColumn 79 224 234 $N $Wall3 $GeoTranPdelta;
element forceBeamColumn 80 234 244 $N $Wall4 $GeoTranPdelta;
```

Frame C

```
*****
```

4th storey*****

```
node 341 60. [expr $h1+3*$h2];
mass 341 [expr (($h2/2)*$Acb*$m)+(($L1/2)*$Abs*$m)+(17900.*$L1)/2./$g] 0. 0.;
node 342 [expr 60.+$L1] [expr $h1+3*$h2];
mass 342 [expr (($h2/2)*$Aci*$m)+(($L1/2)*$Abs*$m)+(($L1/2)*$Abl*$m)
        +(17900.*$L1)/$g] 0. 0.;
node 343 [expr 60.+2*$L1] [expr $h1+3*$h2];
mass 343 [expr (($h2/2)*$Aci*$m)+(($L1/2)*$Abl*$m)+(($L2/2)*$Abl*$m)
        +(17900.*$L1)/2/$g+(17900.*$L2)/2/$g] 0. 0.;
node 344 [expr 60.+2*$L1+$L2] [expr $h1+3*$h2];
mass 344 [expr (($h2/2)*$Aci*$m)+(($L1/2)*$Abl*$m)+(($L2/2)*$Abl*$m)
        +(17900.*$L1)/2/$g+(17900.*$L2)/2/$g] 0. 0.;
node 345 [expr 60.+3*$L1+$L2] [expr $h1+3*$h2];
mass 345 [expr (($h2/2)*$Aci*$m)+(($L1/2)*$Abs*$m)+(($L1/2)*$Abl*$m)
        +(17900.*$L1)/$g] 0. 0.;
node 346 [expr 60.+4*$L1+$L2] [expr $h1+3*$h2];
mass 346 [expr (($h2/2)*$Acb*$m)+(($L1/2)*$Abs*$m)+(17900.*$L1)/2./$g] 0. 0.;
```

```

# 3rd storey
#*****
node 331 60. [expr $h1+2*$h2];
mass 331 [expr ($h2*$Acb*$m)+(($L1/2)*$Abs*$m)+(28100.*$L1)/2./$g] 0. 0.;
node 332 [expr 60.+$L1] [expr $h1+2*$h2];
mass 332 [expr ($h2*$Aci*$m)+(($L1/2)*$Abs*$m)+(($L1/2)*$Abl*$m)
        +(28100.*$L1)/$g] 0. 0.;
node 333 [expr 60.+2*$L1] [expr $h1+2*$h2];
mass 333 [expr ($h2*$Aci*$m)+(($L1/2)*$Abl*$m)+(($L2/2)*$Abl*$m)
        +(28100.*$L1)/2/$g+(28100.*$L2)/2/$g] 0. 0.;
node 334 [expr 60.+2*$L1+$L2] [expr $h1+2*$h2];
mass 334 [expr ($h2*$Aci*$m)+(($L1/2)*$Abl*$m)+(($L2/2)*$Abl*$m)
        +(28100.*$L1)/2/$g+(28100.*$L2)/2/$g] 0. 0.;
node 335 [expr 60.+3*$L1+$L2] [expr $h1+2*$h2];
mass 335 [expr ($h2*$Aci*$m)+(($L1/2)*$Abs*$m)+(($L1/2)*$Abl*$m)
        +(28100.*$L1)/$g] 0. 0.;
node 336 [expr 60.+4*$L1+$L2] [expr $h1+2*$h2];
mass 236 [expr ($h2*$Acb*$m)+(($L1/2)*$Abs*$m)+(28100.*$L1)/2./$g] 0. 0.;

# 2nd storey
#*****
node 321 60. [expr $h1+$h2];
mass 321 [expr ($h2*$Acb*$m)+(($L1/2)*$Abs*$m)+(28100.*$L1)/2./$g] 0. 0.;
node 322 [expr 60.+$L1] [expr $h1+$h2];
mass 322
[expr ($h2*$Aci*$m)+(($L1/2)*$Abs*$m)+(($L1/2)*$Abl*$m)
+(28100.*$L1)/$g] 0. 0.;
node 323 [expr 60.+2*$L1] [expr $h1+$h2];
mass 323
[expr($h2*$Aci*$m)+(($L1/2)*$Abl*$m)+(($L2/2)*$Abl*$m)
+(28100.*$L1)/2/$g+(28100.*$L2)/2/$g] 0. 0.;
node 324 [expr 60.+2*$L1+$L2] [expr $h1+$h2];
mass 324
[expr($h2*$Aci*$m)+(($L1/2)*$Abl*$m)+(($L2/2)*$Abl*$m)
+(28100.*$L1)/2/$g+(28100.*$L2)/2/$g] 0. 0.;
node 325 [expr 60.+3*$L1+$L2] [expr $h1+$h2];
mass 325
[expr ($h2*$Aci*$m)+(($L1/2)*$Abs*$m)+(($L1/2)*$Abl*$m)+
(28100.*$L1)/$g] 0. 0.;
node 326 [expr 60.+4*$L1+$L2] [expr $h1+$h2];
mass 326 [expr ($h2*$Acb*$m)+(($L1/2)*$Abs*$m)+(28100.*$L1)/2./$g] 0. 0.;

# 1st storey

```

```

*****
node 311 60. $h1;
mass 311 [expr ((h1/2)*$Acb*$m)+((h2/2)*$Acb*$m)+(($L1/2)*$Abs*$m)
          +(28100.*$L1)/2./$g] 0. 0.;
node 312 [expr 60.+$L1] $h1
mass 312 [expr ((h1/2)*$Aci*$m)+((h2/2)*$Aci*$m)+(($L1/2)*$Abs*$m)
          +(($L1/2)*$Abl*$m)+(28100.*$L1)/$g] 0. 0.;
node 313 [expr 60.+2*$L1] $h1
mass 313 [expr ((h1/2)*$Aci*$m)+((h2/2)*$Aci*$m)+(($L1/2)*$Abl*$m)
          +(($L2/2)*$Abl*$m)+(28100.*$L1)/2/$g+(28100.*$L2)/2/$g] 0. 0.;
node 314 [expr 60.+2*$L1+$L2] $h1
mass 314 [expr ((h1/2)*$Aci*$m)+((h2/2)*$Aci*$m)+(($L1/2)*$Abl*$m)
          +(($L2/2)*$Abl*$m)+(28100.*$L1)/2/$g+(28100.*$L2)/2/$g] 0. 0.;
node 315 [expr 60.+3*$L1+$L2] $h1;
mass 315 [expr ((h1/2)*$Aci*$m)+((h2/2)*$Aci*$m)+(($L1/2)*$Abs*$m)
          +(($L1/2)*$Abl*$m)+(28100.*$L1)/$g] 0. 0.;
node 316 [expr 60.+4*$L1+$L2] $h1;
mass 316 [expr ((h1/2)*$Acb*$m)+((h2/2)*$Acb*$m)+(($L1/2)*$Abs*$m)
          +(28100.*$L1)/2./$g] 0. 0.;

# Ground floor
*****
node 301 60. 0.;
mass 301 0. 0. 0.;
node 302 [expr 60.+$L1] 0.;
mass 302 0. 0. 0.;
node 303 [expr 60.+2*$L1] 0.;
mass 303 0. 0. 0.;
node 304 [expr 60.+2*$L1+$L2] 0.;
mass 304 0. 0. 0.;
node 305 [expr 60.+3*$L1+$L2] 0.
mass 305 0. 0. 0.;
node 306 [expr 60.+4*$L1+$L2] 0.;
mass 306 0. 0. 0.;

# Define restraints
*****
fix 301 1 1 1;
fix 302 1 1 1;
fix 303 1 1 1;
fix 304 1 1 1;
fix 305 1 1 1;
fix 306 1 1 1;

```


Define columns

element forceBeamColumn 81 301 311 \$N \$BorderColumn \$GeoTranPdelta;
 element forceBeamColumn 82 302 312 \$N \$InteriorColumn \$GeoTranPdelta;
 element forceBeamColumn 83 303 313 \$N \$InteriorColumn \$GeoTranPdelta;
 element forceBeamColumn 84 304 314 \$N \$InteriorColumn \$GeoTranPdelta;
 element forceBeamColumn 85 305 315 \$N \$InteriorColumn \$GeoTranPdelta;
 element forceBeamColumn 86 306 316 \$N \$BorderColumn \$GeoTranPdelta;

element forceBeamColumn 87 311 321 \$N \$BorderColumn \$GeoTranPdelta;
 element forceBeamColumn 88 312 322 \$N \$InteriorColumn \$GeoTranPdelta;
 element forceBeamColumn 89 313 323 \$N \$InteriorColumn \$GeoTranPdelta;
 element forceBeamColumn 90 314 324 \$N \$InteriorColumn \$GeoTranPdelta;
 element forceBeamColumn 91 315 325 \$N \$InteriorColumn \$GeoTranPdelta;
 element forceBeamColumn 92 316 326 \$N \$BorderColumn \$GeoTranPdelta;

element forceBeamColumn 93 321 331 \$N \$BorderColumn \$GeoTranPdelta;
 element forceBeamColumn 94 322 332 \$N \$InteriorColumn \$GeoTranPdelta;
 element forceBeamColumn 95 323 333 \$N \$InteriorColumn \$GeoTranPdelta;
 element forceBeamColumn 96 324 334 \$N \$InteriorColumn \$GeoTranPdelta;
 element forceBeamColumn 97 325 335 \$N \$InteriorColumn \$GeoTranPdelta;
 element forceBeamColumn 98 326 336 \$N \$BorderColumn \$GeoTranPdelta;

element forceBeamColumn 99 331 341 \$N \$BorderColumn \$GeoTranPdelta;
 element forceBeamColumn 100 332 342 \$N \$InteriorColumn \$GeoTranPdelta;
 element forceBeamColumn 101 333 343 \$N \$InteriorColumn \$GeoTranPdelta;
 element forceBeamColumn 102 334 344 \$N \$InteriorColumn \$GeoTranPdelta;
 element forceBeamColumn 103 335 345 \$N \$InteriorColumn \$GeoTranPdelta;
 element forceBeamColumn 104 336 346 \$N \$BorderColumn \$GeoTranPdelta;

Define beams

element forceBeamColumn 105 311 312 \$N \$InteriorBeamSmall \$GeoTranPdelta;
 element forceBeamColumn 106 312 313 \$N \$InteriorBeamLarge \$GeoTranPdelta;
 element forceBeamColumn 107 313 314 \$N \$InteriorBeamLarge \$GeoTranPdelta;
 element forceBeamColumn 108 314 315 \$N \$InteriorBeamLarge \$GeoTranPdelta;
 element forceBeamColumn 109 315 316 \$N \$InteriorBeamSmall \$GeoTranPdelta;

element forceBeamColumn 110 321 322 \$N \$InteriorBeamSmall \$GeoTranPdelta;
 element forceBeamColumn 111 322 323 \$N \$InteriorBeamLarge \$GeoTranPdelta;
 element forceBeamColumn 112 323 324 \$N \$InteriorBeamLarge \$GeoTranPdelta;
 element forceBeamColumn 113 324 325 \$N \$InteriorBeamLarge \$GeoTranPdelta;
 element forceBeamColumn 114 325 326 \$N \$InteriorBeamSmall \$GeoTranPdelta;

```

element forceBeamColumn 115 331 332 $N $InteriorBeamSmall $GeoTranPdelta;
element forceBeamColumn 116 332 333 $N $InteriorBeamLarge $GeoTranPdelta;
element forceBeamColumn 117 333 334 $N $InteriorBeamLarge $GeoTranPdelta;
element forceBeamColumn 118 334 335 $N $InteriorBeamLarge $GeoTranPdelta;
element forceBeamColumn 119 335 336 $N $InteriorBeamSmall $GeoTranPdelta;

element forceBeamColumn 120 341 342 $N $InteriorBeamSmall $GeoTranPdelta;
element forceBeamColumn 121 342 343 $N $InteriorBeamLarge $GeoTranPdelta;
element forceBeamColumn 122 343 344 $N $InteriorBeamLarge $GeoTranPdelta;
element forceBeamColumn 123 344 345 $N $InteriorBeamLarge $GeoTranPdelta;
element forceBeamColumn 124 345 346 $N $InteriorBeamSmall $GeoTranPdelta;

```

C.5 Constraints

```

# **** Define constraints ****
#*****
equalDOF 241 146 1; # Connect Frame B to Frame A
equalDOF 231 136 1;
equalDOF 221 126 1;
equalDOF 211 116 1;

equalDOF 247 341 1; # Connect Frame B to Frame C
equalDOF 237 331 1;
equalDOF 227 321 1;
equalDOF 217 311 1;

equalDOF 244 243 1 2 3; # Impose wall DOF's
equalDOF 244 245 1 2 3; # Impose wall DOF's

equalDOF 234 233 1 2 3; # Impose wall DOF's
equalDOF 234 235 1 2 3; # Impose wall DOF's

equalDOF 224 223 1 2 3; # Impose wall DOF's
equalDOF 224 225 1 2 3; # Impose wall DOF's

equalDOF 214 213 1 2 3; # Impose wall DOF's
equalDOF 214 215 1 2 3; # Impose wall DOF's

```

C.6 Gravity loads

```

# **** Gravity loads ****
#*****
#*****

```

Gravity loads

```
# See steps in the non-linear static analysis for explanation of steps.

# Define gravity loads
#*****
set ALoadBeam4th -9100.;
set ALoadBeam1st2nd3rd -14300.;

set BLoadBeam4th -23100.;
set BLoadBeam1st2nd3rd -36300.;

set CLoadBeam4th -17900.;
set CLoadBeam1st2nd3rd -28100.;

pattern Plain 991 Constant {
eleLoad -ele 40 41 42 43 44 -type -beamUniform $ALoadBeam4th
eleLoad -ele 25 26 27 28 29 30 31 32 32 34 35 36 37 38 39
-type -beamUniform $ALoadBeam1st2nd3rd

eleLoad -ele 73 74 75 76 -type -beamUniform $BLoadBeam4th
eleLoad -ele 61 62 63 64 65 66 67 68 69 70 71 72
-type -beamUniform $BLoadBeam1st2nd3rd
load 244 0.0 -104000. 0.0;
load 234 0.0 -163400. 0.0;
load 224 0.0 -163400. 0.0;
load 214 0.0 -163400. 0.0;

eleLoad -ele 120 121 122 123 124 -type -beamUniform $CLoadBeam4th
eleLoad -ele 105 106 107 108 109 110 111 112 113 114 115 116 117 118 119
-type -beamUniform $CLoadBeam1st2nd3rd
}

# Apply loads
#*****
set TestType EnergyIncr;
set Tol 1.e-3;
set maxNumIter 150;
test $TestType $Tol $maxNumIter;
constraints Plain;
numberer Plain;
system BandGeneral;
algorithm Newton;
set NstepGravity 10;
set DGravity [expr 1./$NstepGravity];
integrator LoadControl $DGravity;
```

```
analysis Static;
set Gravity [analyze $NstepGravity];
if {$Gravity != 0} {
puts "Gravity loads not OK"
}
loadConst -time 0.0
puts "Model including gravity loads has been built."
```

C.7 Records

```
***** Record Data ****
*****
*****

# Displacements
*****
recorder Node -file ControlDisp4th.out -time -node 244 -dof 1 disp;
recorder Node -file ControlDisp3rd.out -time -node 234 -dof 1 disp;
recorder Node -file ControlDisp2nd.out -time -node 224 -dof 1 disp;
recorder Node -file ControlDisp1st.out -time -node 214 -dof 1 disp;

# Drift histories
*****
recorder Drift -file Drift_4th.out -time -iNode 244 -jNode 234 -dof 1 -perpDirn 2;
recorder Drift -file Drift_3rd.out -time -iNode 234 -jNode 224 -dof 1 -perpDirn 2;
recorder Drift -file Drift_2nd.out -time -iNode 224 -jNode 214 -dof 1 -perpDirn 2;
recorder Drift -file Drift_1st.out -time -iNode 214 -jNode 204 -dof 1 -perpDirn 2;
```

C.8 Non-linear static analysis

```
# **** Non-linear static analysis ****
*****
*****

# Constraints
*****
constraints Plain;

# Numberer
*****
numberer Plain;

# System
```

```

*****
system BandGeneral;

# Convergence criteria
*****
set TestType EnergyIncr;
set Tol 1.e-3;
set maxNumIter 200;
set printFlag 0;
test $TestType $Tol $maxNumIter;

# Algorithm selection
*****
set algorithmType Newton
algorithm $algorithmType;

# Integrator
*****
set ControlDisplacementNode 244
set ControlDisplacementDOF 1;
set Dmax 0.7;
set Dincr [expr (1/1000.)];
integrator DisplacementControl $ControlDisplacementNode
$ControlDisplacementDOF $Dincr;

# Load pattern
*****
pattern Plain 992 Linear {
load 244 1. 0.0 0.0;load 234 0.673 0.0 0.0;
load 224 0.363 0.0 0.0;load 214 0.137 0.0 0.0;
}

# Perform non-linear static analysis
*****
analysis Static;
set Nsteps [expr int($Dmax/$Dincr)];
set NSA [analyze $Nsteps];

if {$NSA == 0} {
puts "All steps have converged. Non-linear static analysis OK."
}
if {$NSA != 0} {
puts " No convergence.. must try something else."
set NSA 0;
}

```

```

set controlDisp 0.0;
set D0 0.0;
set Dstep [expr ($controlDisp-$D0)/($Dmax-$D0)]
while {$Dstep < 1.0 && $NSA == 0} {
set controlDisp [nodeDisp $ControlDisplacementNode $ControlDisplacementDOF]
set Dstep [expr ($controlDisp-$D0)/($Dmax-$D0)]
set NSA [analyze 1]
if {$NSA != 0} {
puts "Trying Newton with Initial Tangent .."
test NormDispIncr $Tol 2000 0
algorithm Newton -initial
set NSA [analyze 1 ]
test $TestType $Tol $maxNumIter 0
algorithm $algorithmType
}
if {$NSA != 0} {
puts "Trying Broyden .."
algorithm Broyden 8
set NSA [analyze 1 ]
algorithm $algorithmType
}
if {$NSA != 0} {
puts "Trying NewtonWithLineSearch .."
algorithm NewtonLineSearch .8
set NSA [analyze 1 ]
algorithm $algorithmType
}
}
}
puts "Non-linear static analysis finished"

```

C.9 Non-linear time-history analysis

```

# **** Non-linear time history analysis ****
#*****
#*****

# Set scale factor
#*****
set Scalefactor 1.5;

# Define time series
#*****

```

Non-linear time-history analysis

```
timeSeries Path 992 -dt 0.01 -filePath IW_scaled.txt -factor $Scalefactor;

# Apply time series
#*****
pattern UniformExcitation 2 1 -accel 992;

# Define damping
#*****
set alphaM 0.83775733;
set betaK 0.00169765;
set betaKinit 0.00;
set betaKcomm 0.00;
rayleigh $alphaM $betaK $betaKinit $betaKcomm;
wipeAnalysis;

# Analysis
#*****
constraints Plain
numberer RCM
system UmfPack
test NormDispIncr 1.0e-3 200;
algorithm Linear

# Hilber-Hughes-Taylor Method
#*****
set HHTalpha 0.9;
integrator HHT $HHTalpha;

# Newmarks method
#*****
set Ngamma 0.5;
set Nbeta 0.25;
integrator Newmark $Ngamma $Nbeta;

# Perfrom analysus
#*****
analysis Transient;
set NTHA [analyze 10015 0.01];
if {$NTHA == 0} {
puts "All steps have converged. Non-linear time history analysis OK."
}
if {$NTHA != 0} {
puts "Convergence issues. Non-linear time history analysis not OK."
}
}
```